

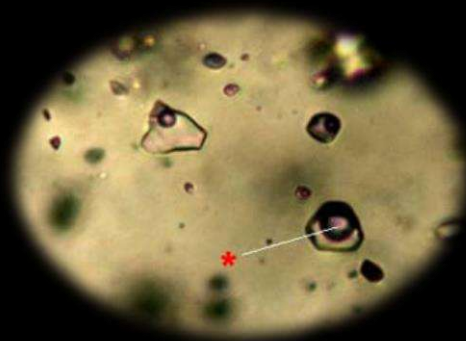
PACROFI XII

12th Biennial Conference
Pan-American Current
Research On Fluid
Inclusions

U.S. Geological Survey
Colorado State University



Program and Abstracts



June 2-6 2014

PACROFI XII

ABSTRACT VOLUME



Edited by

John Ridley

Al Hofstra

June – 2014

Colorado USA




UNLIMITED SCOPE

in Fluid Inclusion Research


For more than 50 years, McCrone Microscopes & Accessories has provided instrumentation and expert consultation to geologists worldwide. We are proud to sponsor the PACROFI 2014 meeting.

Let our technical experts show you how a McCrone fluid inclusion microscope system effectively allows fluid inclusionists to study melt and fluid inclusion behavior. With research-grade Olympus microscopes, Linkam thermal stages, and Q-Imaging microscope cameras, the McCrone fluid inclusion microscope system remains the industry standard.

Call today, 800-622-8122, or email mmaorder@mccrone.com to find the optimal equipment for you and your geological laboratory.



McCRONE
MICROSCOPES & ACCESSORIES
www.mccronemicroscopes.com
850 Pasquinelli Drive • Westmont, Illinois 60559



Contents

	page
PACROFI-XII 2014 Program	1
Tuesday June 3rd	1
Session 1: Instrumental methods, synthetic inclusions, and phase relations	1
Session 2: CL, data integration, and chemical modeling	2
Wednesday June 4th	3
Session 3: Silicic Melts, magmatic fluids, and Mo porphyry-epithermal systems	3
Session 4: Mafic to Intermediate Melts and Cu porphyry-epithermal systems	5
Thursday June 5th	6
Session 5: Mineral and energy resources in sedimentary basins	6
Friday June 6th	7
Posters	8
Oral Abstracts	10
Protocol for collecting, interpreting and reporting fluid and melt inclusion data	11
Bodnar R.J. ^a , Fall A. ^b , Esposito R. ^c , Moore L. ^a , Gazel E. ^a	
Synthetic fluid inclusions in opaque ore minerals as potential standards for NIR-light microthermometry experiments	13
Casanova, V.* , Kouzmanov, K.* , Audétat, A.** , Fontboté, L.*	
Dark secrets of hydrothermal fluid inclusions in quartz revealed by cathodoluminescence imaging	15
Diamond, L.W.* , Lambrecht, G.*	
Origin and evolution of ore-forming brines in sedimentary basins: Perspectives from MVT, sedex, and sedimentary Cu deposits	17
Emsbo, P.* , Hitzman, M.W.**	
Upper Cretaceous melt evolution in the eastern North China Craton: Evidence from clinopyroxene-hosted melt inclusions in mafic dikes	19
Hong-Rui Fan, Ya-Chun Cai, Fang-Fang Hu, Kui-Feng Yang	
Magmatic Steam Alunite Veins: The Epithermal Expression of UST Layers in Porphyry Intrusions?	21
Hofstra, A.H., Landis, G.P. and Rye, R.O.	
Fluid inclusion petrography, microthermometry, and geobiology in modern gypsum from acid saline Salar Ignorado, northern Chile	23
Karmanocky, F.J. and Benison, K.C.*	
Halogens and noble gases in fluid inclusions from sediment-hosted ore deposits and deeper metamorphic settings	25
Kendrick M.A.	
Anomalous physical and thermodynamic properties of H₂O-NaCl fluids in the critical region	27
Klyukin, Yu.I.* , Driesner, T.** , Lowell R.P.* , Bodnar R.J.*	
Evaporate Mound Chemistry: An Effective but Under-utilized Method to Document the Nature and Origin of fluids in Hydrothermal Ore- deposit Settings	29
Kontak, D.J.	

Using synthetic fluid inclusions in ultramafic minerals to monitor hydration – dehydration processes in the oceanic crust.	31
Lamadrid, H.M. *, Schwarzenback, E. *, Caddick, M. *, Rimstidt, D. *, Bodnar, R.J. *	
Vapor-saturated liquidus of the system H₂O-NaCl-FeCl₂	33
Lecumberri-Sanchez, P. *, Steele-MacInnis, M. *, Bodnar, R.J. **	
Stable carbon isotope ratios of CH₄-rich gas inclusions in shale-hosted fracture-fill mineralization: a tool for tracing hydrocarbon generation and estimation of gas potential.	34
Lüders, V. and Plessen, B.	
Petrography of silicate melt inclusions in quartz phenocrysts from porphyry Mo deposit at Bangpu, Tibet, China	35
Luo, M.C. *, Moncada, D. ** and Bodnar, R.J. **	
Noble gas isotope data from the Goldfield high sulfidation epithermal deposit, Nevada: Evidence for helium input from a primitive mantle source during ore formation	37
Manning, A.H. * and Hofstra, A.H. *	
Pre-Eruptive Conditions of the Hideaway Park Topaz Rhyolite, Colorado: Insights into Metal Source and Evolution of Magma Parental to the Henderson Porphyry Mo Deposit	39
Mercer, C.N. *, Hofstra, A.H. *, Todorov, T.I. **, Roberge, J. ***, Sisson, T.W. ****, Burgisser, A. ****, Adams, D.T. *****, and Cosca, M. *	
Fluid Inclusion and Mineral Texture based Exploration Targeting in the El Oro Gold District, Mexico and Michoacán states, Mexico.	41
Moncada, D. *, Freeze, J. **, and Bodnar R. J. *,	
Evidence for a magmatic source for Cu, Zn and Au in epithermal deposits in the Hauraki Goldfield, New Zealand	42
Sabina Strmic Palinkas*, Jeffrey L. Mauk**, Robert J. Bodnar***, Mathijs A. Booden****, Mark P. Simpson*****	
Matching low-temperature microthermometric observations and LA-ICP-MS fluid composition data.	44
John Ridley	
Petrogenesis and metal budget of three volcanoes in the Chichinautzin monogenetic field, Mexico: A Melt Inclusion Study	46
Roberge, J. *, Mercer, C.N. **, Kent, A.J.R. ***, Guilbaud, M-N. ****, Arrieta-Garcia G. ****	
Ore-forming fluids associated with the early mineralization at Cerro de Pasco, Peru	48
Rottier B. *, Kouzmanov K. * Fontboté L. *, Wälle M. **,	
Fluid evolution in an Andean geothermal system: coupling fluid inclusions thermometry, LA-ICP-MS and geochemical modeling	50
Sánchez-Alfaro, P. ^{1,2} , Driesner, T. ³ , Heinrich, C. ³ , Reich, M. ^{1,2} , Pérez-Flores, P. ^{2,4} , Arancibia, G. ^{2,4} , Cembrano, J. ^{2,4} , Campos, E. ^{2,5} and Lohmar, S. ⁶ .	
Developments in fluid inclusion compositional estimation from combined microthermometric and microanalytical data	51
Steele-MacInnis, M. *	
Liquid immiscibility – important processes during pegmatite formation	52
Thomas, R. *, Davidson, P. **	
Using Evaporate Mound Chemistry of Fluid Inclusions to Assess the Metal Fertility and Fluid: Rock Interaction in a Large Peraluminous Batholith: A Case Study of the Mineralized (Sn-W-U-Cu-Zn-Ag) South Mountain Batholith, Nova Scotia, Canada	54
Tweedale, F. *, Hanley, J. *, Kontak, D.J. **, and Rogers, N. ***	
Poster Abstracts	56

Fluid Inclusions and Stable Isotopes (O, H, S, C) Document Fluid Mixing in the Ore-forming Systems of the Daraloo and Sarmeshk Porphyry Cu Deposits, Central Part of the Dehaj-Sardoeieh Belt, South Iran	57
Alimohammadi, M.* , Kontak, D.J.** , Alirezaei, S.* , and Kyser, K.T.**	
Testing Established Models of Hydrothermal Fluid Distribution Around Porphyry Deposits: The Application of Fluid Inclusion Research to Porphyry Exploration	59
Bain, W.B.* , Cline, J.S.* , Marsh, T.M.**	
Cathodoluminescence and Fluid Inclusion Characteristics of Porphyry Vein Quartz	61
Bennett, M.* , Monecke, T.* , Reynolds, T.J.** , Ricks, J.* , and Muntean, J.***	
Fluid inclusion and stable isotope study of Magino; a magmatic related Archean gold deposit.	63
Haroldson, E.H.* , Brown, P.E.*	
Geochemistry of Fluid Inclusions in the Vazante Zinc Deposit, Minas Gerais, Brazil.	65
Hassan, A. M* and Appold, M. S*	
Petrography of fluid inclusions in modern gypsum precipitated from volcanoclastic hosted acid saline Salar Ignorado, northern Chile	67
Karmanocky, F.J. and Benison, K.C.*	
Low-salinity fluids associated with the Geumeum Mo mineralization in the late Cretaceous granitic rocks of the Gyeongsang Basin, South Korea	69
Kim, H.* , Seo, M.* , Yang, K.*	
Characteristics of tin-tungsten mineralizing fluids at Panasqueira, Portugal	71
Lecumberri-Sanchez, P.* , Heinrich, C. A.* , Wälle, M.* , Vieira, R.** , Pinto, F.**	
Paragenesis of quartz, FIA's, and associated alteration and sulfide minerals in the Pebble Porphyry Cu-Au-Mo Deposit, SW Alaska resolved by Cathodoluminescence	72
Marsh, E.E.	
Generation of monazite and other REE-bearing phases during secondary fluid events: Pea Ridge iron oxide-apatite-REE deposit, Southeast Missouri, USA	74
Meighan, C.J.* , Hofstra, A.H.* , Marsh, E.E.* , Lowers, H.A.* , Emsbo, P.* , Hitzman, M.W.**	
Estimates of the amount of time required to form an epithermal precious metal deposit based on ore grade & tonnage, fluid flow rate, and metal content of ore fluids.	76
Moncada, D.* , Rimstidt, J.D.* , and Bodnar, R.J.*	
Fluid inclusion & stable isotopic evidence for extreme degassing of melt & condensation of brine in the Henderson porphyry Mo deposit	77
Melanie N. Newton* and Albert H. Hofstra**	
Critical PTX properties of FeCl₂-bearing fluids	79
Steele-MacInnis, M.* , Lecumberri-Sanchez, P.* , Bodnar, R.J.**	
CO₂-rich fluid inclusions in Silica- and LREE-enriched spinel peridotite xenoliths from the Quaternary intraplate alkali basalt, Jeju island, South Korea: A preliminary study	80
Woo, Y.H. , Yang, K.H	
Author Index	82

PACROFI XII – 2014 Program

Tuesday June 3rd

Session 1: Instrumental methods, synthetic inclusions, and phase relations

8:30-8:40

Welcome to USGS

–Al Hofstra

8:40-9:20

Keynote: Halogens and noble gases in fluid inclusions from sediment-hosted ore deposits and deeper metamorphic settings

–Kendrick M.A.

9:20-9:40

Evaporate Mound Chemistry: An Effective but Under-utilized Method to Document the Nature and Origin of fluids in Hydrothermal Ore-deposit Settings

–Kontak, D.J.

9:40-10:00

Synthetic fluid inclusions in opaque ore minerals as potential standards for NIR-light microthermometry experiments

–Casanova, V., Kouzmanov, K., Audétat, A., and Fontboté, L.

Break

10:15-10:35

Using synthetic fluid inclusions in ultramafic minerals to monitor hydration – dehydration processes in the oceanic crust

–Lamadrid, H.M., Schwarzenback, E., Caddick, M., Rimstidt, D., and Bodnar, R.J.

10:35-10:55

Anomalous physical and thermodynamic properties of H₂O-NaCl fluids in the critical region

–Klyukin, Y.I., Driesner, T., Lowell R.P., and Bodnar R.J.

11:00-12:00 Lab tour

12:00-1:00 Lunch

1:00-4:30 Transport to Pingree Park

5:40-6:00 Pingree Park Orientation

5:00-6:00 Happy Hour

6:00-7:00 Dinner

Session 2: CL, data integration, and chemical modeling

7:30-7:40pm

Welcome to CSU at Pingree Park, info

–John Ridley

7:40-8:00

Dark secrets of hydrothermal fluid inclusions in quartz revealed by cathodoluminescence imaging

–Diamond, L.W., and Lambrecht, G.

8:00-8:20

Vapor-saturated liquidus of the system $\text{H}_2\text{O}-\text{NaCl}-\text{FeCl}_2$

–Lecumberri-Sanchez, P., Steele-MacInnis, M., and Bodnar, R.J.

8:20-8:40

Matching low-temperature microthermometric observations and LA-ICP-MS fluid composition data

–Ridley, J.

Break

9:00-9:20

Developments in fluid inclusion compositional estimation from combined microthermometric and microanalytical data

–Steele-MacInnis, M.

9:20-9:40

Protocol for collecting, interpreting and reporting fluid and melt inclusion data

–Bodnar, R.J., Fall, A., Esposito, R., Moore, L., and Gazel, P.

9:40-10:00

Discussion

Wednesday June 4th

Session 3: Silicic Melts, magmatic fluids, and Mo porphyry-epithermal systems

8:30-9:10

Keynote: Liquid immiscibility – important processes during pegmatite formation

–Thomas, R., and Davidson, P.

9:10-9:30

Using Evaporate Mound Chemistry of Fluid Inclusions to Assess the Metal Fertility and Fluid: Rock Interaction in a Large Peraluminous Batholith: A Case Study of the Mineralized (Sn-W-U-Cu-Zn-Ag) South Mountain Batholith, Nova Scotia, Canada

–Tweedale, F., Hanley, J., Kontak, D.J., and Rogers, N.

9:30-9:50

Petrography of silicate melt inclusions in quartz phenocrysts from porphyry Mo deposit at Bangpu, Tibet, China

–Luo, M.C., Moncada, D., and Bodnar, R.J.

Break

10:10-10:30

Pre-Eruptive Conditions of the Hideaway Park Topaz Rhyolite, Colorado: Insights into Metal Source and Evolution of Magma Parental to the Henderson Porphyry Mo Deposit

–Mercer, C.N., Hofstra, A.H., Todorov, T.I., Roberge, J., Sisson, T.W., Burgisser, A., Adams, D.T., and Cosca, M.

10:30-10:50

Magmatic Steam Alunite Veins: The Epithermal Expression of UST Layers in Porphyry Intrusions?

–Hofstra, A.H., Landis, G.P., and Rye, R.O.

10:50-11:10

Fluid evolution in an Andean geothermal system: coupling fluid inclusions thermometry, LA-ICP-MS and geochemical modeling

–Sánchez-Alfaro, P., Driesner, T., Heinrich, C., Reich, M., Pérez-Flores, P., Arancibia, G., Cembrano, J., Campos, E., and Lohmar, S.

11:10-11:40

Discussion

12:00-1:00 Lunch

1:00-4:00 Free time

4:00-6:00 Posters/Happy Hour

6:00-7:00 Dinner

Session 4: Mafic to Intermediate Melts and Cu porphyry-epithermal systems

7:30-7:50

Upper Cretaceous melt evolution in the eastern North China Craton: Evidence from clinopyroxene-hosted melt inclusions in mafic dikes

–Hong-Rui Fan, Ya-Chun Cai, Fang-Fang Hu, and Kui-Feng Yang

7:50-8:10

Petrogenesis and metal budget of three volcanoes in the Chichinautzin monogenetic field, Mexico: A Melt Inclusion Study

–Roberge, J., Mercer, C.N., Kent, A.J.R., Guilbaud, M-N., and Arrieta-Garcia G.

8:10-8:30

Ore-forming fluids associated with the early mineralization at Cerro de Pasco, Peru

–Rottier B., Kouzmanov K., Fontboté L., and Wälle M.

Break

8:50-9:10

Noble gas isotope data from the Goldfield high sulfidation epithermal deposit, Nevada: Evidence for helium input from a primitive mantle source during ore formation

–Manning, A.H., and Hofstra, A.H.

9:10-9:40

Evidence for a magmatic source for Cu, Zn and Au in epithermal deposits in the Hauraki Goldfield, New Zealand

–Sabina Strmic Palinkas, Jeffrey L. Mauk, Robert J. Bodnar, Mathijs A. Booden, and Mark P. Simpson

9:40-10:00

Fluid Inclusion and Mineral Texture based Exploration Targeting in the El Oro Gold District, Mexico and Michoacán states, Mexico.

–Moncada, D., Freeze, J., and Bodnar R.J.

Thursday June 5th

Session 5: Mineral and energy resources in sedimentary basins

8:30-9:10

Keynote: Origin and evolution of ore-forming brines in sedimentary basins: Perspectives from MVT, sedex, and sedimentary Cu deposits

–Emsbo, P., and Hitzman, M.W.

9:10-9:30

Stable carbon isotope ratios of CH₄-rich gas inclusions in shale-hosted fracture-fill mineralization: a tool for tracing hydrocarbon generation and estimation of gas potential.

–Lüders, V., and Plessen, B.

9:30-9:50

Fluid inclusion petrography, microthermometry, and geobiology in modern gypsum from acid saline Salar Ignorado, northern Chile

–Karmanocky, F.J., and Benison, K.C.

9:50-10:10 PACROFI 2016

10:10-noon Posters

12:00-1:00 Lunch

1:00-5:00 Free Time

5:00-7:00 Posters/Happy Hour

7:00-9:00 Banquet and Band

9:00-12:00 Bonfire and Band

Friday June 6th

Transport to Ft. Collins shuttle station

with service to Denver International Airport

Posters

Fluid Inclusions and Stable Isotopes (O, H, S, C) Document Fluid Mixing in the Ore-forming Systems of the Daraloo and Sarmeshk Porphyry Cu Deposits, Central Part of the Dehaj-Sardoeieh Belt, South Iran

–Alimohammadi, M., Kontak, D.J., Alirezaei, S., and Kyser, K.T.

Testing Established Models of Hydrothermal Fluid Distribution Around Porphyry Deposits: The Application of Fluid Inclusion Research to Porphyry Exploration

–Bain, W.B., Cline, J.S., and Marsh, T.M.

Cathodoluminescence and Fluid Inclusion Characteristics of Porphyry Vein Quartz

–Bennett, M., Monecke, T., Reynolds, T.J., Ricks, J., and Muntean, J.

Fluid inclusion and stable isotope study of Magino; a magmatic related Archean gold deposit

–Haroldson, E.H., and Brown, P.E.

Geochemistry of Fluid Inclusions in the Vazante Zinc Deposit, Minas Gerais, Brazil.

–Hassan, A.M., and Appold, M.S.

Petrography of fluid inclusions in modern gypsum precipitated from volcanoclastic hosted acid saline Salar Ignorado, northern Chile

–Karmanocky, F.J., and Benison, K.C.

Low-salinity fluids associated with the Geumeum Mo mineralization in the late Cretaceous granitic rocks of the Gyeongsang Basin, South Korea

–Kim, H., Seo, M., and Yang, K.

Characteristics of tin-tungsten mineralizing fluids at Panasqueira, Portugal

–Lecumberri-Sanchez, P., Heinrich, C.A., Wälle, M., Vieira, R., and Pinto, F.

Paragenesis of quartz, FIA's, and associated alteration and sulfide minerals in the Pebble Porphyry Cu-Au-Mo Deposit, SW Alaska resolved by Cathodoluminescence

–Marsh, E.E.

Generation of monazite and other REE-bearing phases by secondary fluid events, Pea Ridge iron oxide-apatite-REE deposit, Southeast Missouri, USA

– Meighan, C.J., Hofstra, A.H., Marsh, E.E., Lowers, H.A., Emsbo, P., and Hitzman, M.W.

Estimates of the amount of time required to form an epithermal precious metal deposit based on ore grade & tonnage, fluid flow rate, and metal content of ore fluids.

–Moncada, D., Rimstidt, J.D., and Bodnar, R.J.

Fluid inclusion & stable isotopic evidence for extreme degassing of melt & condensation of brine in the Henderson porphyry Mo deposit

–Newton, M.N., and Hofstra, A.H.

Critical PTX properties of FeCl₂-bearing fluids

–Steele-MacInnis, M., Lecumberri-Sanchez, P., and Bodnar, R.J.

CO₂-rich fluid inclusions in Silica- and LREE-enriched spinel peridotite xenoliths from the Quaternary intraplate alkali basalt, Jeju island, South Korea: A preliminary study

–Woo, Y.H., and Yang, K.H

Abstracts

Oral abstracts

Protocol for collecting, interpreting and reporting fluid and melt inclusion data

Bodnar R.J.^a, Fall A.^b, Esposito R.^c, Moore L.^a, Gazel E.^a

^a Fluids Research Laboratory, Virginia Tech, Blacksburg, VA USA 24061 (rjb@vt.edu). ^b Texas Bureau of Economic Geology, University of Texas, Austin, TX USA 78713). ^c DiSTAR, Università di Napoli (Federico II), Italy.

The concept of the *Fluid Inclusion Assemblage* (*FIA*) was reported two decades ago (Goldstein and Reynolds, 1994), and the comparable *Melt Inclusion Assemblage* (*MIA*) was described in 2006 (Bodnar and Student, 2006). These protocols describe the methods that should be followed to collect defensible fluid and melt inclusion data that can be used to understand the fluid and melt properties associated with a wide range of geologic processes. Yet, today, many inclusionists, including very experienced workers, do not understand and do not apply these fundamental concepts that form the basis of fluid and melt inclusion research. Here, we reiterate the principles behind these concepts and describe the protocol that should be followed during collection, interpretation and reporting of fluid and melt inclusion data.

Perhaps the reason that many inclusionists do not follow the *FIA* approach is that they confuse *FIAs* with fluid inclusion “types”. Thus, when asked to define an *FIA*, many inclusionists respond that they have, for example, two-phase liquid-rich inclusions, but they are describing the types of inclusions present and not the *FIAs*. While an *FIA* can be composed of two-phase, liquid-rich fluid inclusions, this type of FI does not constitute an *FIA*. Stated in its simplest form, an *FIA* represents a group of petrographically-associated fluid inclusions, or a group of fluid inclusions that were all trapped at the same time. Thus, an *FIA* is recognized as a group of FI that outline a former growth surface in a crystal (primary inclusions, Fig. 1) or occur along a linear trail representing a healed fracture (secondary FI). Individual *FIAs* typically have dimensions such that the entire *FIA* is observable in a single field of view when the sample is examined at low to moderate magnification using a 10x or 20x objective. Most *FIAs* are limited to a single crystal, although *FIAs* composed of secondary FI may extend from one crystal into the adjoining crystal.

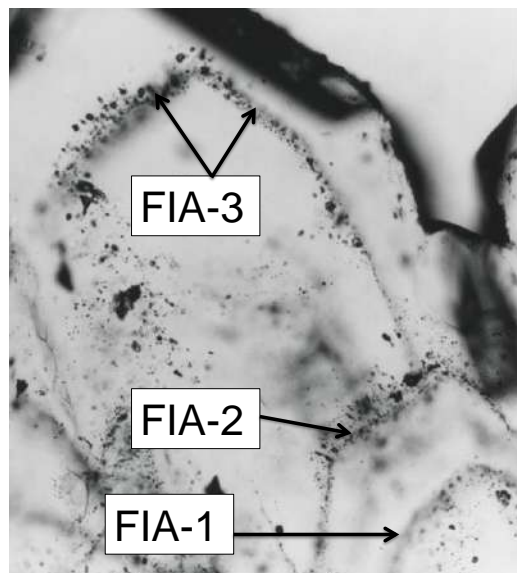


Figure 1. Photomicrograph showing three *FIAs* composed of primary fluid inclusions in quartz.

Why should we study *FIAs* and *MIAs*?

The assumption that is made when we study fluid (and melt) inclusions is that the fluid properties (density, composition) that are determined from analysis of inclusions represent the properties of the fluid at the time of trapping. Thus, in order for an inclusion to preserve and record the original fluid properties, the fluid inclusion must trap a single, homogeneous fluid, the volume of the inclusion must remain constant (isochoric), and nothing can be lost from, or added to, the inclusion after trapping (Roedder's/Sorby's Rules). However, if we measure a single fluid inclusion and it homogenizes at, for example, 250°C and has a salinity of 10 wt.% NaCl equivalent, there is no way *a priori* to know that this represents the original homogenization temperature (density) and salinity of the trapped fluid. Conversely, if we measure an *FIA* (group of inclusions that were all trapped at the same time), and if all the FI in the *FIA* show the same homogenization temperature and salinity, then these represent the original trapping conditions because we know from studies of synthetic and natural inclusions that it is statistically improbable for a group of FI to reequilibrate and to all show the same homogenization temperature and salinity after reequilibration.

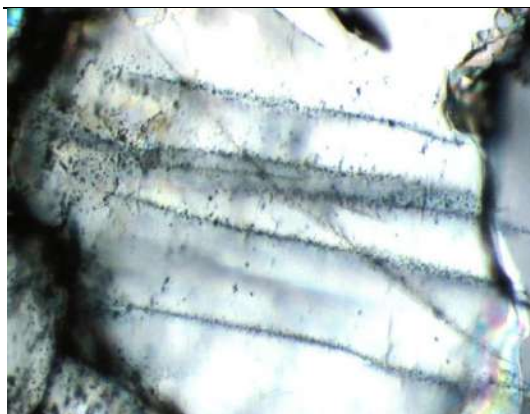


Figure 2. Photomicrograph showing several FIAs composed of secondary fluid inclusions along healed fractures in quartz.

While many fluid inclusionists strive to identify and study *FIAs*, few workers who study melt inclusions study *MIAs*. There are many reasons why so few melt inclusionists study *MIAs*, but perhaps the main one is that *MIAs* are less common because many phenocrysts contain only one or a few MI, and identifying two or more MI that were trapped at the same time is time-consuming and difficult. However, *MIA* do occur in many environments (Fig. 3). The failure to study *MIA* or, stated differently, by studying

randomly-selected MI with unconstrained paragenetic relationships, has led to many incorrect (or at least indefensible) interpretations of melt inclusion data. This has been especially apparent in studies that use melt inclusions to constrain magma degassing paths (Esposito et al., 2014; Moore et al., 2014, Steele-MacInnis et al., 2011).

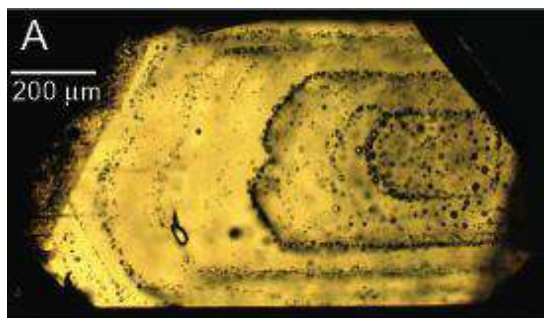


Figure 3. Photomicrograph showing several MIAs composed of primary melt inclusions along growth zones in pyroxene.

Reporting data for *FIAs* and *MIAs*?

Most often, fluid and, to a lesser extent, melt inclusion data are reported as histograms showing the frequency of homogenization temperatures, salinity, etc. Moreover, the data are generally grouped according to inclusion type,

such as two-phase liquid-rich, halite-bearing, CO₂ inclusions, etc. While this method of data reporting provides some information on the broad variation in the properties of the fluid inclusion types in the geological environment being studied, it provides little information concerning the reliability of the data and temporal variations in fluid properties. As such, data for individual *FIAs* should be reported, and these should show the complete range of data as well as the average and 75th and 25th percentiles. In most fluid inclusion studies, several tens or hundreds of *FIAs* will be measured, and each should be plotted separately. If the number of *FIAs* measured is too large to be practical to plot individually, a representative number of *FIAs* should be shown graphically, but *all FIAs* should be listed in a table or in supporting information. Only by reporting the data in this manner can the informed reader evaluate the data and place it into a paragenetic context.

REFERENCES

- Bodnar, R.J., Student, J.J. (2006) Melt inclusions in plutonic rocks: Petrography and microthermometry. *In* Melt Inclusions in Plutonic Rocks (J. D. Webster, ed.) Mineral. Assoc. Canada, Short Course **36**, 1-26.
- Esposito, R., Hunter, J., Schiffbauer, J., Shimizu, N., Bodnar, R.J. (2014) An assessment of the reliability of melt inclusions as recorders of the pre-eruptive volatile content of magmas. *American Mineralogist*, in press.
- Goldstein, R.H., Reynolds, T.J. (1994) Systematics of fluid inclusions in diagenetic minerals. *SEPM Short Course*, **31**.
- Moore, L., Gazel, E., Tuohy, R., Lloyd, A., Esposito, R., Hauri, E., Wallace, P., Plank, T., Bodnar, R.J. (2014) Bubbles matter: An assessment of the contribution of vapor bubbles to melt inclusion volatile budgets. *American Mineralogist* (in review).
- Steele-MacInnis, M., Esposito, R., Bodnar, R.J. (2011) Thermodynamic model for the effect of post-entrapment crystallization on the H₂O-CO₂ systematics of volatile-saturated silicate melt inclusions. *Journal of Petrology*, **52**, 2461-2482.

Synthetic fluid inclusions in opaque ore minerals as potential standards for NIR-light microthermometry experiments

Casanova, V.*, Kouzmanov, K.*, Audétat, A.**, Fontboté, L.*

* *Earth and Environmental Sciences, University of Geneva, Switzerland*

** *Bayerisches Geoinstitut, Universität Bayreuth, Germany*

Fluid inclusions (FIs) are an essential tool to study ore deposits formation. However, most studies are performed using classical microscopy. They are therefore limited to transparent minerals, of which only cassiterite and Fe-poor sphalerite are ore minerals, and rely mostly on gangue minerals interpreted to be cogenetic with ore-formation. Near-infrared (NIR) microscopy of ore minerals can be used to study internal textures of minerals that are opaque to the visible light, such as pyrite, enargite, wolframite, hematite, stibnite. It has also been used to study FIs hosted in ore minerals, thus providing direct insights into ore-forming fluids.

An earlier study on enargite-hosted FIs (Moritz, 2006) pointed out important overestimation of fluid salinities and underestimation of homogenization temperatures owing to shifts in recorded phase transition temperatures as a function of the used light intensity. More recent work (Zhu et al., 2013) did not notice drastic light intensity-dependant temperature shifts in pyrite-hosted FIs. It is critical to understand the processes behind light intensity-driven temperature shifts encountered in some NIR-transparent minerals in order to bring meaningful results to ore geology.

Here we report results of the first systematic study of synthetic FIs in a variety of NIR-transparent ore minerals in an attempt to create standards for NIR-microthermometry.

Natural samples of enargite, pyrite, stibnite, hematite, Fe-rich, and Fe-poor sphalerite were selected upon their paucity in fluid inclusions and their transparency to NIR. Each opaque mineral was loaded together with powdered equivalent and synthetic quartz into a gold capsule to which a 10 wt% NaCl aqueous solution spiked with Cs was added. After several days of equilibration in an autoclave at fixed P-T conditions, the samples were cracked in situ and held at the same P-T conditions for several more days in order for the cracks to seal. The recovered samples were prepared as doubly polished thin sections with respective thickness of 150 μm and -500 μm .

Microthermometric measurements were performed using a Linkam FTIR-600 mounted on an Olympus BX51 microscope equipped with IR Olympus objectives. The microscope has been modified to accept a removable 1200 nm low-pass filter placed at the exit of the light source. NIR observations and image acquisition were done using an Olympus XM10 camera or a Hamamatsu C2400-03d camera, both connected to the CellP® software. The 100 W lamp intensity is controlled by an Olympus TH4-200 controller and recorded by a voltmeter mounted in parallel.

Synthetic FIs (up to 70 μm in size) were obtained in enargite, pyrite, Fe-rich, and Fe-poor sphalerite as well as in all quartz samples. Microthermometry performed under low light intensity yields similar apparent salinities for FIs trapped in quartz and NIR-transparent minerals from the same batch. With increasing light intensity, important shifts are recorded. These correlation trends are different for each mineral. In contrast to results reported by Moritz (2006), they are not linearly correlated with the light intensity but rather define exponential trends. It is important here to stress that not only the intensity of the light source affects the intensity of light reaching the sample, but all optical components situated in the light path in between (e.g. filters, diaphragms, polarizer) as shown in Figure 1A. This kind of diagram is limited to produce curves for fixed microscope settings. However it is possible to assess the light intensity reaching the sample by using the dwell time of the camera as a proxy, which is directly linked to the amount of light exiting the sample. It now appears that there is a range of microscope and light settings for which the error is acceptable (Fig. 1B).

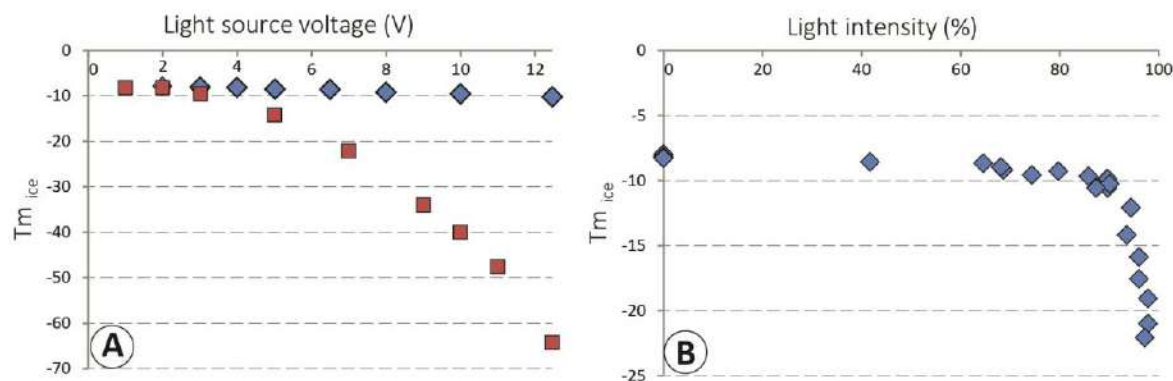


Figure 1: A. Correlations curves between recorded final ice melting temperature ($T_{m_{ice}}$) and light source intensity for two microscope settings: **Square:** Diaphragm fully open and 1200 nm filter on; **Diamonds:** Diaphragm closed at 95% and 1200 nm filter removed. **B.** Correlation curve between $T_{m_{ice}}$ and assessed light intensity reaching the sample for various light and microscope settings; light intensity is assessed using the camera dwell time (Dwt): [light intensity (%)]= $100 \cdot (Dwt_{max} - Dwt_{measured}) / Dwt_{max}$

This study shows that under the same conditions, gangue and ore minerals trap the same fluid in terms of major elements. It also confirms that under poorly controlled light settings during NIR-microthermometry, important underestimation of phase change temperatures can be recorded leading to overestimation of salinities (up to more than 100%). This directly translate into important errors when interpreting fluid origins or assessing the internal standard for LA-ICP-MS analyses. However for each NIR-transparent ore mineral, there is a range of light and microscope settings for which no shift is noticeable. Reflectance and transmittance FTIR-spectra for each sample will be acquired in order to establish relationship between mineral absorbance and recorded temperature shifts.

REFERENCES

- Moritz R. (2006) Fluid salinities obtained by infrared microthermometry of opaque minerals: Implications for ore deposit modeling — A note of caution. *Journal of Geochemical Exploration*. v.89. p 284-287.
- Zhu M. T., Zhang L. C., Wu G., He H. Y., Cui M. L. (2013) Fluid inclusions and He\Ar isotopes in pyrite from the Yinjiagou deposit in the southern margin of the North China Craton: A mantle connection for poly-metallic mineralization. *Chemical Geology*. v. 351. p. 1-14.

Dark secrets of hydrothermal fluid inclusions in quartz revealed by cathodoluminescence imaging

Diamond, L.W.*, Lambrecht, G.*

**Rock-Water Interaction Group, Institute of Geological Sciences, University of Bern, Switzerland*

Cathodoluminescence (CL) studies have previously shown that some secondary fluid inclusions in luminescent quartz are surrounded by dark, non-luminescent patches, resulting from fracture-sealing by late, trace-element-poor quartz. This finding has led to the tacit generalization that all dark CL patches indicate influx of low temperature, late-stage fluids. In this study we have examined natural and synthetic hydrothermal quartz crystals using a type of CL imaging (SEM-VPSE) supplemented by in-situ elemental analysis. The results lead us to propose that all natural, water-bearing inclusions in quartz, whether trapped on former crystal growth surfaces (i.e. of primary origin) or in healed fractures (i.e. of pseudosecondary or secondary origin), are surrounded by three-dimensional, non-luminescent patches (Fig. 1). Cross-cutting relations show that the patches form after entrapment of the fluid inclusions and therefore they are not diagnostic of the timing of fluid entrapment. In particular, the presence of dark patches cannot be taken as evidence that the associated fluid inclusion is of secondary origin. Instead, the dark patches reveal the mechanism by which fluid inclusions spontaneously approach morphological equilibrium and purify their host quartz over geologic time.

The dark-CL patches are interpreted to form as follows. Fluid inclusions containing solvent water perpetually dissolve and reprecipitate their walls, gradually adopting low-energy euhedral and equant shapes. Defects in the host quartz constitute solubility gradients that drive physical migration of the inclusions over distances of tens of μm (commonly) up to several mm (rarely). Inclusions thus sequester from their walls any trace elements (e.g., Li, Al, Na, Ti) present in excess of equilibrium concentrations, thereby chemically purifying their host crystals in a process analogous to industrial zone refining. Non-luminescent patches of quartz are left in their wake. Fluid inclusions that contain no solvent water (e.g., inclusions of low-density H_2O vapor or other non-aqueous volatiles) do not undergo this process and therefore do not migrate, do not modify their shapes with time and are not associated with dark CL patches.

This new understanding has implications for the interpretation of certain solid crystallites within fluid inclusions. As Ti and Al are commonly transferred from the quartz host to the fluid inclusion by zone refining, Ti- and Al- minerals may saturate within the fluid inclusions long after the initial entrapment of the fluid inclusions. Likely candidates here are TiO_2 polymorphs (e.g., rutile, anatase, brookite) and phyllosilicates (e.g., muscovite; the addition of Al perhaps having triggered precipitation from a K-bearing solution). Many such crystallites in fluid inclusions may therefore be more accurately classified as step-daughter minerals rather than daughter or captured phases. Similarly, the post-entrapment enrichment of fluid inclusions in Li, Al and Ti by zone refining needs to be taken into account when using chemical analyses of fluid inclusions to reconstruct the composition of the parent hydrothermal fluid. Although Na is also subject to this process, its enrichment is negligible considering the initial Na contents of common hydrothermal fluids.

In-situ microbeam analytical methods for element ratios in fluid inclusions, such as laser-ablation-ICP-MS, SIMS, SXRF and PIXE, usually rely on the proper quantification of separate background (mineral host) and fluid inclusion signals. Dark-CL patches, being purified quartz, thus constitute an ideal background matrix for sensitive analyses of Ti, Al, Li, Ge, Na, K and Fe in fluid inclusions (although background values are relatively unimportant to Na and K, as these elements are normally so abundant in fluid inclusions). However, as the dark-CL patches have variable shapes and sizes and envelop fluid inclusions asymmetrically, use of SEM-CL images is recommended to select appropriate sites for background analyses.

The observed sequestration of Ti by fluid inclusions and its depletion in dark patches around fluid inclusions impacts on applications of the Ti-in-quartz geothermometer. As zone-refined dark patches in quartz are post-crystallization features depleted in Ti, their unwitting analysis will yield erroneously low temperatures when inserted into the geothermometer equations. Individual dark patches may have spatial extents up to several square micrometers (mm^2). Therefore, CL images should be used to select luminescent sample spots for microbeam analysis. However, when using depth-profiling methods such as

LA-ICP-MS and SIMS, the danger still remains that invisible zone-refined patches may be traversed below the sample surface.

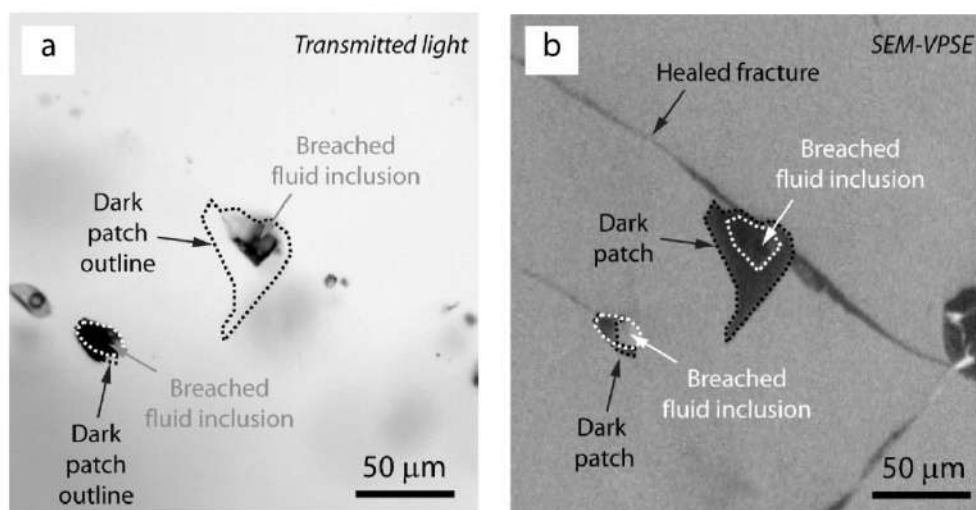


Fig. 1.
a: Hydrothermal fluid inclusions in quartz viewed in transmitted light.
b: Same field of view as (a) in SEM-VPSE illumination, showing dark patches around the inclusions.

Origin and evolution of ore-forming brines in sedimentary basins: Perspectives from MVT, sedex, and sedimentary Cu deposits

Emsbo, P.*, Hitzman, M.W.**

**U.S. Geological Survey, Denver, CO, **Colorado School of Mines, Golden, CO*

Sedimentary basins host a spectrum of sediment-hosted ore deposits, including Mississippi Valley-type (MVT) Zn-Pb-Ag, sedimentary exhalative Zn-Pb-Ag (sedex), and sediment-hosted Cu-Co-Ag (sed Cu) deposits that, together, account for a significant proportion of the world's base metal resources. Fluid inclusion studies of these deposits have shown that most formed from moderate temperature (50 to 200°C) high-salinity (15 to 30 wt % NaCl_{eq}) brines. Geochemical models and chemical analyses of modern brines have demonstrated that chloride is the primary ligand for the transport of metals. Despite the importance of high-salinity brines in the genesis of these ore deposits, the source(s) of dissolved salt (and water) in the brines is still not well understood. New data from a reconnaissance study of fluid inclusion solute compositions in ore minerals from the world's great sediment-hosted mining districts demonstrates that they formed, almost exclusively, from residual brine produced by the evaporation of seawater. This observation places significant geologic, geochemical, mass balance, and hydrologic constraints on genetic models for these tremendous hydrothermal systems.

Much of our current understanding about the generation and evolution of brines has come from geochemical and stable/radiogenic isotopic studies of brines in modern basins. These studies have identified two processes for generating high salinity basinal brines, both ultimately related to subaerial evaporation of seawater. Major solutes in basinal brines are derived from either 1) residual brine that infiltrated down into underlying sedimentary sequences during evaporation, or 2) dissolution of evaporite minerals (primarily halite) by infiltrating meteoric or marine water in the subsurface. A third proposed mechanism, membrane filtration, has not been demonstrated in natural environments and is probably untenable for large-scale production of highly saline brines. The seminal studies of Rittenhouse (1967), Carpenter (1978), and Hanor (1994) demonstrated the ability of brine solutes, such as Cl, Br, I, Na, K, Ca, Mg, SO₄, to discriminate between the two possible brine sources in modern basinal brines and to track the chemical evolution of brines in sedimentary basins.

Historically, the source for dissolved salts in ore fluids was primarily considered to be from the dissolution of evaporites in the flow path of meteoric/marine waters. The advent of fluid inclusion solute analysis and ion ratio plots to discriminate the source of salt and their application to MVT deposits changed this perception by demonstrating that the ores formed from residual brine derived from the evaporation of seawater (Kesler et al., 1995; Viets et al., 1996). Subsequent work has demonstrated that solute data from fluid inclusions in sphalerite from more than 20 MVT districts in North America, Europe, and northern Africa, show little, or no, evidence of halite dissolution.

Despite the absence of salt sequences in the inferred fluid path of sedex deposits, salt dissolution has dominated proposed genetic models. The new fluid inclusion solute data from seven sedex deposits (Century, McArthur River, Sullivan, Red Dog, Watson's Load, Silver King, and Rammelsberg) show that the primary source of salt in ore fluids was evaporated seawater. The data plot in the center of the compositional field for (MVT) basinal brines with ion ratios that indicate that the brines formed from evaporated seawater that attained halite saturation. The compositional similarity of fluids in sedex and MVT deposits confirms hypotheses that the two deposit types formed from brines of similar origin. Because neither deposit type provides evidence for halite dissolution as a primary source for the parent fluid, residual brines are appear fundamental to the genesis of basin-hosted Zn-Pb-Ag deposits.

In the case of sed Cu, the spatial association between deposits and large salt bodies has led to a dominance of salt-dissolution models. The new data on fluid inclusions in ore minerals from deposits in the Kupferschiefer, situated a few 10's of meters below the footwall of one of the great salt mining districts of the world, show no evidence of salt dissolution. Similarly, pre-orogenic Congolese *écaillé* deposits (Kolwezi, Kamoya, Kisanfu) and arenite-hosted deposits in the Zambian Copperbelt (Chibuluma West, Nchanga) plot close to the seawater evaporation curve with no direct evidence for the dissolution of salt.

The application of solute systematics developed in modern basins allow tracking the chemical evolution of ore-forming brines in basins through space and time. With the source of the brine constrained, the comparison of conservative elements like Br, and to some degree Cl, with other solutes can be used to evaluate the chemical evolution of brines. Changes in the relative proportions of non-conservative elements in fluid inclusions can be used to monitor water rock interactions, such as stoichiometric replacement of Mg by Ca (dolomitization), Na depletion in brine (abitization), etc. Mixing between, and changes of, brine sources can be recognized by changes in conservative solutes. Because conservative solutes provide a direct measure of the degree of evaporation and, thus, the salinity of the starting brine, the salinity measured in fluid inclusions can be used to determine the amount of dilution by other fluids. Moreover, the introduction of externally derived redox sensitive components like NH₄ and organic acids can be used to identify redox environments and monitor processes of ore deposition.

An exciting outcome of this work is the realization that once residual brines are generated they can influence the metallogenic evolution of sedimentary basins over 100's of millions of years. For example, the brine compositions of the syn/post orogenic Mount Isa copper deposit appears to be the same source as the brines that formed the great sedex deposits during early stages of the MacArthur Basin. Similarly, at least three very broad and individually diachronous mineralizing events are evident in the Central African Copperbelt that are coincident with diagenesis, Lufilian inversion and metamorphism, and post-metamorphic brittle deformation and vein emplacement that span at least 300 million years of basin history. It is only during the latest stages of this protracted basin history in post-metamorphic mineralization events (e.g. Kansanshi, Kipushi and Shinkolobwe deposits,) that evidence of salt dissolution is observed.

Taken together, the results of this reconnaissance study indicate that residual brine generated from the evaporation of ancient seawater was responsible for the formation of much of the world's base metal reserves. This work demonstrates the potential of fluid inclusion solute analysis to identify and map brine provinces, subsequent compositional modifications resulting from fluid-rock reactions and fluid mixing, mechanisms of ore deposition, and mass balance and fluid flow paths that, ultimately, provide crucial constraints on genetic models for basin-hosted ore deposits.

REFERENCE

- Carpenter, A. B., 1978, Origin and chemical evolution of brines sedimentary basins: Oklahoma Geological Survey Circular, v. 79, p. 60-77.
- Hanor, J. S., 1994, Origin of saline fluids in sedimentary basins, *in* Parnell, ed., *Geofluids; origin, migration and evolution of fluids in sedimentary basins*, 78, Geological Society Special Publications, p. 151-174.
- Kesler, S. E., Appold, M. S., Martini, A. M., Walter, L. M., Huston, T. J., and Kyle, J. R., 1995, Na-Cl-Br systematics of mineralizing brines in Mississippi Valley-type deposits: *Geology*, v. 23, p. 641–644.
- Rittenhouse, G., 1967, Bromide in oilfield waters and its use in determining possibilities of origins its waters: *American Association of Petroleum Geologists Bulletin* v. 51.
- Viets, J., Hofstra, A. H., and Emsbo, P., 1996, Solute composition of fluid inclusions in sphalerite from North America and European Mississippi Valley-Type ore deposits: ore fluid derived from evaporated seawater, *in* Sangster, D. F., ed., *Carbonate-Hosted Lead-Zinc Deposits*, SEG special Publication No. 4, p. 465-483.

Upper Cretaceous melt evolution in the eastern North China Craton: Evidence from clinopyroxene-hosted melt inclusions in mafic dikes

Hong-Rui Fan, Ya-Chun Cai, Fang-Fang Hu, Kui-Feng Yang

**Institute of Geology and Geophysics, Chinese Academy of Sciences, Beijing 100029, China*

Silicate melt inclusions (SMIs) in magmatic minerals provide key information on the chemical and mineralogical evolution of source magmas (Roedder, 1979). The widespread Cretaceous mafic dikes in the Jiaobei region of the eastern North China Craton (Cai et al., 2013) contain abundant SMIs within clinopyroxene phenocrysts. The daughter minerals in these SMIs include amphibole, plagioclase, pyrite and ilmenite, together with $\text{CO}_2 + \text{CH}_4$ and CH_4 as the major volatile phase (Fig. 1). The total homogenization temperatures of the SMIs range between 1280 and 1300 °C. The host clinopyroxene phenocrysts in these dolerite dikes are dominantly augite with minor diopside.

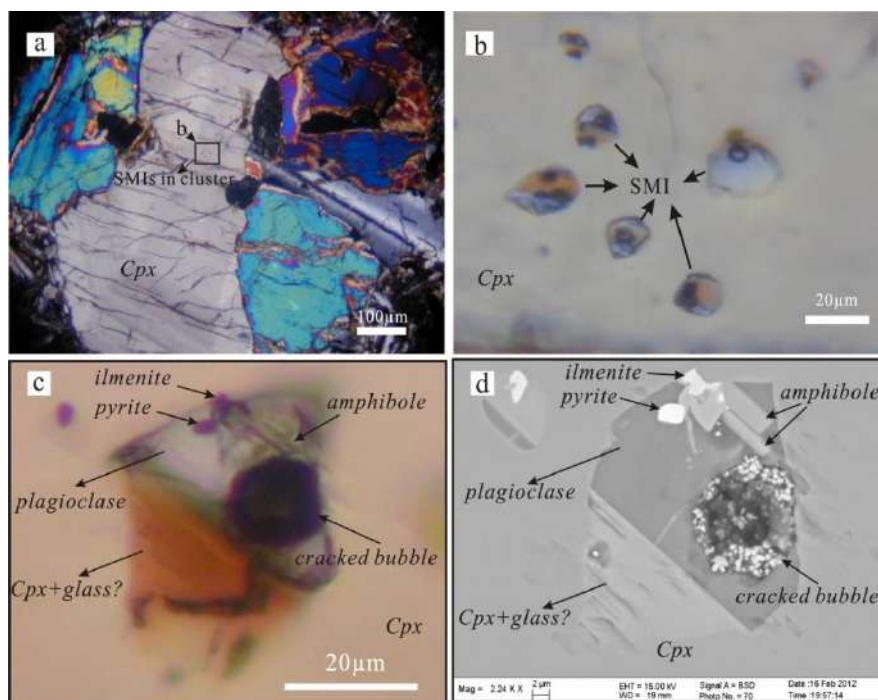


Fig 1. (a) SMIs in cluster hosted in clinopyroxene phenocryst; (b) Representative photomicrographs of multiphase crystallized SMIs in clinopyroxene.; (c) and (d) Photomicrograph and BSE images of representative polished SMI showing typical texture and daughter mineral phases in the SMIs.

From LA ICP-MS *in situ* analyses, two compositional groups of the SMIs are identified, low-MgO (6.0–7.6 wt. %) and high-MgO (11.2–13.9 wt. %) SMIs. The Low-MgO SMIs exhibit higher concentrations of TiO_2 , Al_2O_3 , Na_2O , P_2O_5 and lower CaO and $\text{CaO}/\text{Al}_2\text{O}_3$ ratio as compared to the high-MgO ones. The trace element patterns of the two types of SMIs are similar to those of the host mafic dikes. However, the low-MgO SMIs and host mafic dikes are clearly more enriched in all the trace elements as compared to the high-MgO type, especially with regard to the highly incompatible elements. The estimated capture temperatures and pressures are 1351–1400 °C and 16.2–21.0 kbar for the high-MgO SMIs and 1177–1215 °C and 5.5–10.9 kbar for the low-MgO type. The high-MgO and low-MgO SMIs were trapped at depths of ~51–68 km and ~20–35 km, respectively. Computations show that the parental melt is basic with SiO_2 content 49.6 wt % and Mg# 80.0 with relatively low total alkali contents (1.35 wt % $\text{Na}_2\text{O} + \text{K}_2\text{O}$) and high CaO (15.2 wt %) (Table 1).

Table 1. Composition estimations for the parental melt of dolerite dikes from the Jiaobei area

	Primitive melt	Fe ₂ O ₃ /FeO calculated	Cpx(core) with Mg# 81.8	Ol with Fo 82.1	30 wt. % Cpx and 12 wt. % Ol added
SiO ₂	50.30	50.30	52.15	39.54	49.62
TiO ₂	1.38	1.38	0.75	0.06	1.03
Al ₂ O ₃	6.85	6.85	3.20	0.06	4.92
Fe ₂ O ₃		2.22			1.28
FeO	9.19	7.20	6.31	16.16	8.06
MnO	0.19	0.19	0.15	0.20	0.18
MgO	14.06	14.06	15.88	41.70	18.07
CaO	15.76	15.76	20.29	0.27	15.23
Na ₂ O	1.57	1.57	0.46	0.32	1.08
K ₂ O	0.45	0.45		0.11	0.27
P ₂ O ₅	0.23	0.23			0.13
Cr ₂ O ₃			0.52	0.03	0.16
SUM	100.0	100.2	99.7	98.71	100.1
Mg#	73.2	77.7	81.8	82.1	80.0
CaO/Al ₂ O ₃	2.3	2.3	6.3	4.3	3.1

Major elements in wt %

Exploratory runs with the program MELTS (for pressures < 10 kbar) and pMELTS (pressures 10–20 kbar) (Ghiorso et al., 2002) show that the low-MgO and high-MgO SMLs were derived from the same parental melt through different degrees of crystallization. Clinopyroxene and a small amount of olivine were the fractionating phases during the evolution from parental melts to low MgO melts, while the low MgO melts experienced significant fractional crystallization of olivine and clinopyroxene. We postulate the newly accreted lithospheric clinopyroxenite as the major source for the Jiaobei dolerite dikes, with melting of the source at a depth of ~68–80 km.

ACKNOWLEDGEMENT

This study was financially supported by the Natural Science Foundation of China (41173056).

REFERENCES

- Cai YC, Fan HR, Santosh M, Liu X, Hu FF, Yang KF, Lan TG, Yang YH, Liu YS. (2013) Evolution of the lithospheric mantle beneath the southeastern North China Craton: Constraints from mafic dikes in the Jiaobei terrain. *Gondwana Research*. 24. 601-621.
- Ghiorso MS, Hirschmann MM, Reiners PW, Kress VC. (2002) The pMELTS: a revision of MELTS for improved calculation of phase relations and major element partitioning related to partial melting of the mantle to 3 GPa. *Geochemistry, Geophysics, Geosystems*. 3. doi:10.1029/2001GC000217.
- Roedder E. (1984) Fluid inclusions. *Review in Mineralogy*. 12. 1-644.

Magmatic Steam Alunite Veins: The Epithermal Expression of UST Layers in Porphyry Intrusions?

Hofstra, A.H., Landis, G.P. and Rye, R.O.

Denver Inclusion Analysis Laboratory, USGS, Denver, CO 80225, USA, ahofstra@usgs.gov

Magmatic steam alunite (MSA) veins form in the epithermal environment from the episodic release of steam from underlying intrusions (Rye et al. 1992). Unidirectional solidification texture (UST) layers comprised of alternating comb α -quartz and aplite at the tops of porphyry intrusions form from the repeated buildup and discharge of exsolved fluid from the interface between quenched and molten magma (Lowenstern & Sinclair, 1996). The common settings, ages, scale, cyclicity, and geochemistry of UST layers and coarse banded MSA veins suggest they may be genetically related to one another. Melt and fluid inclusion and stable isotopic evidence from the Henderson Climax-type Mo porphyry deposit in Colorado and the Alunite Ridge vein deposit in Utah support this interpretation. Although they differ in age (~28 and ~14 Ma), both are associated with bimodal basalt-rhyolite magmatism in a continental rift setting. Alunite Ridge is underlain (~2km) by a Pb-Zn-Ag-Au-Cu manto deposit enriched in Mo and F (Deer Trail; Beaty et al., 1986) that is presumed to emanate from a Mo porphyry.

At Henderson, the composition of phenocrysts and melt inclusions in the 27.6 Ma Hideaway Park tuff indicate parental rhyolite magmas were relatively reduced such that exsolved volatiles at 100 MPa are modeled to contain $\text{H}_2\text{O} > \text{CH}_4 > \text{CO}_2 > \text{H}_2\text{S} > \text{H}_2 > \text{CO} > \text{SO}_2$ (Mercer, et al., 2014). UST layers and vein dikes are well developed and some connect to quartz \pm Mo veins (Carten et al., 1988a). The H-isotope composition of igneous and vein biotite and fluid inclusion water extracted from quartz are indicative of open system magma degassing and condensation of brine from vapor (Carten et al., 1988b; Newton and Hofstra, 2014). The range of homogenization T (550-200°C) and P (75-1 MPa) in hypersaline inclusions trapped at ~3km depth allow that they were trapped during transitions from lithostatic to vaporstatic conditions as volatiles discharged to the paleosurface (Carten et al., 1988a; Seedorff, 1987; Newton and Hofstra, 2014). The high enthalpy and $f\text{H}_2$ of fluid discharged from UST layers may promote quenching of melt against comb quartz and increase the oxidation state of volatile-depleted melt and condensed brine. Such oxidation may be indicated by hematite daughter minerals in hypersaline inclusions.

At Alunite Ridge, no coeval intrusions are exposed, but the isotopic compositions of He, Ne, and Ar in fluid inclusion extracts from early bladed calcite and drusy quartz veins and later MSA veins with trace hematite provide constraints on the nature of concealed intrusions. Calcite and quartz have high He R/Ra (0.3-30) that require a juvenile mantle source, such as basalt. MSA bands have low He R/Ra (0.004-0.3) indicative of a crustal source, such as rhyolite produced by country rock assimilation and fractional crystallization. The lowest R/Ra (0.004) and $^{20}\text{Ne}/^{22}\text{Ne}$ (7) and the highest $^{38}\text{Ar}/^{36}\text{Ar}$ (0.9) provide evidence for production of ^4He , ^{22}Ne , and ^{38}Ar from U decay in a F- and K-bearing source, such as a highly fractionated rhyolite intrusion. The abundance of K in alunite and its H and O isotopes indicate fluids ($\delta\text{D}_{\text{H}_2\text{O}}$ -78 to -55‰, $\delta^{18}\text{O}_{\text{H}_2\text{O}}$ 2.3 to 10.6‰) were derived from potassic melts. Vapor-rich inclusions in the coarse banded MSA veins are comprised of $\text{H}_2\text{O} > \text{CH}_4 > \text{H}_2 > \text{CO}_2$ with trace H_2S and SO_2 . Gas geothermometry and calculated $f\text{O}_2$ values plot along the projection of QFM from 700 to 200°C with a mode at 280°C. Although the high T's may be spurious, corresponding $f\text{O}_2$ values are indicative of reduced magma, as at Henderson. The mode is at the high end of $\Delta^{34}\text{S}_{\text{sph-gal}}$ temperatures (235-280°C) and Th (160-300°C) of liquid-rich inclusions in the underlying Deer Trail deposit (Beaty et al., 1986). Complete conversion of sulfide to sulfate in the ascending magmatic vapor plume is indicated by the calculated isotopic composition of H_2S (-1‰) in

equilibrium with sulphide minerals in deep polymetallic mineralization (Beatty et al., 1987) and the composition of sulfate (-1 to 2%) in shallow alunite veins.

Chemical models show that conversion of sulfide to sulfate can be accomplished by decompression of magmatic fluid from lithostatic to vaporstatic conditions, which also happens to increase the proportion of K_2SO_4 and CH_4 in the vapor. Precipitation of alunite and hematite from such vapors and their condensates generates H_2 . Discharge of H_2 from fumaroles at the surface drives precipitation of alunite and hematite in underlying fractures. These relationships explain the apparent paradox of reduced gas species (CH_4 and H_2) in oxidized minerals [$KAl_3(SO_4)_2(OH)_6$, Fe_2O_3]. Mass balance calculations based on the concentration of K in exsolved magmatic fluid and K in alunite allow that each alunite band in the veins could have formed from a 1-10 cm thick fluid layer, 10 to 100 m in diameter, in underlying magma chambers, which is similar to the scale of UST layers in porphyry intrusions. Vaporstatic conditions are more likely to form above shallow cupolas hosted in relatively impermeable host rocks where dilatant fractures allow transient jets of magmatic vapor to ascend to the surface with minimal dilution by local ground water. MSA veins are unlikely to form in vapor-dominated reservoirs below hydrostatically pressured caps, rather replacement magmatic hydrothermal alunite with trace pyrite will form.

If UST layers and MSA veins are the deep and shallow products of fluid discharged from porphyry intrusions, then the age, isotopic, and chemical composition of MSA veins may provide valuable insights into the age and nature of their source intrusions and the potential for concealed porphyry deposits. This conclusion is supported by the high F-content (1.9 wt. %) of MSA veins associated with Mo porphyries in the Questa district of New Mexico and the anomalous concentrations of hematite, Au, As, Bi, and Pb in MSA veins at Tambo, Chile (Bove et al., 2009).

REFERENCES

- Bove, D.J., Hofstra, A.H., Koenig, A.E., Lowers, H.A., Rye, R. O. (2009) Chemical compositions of magmatic steam alunite veins. *GSA Abstracts with Programs* v. 41. no. 7. 525.
- Beatty, D.W. and others (1986) Geology and geochemistry of the Deer Trail Pb-Zn-Ag-Au-Cu manto deposits, Marysville District, west-central Utah. *Economic Geology*. 81. 1932-1952
- Carten, R.B., Geraghty, E.P., Walker, B.M., and Shannon, J.R. (1988a) Cyclic development of igneous features and their relationship to high-temperature hydrothermal features in the Henderson Porphyry Molybdenum deposit. Colorado. *Economic Geology*. 83. 266–296.
- Carten, R.B., Rye, R.O., and Landis, G.P. (1988b) Effects of igneous and hydrothermal processes on the composition of ore-forming fluids; stable isotope and fluid inclusion evidence, Henderson porphyry molybdenum deposit, Colorado. *GSA Abstracts with Programs*. 19. A94.
- Lowenstern, J.B. and Sinclair, W.D. (1996) Exsolved magmatic fluid and its role in the formation of comb-layered quartz at the Cretaceous Logtung W-Mo deposit, Yukon Territory, Canada. *Transactions of the Royal Society of Edinburgh*. 87. 291-303.
- Mercer, C.N. and others (2014) Pre-Eruptive Conditions of the Hideaway Park Topaz Rhyolite, Colorado: PACROFI-XII.
- Newton, M.N. and Hofstra, A.H (2014) Fluid inclusion & stable isotopic evidence for extreme degassing of melt & condensation of brine in the Henderson porphyry Mo deposit. PACROFI-XII.
- Rye, R.O.; Bethke, P.M.; Wasserman, M.D. (1992) The stable isotope geochemistry of acid sulfate alteration. *Economic Geology*. 87. 225-262.
- Seedorff, C.E. (1987) Henderson porphyry molybdenum deposit: Cyclic alteration-mineralization and geochemical evolution of topaz- and magnetite-bearing assemblages. Ph.D. dissertation, Stanford University, Stanford, CA, 432.

Fluid inclusion petrography, microthermometry, and geobiology in modern gypsum from acid saline Salar Ignorado, northern Chile

Karmanocky, F.J. and Benison, K.C.*

*West Virginia University, Department of Geology and Geography

Acid Salar Ignorado in the Andes Mountains of Chile precipitates gypsum crystals with abundant primary fluid inclusions. At 4200 m elevation, this salar is situated in a small intervolcanic basin at the southern edge of the Cerro Bayo volcanic complex; local magmatic inflation is ~2.5 cm/year (Froger et al., 2007). This environment is extreme with high winds, large dust devils, high solar radiation, and acid saline waters. During field investigations in the late austral summer, temperature ranged from 1°C to 25°C (Benison and Gonzalez, 2007). Barometric pressures are calculated at 0.58 atm to 0.61 atm, respectively. Salar Ignorado contains shallow pools located in depressions on the wind-scalloped salar. Waters have a pH of 3.3–4.6, salinities of 4.05 to 97.4 ppt TDS, and are rich in SO₄-Al-Cl-Na-K with lesser amounts of Si-Mg-B (listed by relative abundance; Risacher et al., 2002). Acid saline waters here precipitate gypsum, native sulfur, and halite, and groundwaters precipitate alunite, jarosite, hematite, and kaolinite.

Primary fluid inclusions in gypsum from this unusual and extreme environment provide the opportunity to trace water chemistry, environmental conditions, and life in an acid saline volcanic setting. Here we present preliminary results of fluid inclusion characterization of gypsum from Salar Ignorado, using petrography, microthermometry, and laser Raman spectroscopy,

There are two primary growth morphologies of the modern gypsum precipitating in Salar Ignorado. Mounds of needle-shaped crystals were collected from below the air-water interface in the salar pools, and 'stock-work' masses of gypsum crystals were collected from the salar surface. The crystals of the 'stock-work' masses likely precipitated as bottom growth gypsum; however, subsequent reworking by the wind is evident due to abrasions on the gypsum crystals and their discordant arrangement.

Primary fluid inclusions form in rows along prior crystal faces that are parallel to the direction of growth. Three types of primary FIAs have been identified: **Type I** – ~2 to 15 µm long and are negative crystal to sub-horn shaped, highly variable L-V ratio; **Type II** – ~50 to 200 µm long and are triangular shaped, highly variable L-V ratio; and **Type III** – ~20 to 60 µm long and horn shaped, consistently all liquid. Microorganisms and organic compounds have been observed in fluid inclusions from all three types of primary FIAs. Optical petrography of primary FIAs has been used to differentiate between eukaryotes, prokaryotes, and organic compounds.

Diatoms are trapped as clusters in primary fluid inclusions and solid inclusions (Fig. 1A). Clusters contain either (1) pristine diatoms, suggesting entrapment of live diatoms; or (2) abundant broken diatoms, indicating abrasion during wind transport and physical deposition in salar pools prior to entrapment by the growing gypsum (Fig. 1C). Discrete parts of pristine diatoms, likely their chloroplasts, fluoresce blue when exposed to UV-vis light (Fig. 1B).

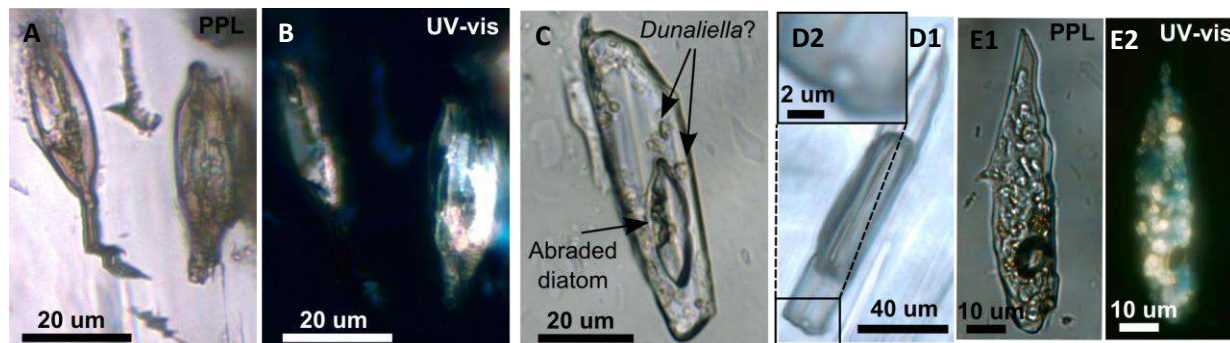


Figure 1. Microorganisms in primary fluid inclusions from modern Salar Ignorado gypsum (see text for details)

Suspect green algae are abundant in Salar Ignorado gypsum (Fig. 1C, 1E1; Fig. 2A). They appear as pale yellow and pale orange dimpled spheres and ovoids that fluoresce blue (Fig. 1E2), range in size from ~3-10 μm , and are observed both as solid inclusions and in fluid inclusions. Multiple spheres and ovoids, likely *Dunaliella* alga, are typically found together, with as many as ~20 in some individual primary fluid inclusions.

Prokaryotes are observed both as solid inclusions and within some fluid inclusions (Fig. 1D1, 2A). They appear as clear, high relief, 1-2 μm diameter spheres and pale yellow-clear (Fig. 1D2), high relief, 4-5 μm long rods. All fluoresce pale green when exposed to UV-vis light. Some of these coccoid and bacilli-shaped cells are likely bacteria and/or archaea.

Some primary fluid inclusions contain 1-3 μm spherical solids (Fig. 2B). These are typically clear, but in some cases have a green hue in transmitted light and can be a bright blue in UV light. They collect in lineations or in clusters. Preliminary laser Raman spectroscopy with 532 nm excitation shows that these spherical solids are high molecular weight, alkane-rich hydrocarbons.

Preliminary freezing-melting behavior of primary fluid inclusions in modern Salar Ignorado gypsum includes: T_{eu} from -60 to -28°C, a small, <1 μm , high relief solid phase that is present in some inclusions from -23 to -9 °C (possibly hydrohalite?), and T_{mice} from -4.3 to -0.2°C. Typically the liquid between the solid phases has a green hue from -25 to -6°C.

Large bubbles in many primary fluid inclusions do not behave as water vapor during microthermometry. When exposed to the atmosphere by crushing, a sulfuric odor is emitted, suggesting the possibility that these are H_2S bubbles.

Further characterization of fluid inclusions in gypsum from this extreme environment may provide a better understanding of acid saline fluids in volcanic settings. These fluids may be considered a type of ore fluid due to their extremely high sulphur and aluminium content. In addition, the geology and geochemistry of Salar Ignorado is an excellent analog for martian environments, informing us about the fossilization styles of possible life on Mars.

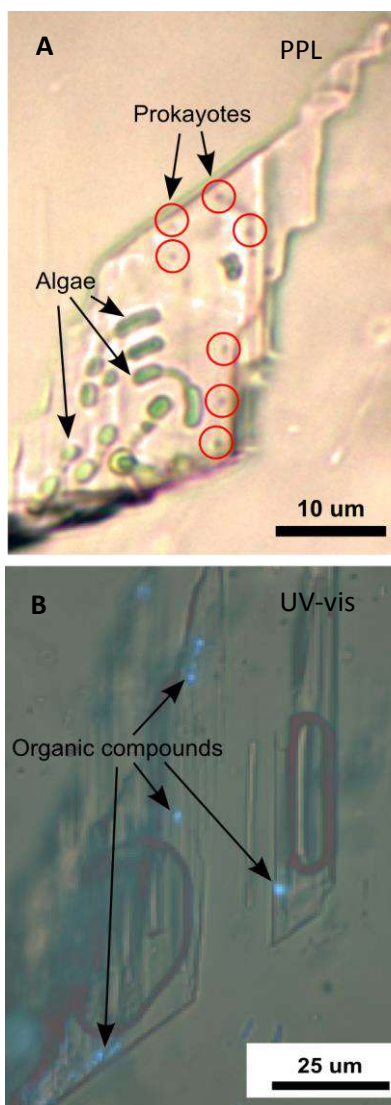


Figure 2. (A) Microorganisms and (B) organic compounds in modern Salar Ignorado gypsum (see text for details)

REFERENCES

- Benison, K.C. and Gonzalez, M.M. (2007) Sedimentology of two acid saline lakes in the high Andes of northern Chile. Geological Society of America Annual Meeting, 39. 433.
- Froger, J.L., Remy, D., Bonvalot, S., and Legrand, D. (2007) Two scales of inflation at Lastarria-Cordon del Azufre volcanic complex, central Andes, revealed from ASAR-ENVISAT interferometric data. Earth and Planetary Science Letters. 255. 148-163.
- Risacher, F., Alonso, H., and Salazar, C. (2002) Hydrochemistry of two adjacent acid saline lakes in the Andes of northern Chile. Chemical Geology. 187. 39-57.

Halogens and noble gases in fluid inclusions from sediment-hosted ore deposits and deeper metamorphic settings

Kendrick M.A.

Research School of Earth Sciences, Australian National University, Canberra, ACT 0200, Australia.
School of Earth Sciences, University of Melbourne, VIC 3010, Australia

The halogens and noble gases provide powerful markers for tracing the sources of volatiles trapped in fluid inclusions, and a direct means for investigating a fluids acquisition of salinity (Böhlke and Irwin, 1992). Combined halogen and noble gas methodologies can be applied to investigate any fluid process fossilised in fluid inclusions. However, the origin of halogens in ore forming fluids has been of special interest because of chlorines essential role as a ligand for efficient metal transport in solution. The halogens (Cl, Br and I) can be measured simultaneously with naturally occurring isotopes of Ar, Kr and Xe in irradiated samples using noble gas methodologies (Kendrick, 2012). Here I present an overview of this technique and recent applications to fluid inclusion studies (see Kendrick and Burnard, 2013 for a comprehensive review).

Chlorine is unique among the halogens and noble gases in that it can be a major component within crustal fluids. The other halogens and noble gases are trace constituents with ppm to ppb abundances, but because their transport is coupled to that of major volatiles they provide important information about the sources and reactions of H₂O and CO₂ in the crust. The heavy halogens (Cl, Br and I) have high solubilities in aqueous fluids, and because they are fractionated by only a small number of processes (e.g. seawater evaporation and biological processes at Earth's surface) they have characteristic abundance ratios (Br/Cl and I/Cl) in different geological reservoirs. The noble gases are

chemically inert tracers with isotopic signatures that vary by orders of magnitude between crustal, mantle and surface reservoirs (Table 1). Mass fractionation contributes negligible variation to noble gas isotope ratios (e.g. ⁴⁰Ar/³⁶Ar, ³He/⁴He), but alters elemental abundance ratios (e.g. ⁴He/⁴⁰Ar) during various processes related to diffusion or solubility.

Early applications of halogens and noble gases to fluid inclusions focused on relatively shallow ore forming environments and because of the low concentrations of these elements in silicate minerals it was often assumed that they are not strongly altered by fluid-rock interaction. Recent work shows that organic matter exerts a significant influence on Br, as well as I, in many geological settings (Fig 1).

Table 1. Noble gases in the Earth

	Mantle	Crust	Surface
³ He/ ⁴ He	8 Ra	0.05 Ra	1 Ra
²⁰ Ne/ ²² Ne	12.5	<9.8	9.8
⁴⁰ Ar/ ³⁶ Ar	>10,000	>300	296

Ra = atmospheric ³He/⁴He ratio of 1.4×10⁻⁶

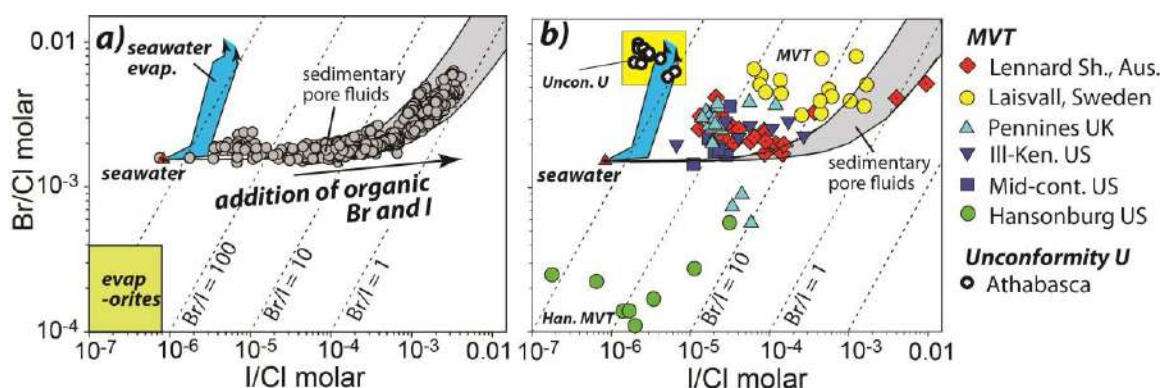


Fig 1. Log-log Br/Cl and I/Cl plots showing sedimentary fluids. a) sedimentary marine pore fluids define a linear array with seawater corrected Br/I of ~1 (it appears curved in log space). b) Most MVT plot between the seawater evaporation trajectory and sedimentary pore fluids. In contrast, unconformity U deposits lie over the seawater evaporation trajectory (see Böhlke and Irwin, 1992; Kendrick et al., 2011a; Richard et al., 2014).

The high salinity of Mississippi Valley type ore fluids (~25-30 wt % salts) coupled with their generally high Br/Cl ratios (Fig 1b), provides evidence for the involvement of evaporated seawater, but a significant part of their Br enrichment is derived from organic matter (Fig 1b; Kendrick et al., 2011a). In contrast, U-rich fluid inclusions (30-35 wt % salts) associated with Athabasca unconformity U deposits lie on the seawater evaporation trajectory (Fig 1b; Richard et al., 2014). Fluid inclusions from both deposit types have low $^{40}\text{Ar}/^{36}\text{Ar}$ ratios of <1000 that are consistent with seawater evaporation as a major source of high salinity fluids in sedimentary basins. However, while the iodine enrichment of MVT fluids is consistent with fluid interaction with organic-rich rocks or gases as a cause of sulphide precipitation, the lack of an iodine enrichment in Athabasca U-deposits does not favour models in which organic matter acted as a reductant for localising U ores (Richard et al. 2014).

Halogens are mobilised during metamorphism meaning organic Br and I are also enriched in some deeper deposits such as greenschist facies orogenic gold deposits (Fig 2). Interpretation of halogens in Victorian gold deposit fluid inclusions (Australia) is analogous to C isotopes because components derived from both altered volcanic rocks (AOC) and organic-rich shale can be recognised (Fig 2; Fu et al., 2012).

Recent work on iron-oxide-copper-gold deposits in the greenschist-amphibolite facies Mt Isa Inlier of Australia has shown CO_2 -rich magmatic fluids have high concentrations of radiogenic noble gases (e.g. ^{40}Ar , ^{21}Ne , ^{134}Xe) and mantle-like Br/Cl and I/Cl ratios (Kendrick et al., 2011b). The high $^{40}\text{Ar}/^{36}\text{Ar}$ of ~30,000 in the magmatic fluid end-member is consistent with these fluids being sourced

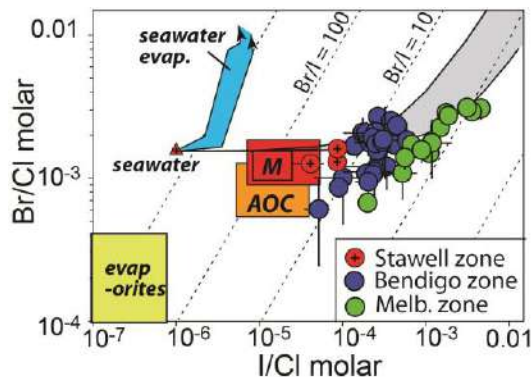


Fig 2. Log-log Br/Cl versus I/Cl plots showing data for Victorian orogenic gold deposits, Aus (Fu et al., 2012). M = mantle; AOC = Altered volcanics (Altered Ocean Crust).

from basement-derived A-type granites. However, the magmatic fluids have been variably overprinted by fluids with $^{40}\text{Ar}/^{36}\text{Ar}$ of 1000 and low Br/Cl and I/Cl ratios similar to those expected in sedimentary formation waters that dissolved evaporites. The data can be explained by mixing magmatic fluids with either sedimentary formation waters or metamorphic fluids derived from the calcsilicate host rocks. In this case there is no evidence for organic I or Br contributions but both the noble gas and halogens signatures have been influenced by various fluid-rock interactions (Kendrick et al., 2011b).

REFERENCES

- Böhlke, J.K., Irwin, J.J., (1992) Brine History Indicated by Argon, Krypton, Chlorine, Bromine and Iodine Analyses of Fluid Inclusions from the Mississippi Valley Type Lead-Fluorite-Barite Deposits at Hansonburg, New-Mexico. *Earth and Planetary Science Letters* 110, 51-66.
- Fu, B., Kendrick, M.A., Fairmaid, A.M., Phillips, D., Wilson, C.J.L., Mernagh, T.P., (2012) New Constraints on Fluid Sources in Orogenic Gold Deposits, Victoria, Australia. *Contributions to Mineralogy and Petrology* 163, 427-447.
- Kendrick, M.A., Burnard, P., (2013) Noble gases and halogens in fluid inclusions: A journey through the Earth's crust, in: Burnard, P. (Ed.), *The Noble Gases as Geochemical Tracers*. Springer-Verlag, Berlin, pp. 319-369.
- Kendrick, M.A., Phillips, D., Wallace, M., Miller, J.M., (2011a) Halogens and noble gases in sedimentary formation waters and Zn-Pb deposits: A case study from the Lennard Shelf, Australia. *Applied Geochemistry* 26, 2089-2100.
- Kendrick, M.A., Honda, M., Oliver, N.H.S., Phillips, D., (2011b). The noble gas systematics of late-orogenic H_2O - CO_2 fluids, Mt Isa, Australia. *Geochimica et Cosmochimica Acta* 75, 1428-1450.
- Richard, A., Kendrick, M.A., Cathelineau, M., (2014) Noble gases (Ar, Kr, Xe) and halogens (Cl, Br, I) in fluid inclusions from the Athabasca Basin (Canada): Implications for unconformity-related U deposits. *Precambrian Research* in press.

Anomalous physical and thermodynamic properties of H₂O-NaCl fluids in the critical region

Klyukin, Yu.I*, Driesner, T.**, Lowell R.P.*, Bodnar R.J.*

*Virginia Tech, Blacksburg, VA 24061, USA (correspondence: yury84@vt.edu)

**IGP, ETH, Zurich, 8092 Switzerland

Mass and energy transfer in hydrothermal systems is controlled by the physical (density) and thermodynamic (enthalpy or heat capacity) properties of the fluid. As such, changes in any of these properties affect the ability of the fluid to transport mass and energy in hydrothermal systems. Johnson and Norton [1] documented that pure H₂O shows large variations in most physical and thermodynamic properties with small changes in temperature (T) and/or pressure (P) in a PT region along the critical isochore (critical wedge). This region is bounded at lower and higher pressures by the 0.2 and 0.42 g/cm³ isochores, and extends from near the critical temperature to approximately 420 °C. While the large temperature and pressure derivatives of the physical and thermodynamic properties of pure H₂O have been well documented, it is not clear if the “critical wedge” migrates to higher temperatures and pressures as the critical temperature and pressure increase as salt and/or gases are added to pure H₂O. In this study, we used the SoWat model [2] to estimate the properties of H₂O-NaCl in the vicinity of the critical point for compositions ranging from 0 to 30 wt. % NaCl. The SoWat model allows the density, specific enthalpy, specific heat capacity and molar volume of fluid to be calculated at any given salinity and PT.

The relative change in density (or volume) of a fluid as a function of T at constant P is defined by the coefficient of thermal expansion, α . Along the critical isochore for pure H₂O, α approaches infinity at the critical point and shows large variation with small changes in P or T near the critical point. Our results show that addition of NaCl to H₂O causes the critical wedge to migrate to higher PT conditions as the critical point migrates to higher P and T, as shown for a 15 wt. % H₂O-NaCl composition in Fig. 1. Compared to H₂O, the critical wedge for H₂O-NaCl compositions is asymmetrical because the wedge is truncated on the high T, low P side by the two-phase (liquid+vapor) region. The region of anomalous fluid properties is stretched from the critical point of H₂O along the two phase boundary towards the critical isochore for a given salinity. Our results suggest that the PT region in which enhanced mass and energy transport occurs in hydrothermal systems is significantly influenced by the fluid composition, as suggested by [3]. Our model shows that the magnitude of α shows an inverse dependence on salinity in the critical region, which is in agreement with [4].

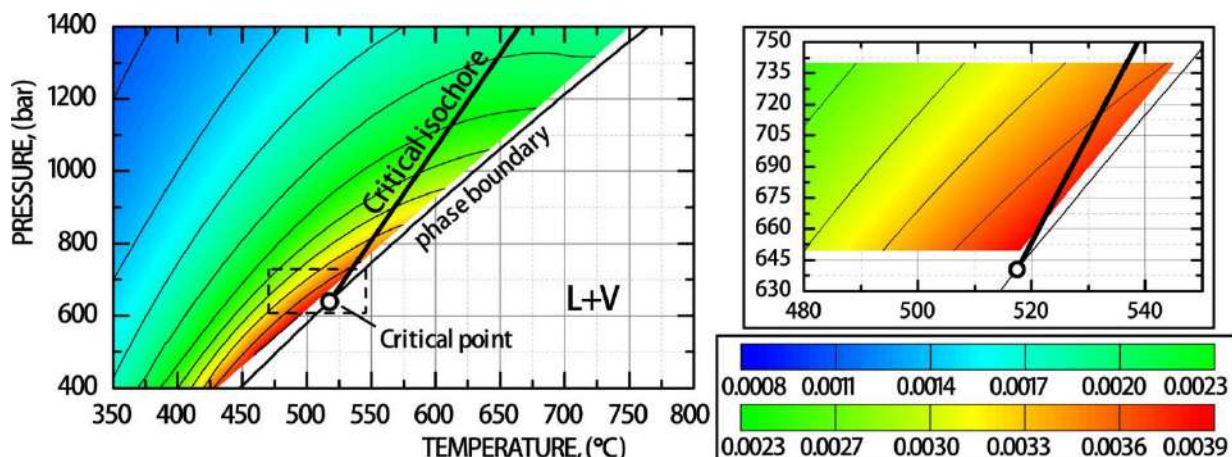


Figure 1: The coefficient of thermal expansion, α , (°C⁻¹) for 15 wt.% H₂O-NaCl, in the region from 350 to 750°C and from 400 to 1400 bar. Inset shows α in the area near the critical point.

The enthalpy, H, of a fluid represents the amount of thermal energy the fluid can transport during fluid migration. The specific heat capacity, C_p , represents the partial derivative of fluid enthalpy with respect to temperature at constant pressure. Thus, variations in the magnitude of the specific heat capacity reflect

variations in the ability of the fluid to transport thermal energy. The distribution of C_p in the vicinity of the critical point varies in a manner similar to the coefficient of thermal expansion: it achieves a maximum value at the critical point, and values of the C_p are highest along the critical isochore. In the H_2O -NaCl system, the magnitude of C_p decreases with increasing salinity, and maximum values of C_p occur along the one-phase/two-phase boundary between the critical point of water and the critical point for a given salinity (Fig. 2).

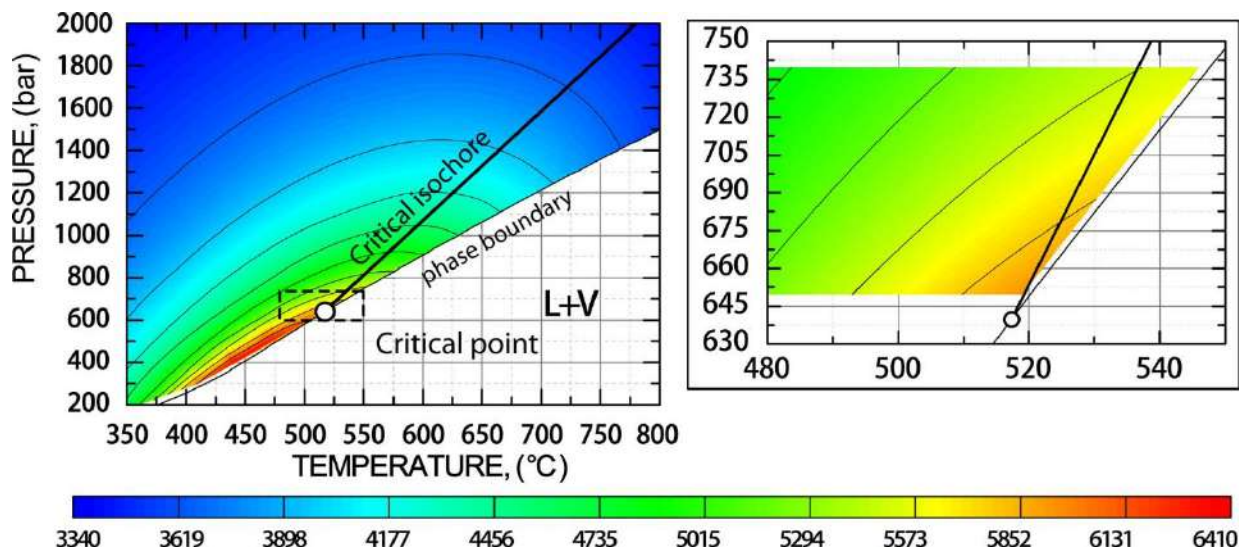


Figure 2: The specific heat capacity, C_p , ($J \cdot kg^{-1} \cdot K^{-1}$) for 15 wt.% NaCl in the region from 350 to 800°C and from 200 to 2000 bar. Inset shows C_p in the area near the critical point.

Quartz is one of the most abundant minerals that form during hydrothermal processes. Model of [5] allow us to estimate solubility of SiO_2 in the fluid for H_2O -salt- CO_2 system, based on this equation:

$$\log m_{SiO_2} = A(T) + B(T) \cdot \log \frac{M_{H_2O}}{V_{H_2O}^*} + 2 \log x_{H_2O}$$

Where $A(T)$ and $B(T)$ are polynomials from [6] equation for quartz solubility in the pure water, x_{H_2O} and $V_{H_2O}^*$ are the mole fraction and effective partial molar volume of H_2O in the fluid, respectively. The value $V_{H_2O}^*$ is calculated from the relation $V_{mix} = x_{H_2O} V_{H_2O}^* + (1 - x_{H_2O}) V_s$, where V_{mix} is the molar volume of fluid mixture and V_s intrinsic volume of the NaCl.

According to the equation above, quartz solubility is a function of fluid density (molar volume). In our calculation the coefficient of thermal expansion α , represents the change in molar volume with respect to T at constant P . Hence, high values α denote large changes in the fluid molar volume over small ranges in P or T . Thus, in regions where α changes by a large amount with a small change in temperature, the solubility of quartz will likewise show large variation with a small change in temperature. This, in turn, could lead to significant quartz dissolution or deposition within the block of rock where the temperature is changing.

Because the magnitude of the physical and thermodynamic properties described above shows an inverse dependence on salinity in the critical region, and that with increasing salinity the region of anomalous behaviour is stretched from the critical point of water to the critical point of the fluid system for a given salinity, we infer that the region of anomalous mass and energy transport will be similarly stretched to higher temperatures and pressures as salt is added to pure H_2O .

REFERENCES

- [1] Johnson & Norton (1991) *Am. J. Sci.* 291, 541-648. [2] Dreisner (2007) *Geochim. Cosmochim. Ac.* 71, 4902-4919. [3] Bodnar & Costain (1991) *Geop. Res. Lett.* 18, 983-986. [4] Pitzer (1986) *J. Phys. Chem.*, 90, 1502-1504 [5] Akinfiev & Diamond (2009) *Geochim. Cosmochim. Ac.* 73, 1597-1608. [6] Manning (1994) *Geochim. Cosmochim. Ac.* 58, 2811-4839

Evaporate Mound Chemistry: An Effective but Under-utilized Method to Document the Nature and Origin of fluids in Hydrothermal Ore- deposit Settings

Kontak, D.J.

Department of Earth Sciences, Laurentian University, 935 Ramsey Lake Road, Sudbury Ontario, Canada,
P3E 2C6, dkonak@laurentian.ca

The bulk chemistry of fluids implicated in a large range of hydrothermal systems, from high -T magmatic to low-T diagenetic, is constrained in part from the measurement of the ice melting temperature ($T_{m_{ice}}$) in previously frozen fluid inclusions or dissolution temperature of halides (Roedder 1984; Bodnar 2003). Given that Na is generally the most common cation in a large range of fluids (i.e., hydrothermal, metamorphic, diagenetic), the NaCl-H₂O binary is used to infer the concentration of dissolved salts, expressed as equivalent wt. % NaCl. This assumption is, however, known to be an over simplification for natural samples based on the observed depression of the NaCl-H₂O eutectic (i.e., <-21.2°C) due to presence of divalent cations (e.g., Ca, Fe, Mg; Crawford 1981) and direct measurement of the solute chemistry using, for example, leachate (Gleeson 2003) and *in situ* LA ICP-MS analyses (Heinrich et al. 1999). Another method which can provide insight into the composition of the fluid, including both the cations (Na, K, Ca, Fe, Mn) and anions (Cl, F, S), is the decrepitate or evaporate mound method, first explored by Edington (1974) and examined more quantitatively by Haynes et al. (1988). Despite its potential application in a wide variety of relevant geological settings, the method has not become incorporated as a routine part of fluid inclusion studies despite the ease to generate meaningful and quantifiable information. In an earlier attempt to effort to promote the use of this method, I presented a summary of work on a variety of settings at the PACROFI VIII meeting, summarized in the subsequent proceedings (Kontak 2004). Continued work in a wide variety of hydrothermal settings over the past decade has only reinforced the application of this method. Examples of representative mounds, presented as back-scattered electron (BSE) images from a scanning electron microscope (SEM), for a variety of hydrothermal settings are shown in Figure 1. Of particular note is the variety of shapes, which often reflects different bulk compositions, as noted earlier by Haynes et al. (1988), and the large range in the abundances of cations, including Na, K, Ca, Fe, Mn, Ba, Sr, and anions, which in addition to Cl also includes S and F which are not easily detected with other methods.

In this presentation the protocol used in such studies will be addressed, including the short-comings of the method, such as fractionation of the fluid and elemental decoupling (e.g., Na and K) during the decrepitation procedure, and how to overcome these problems. However, the emphasis will be placed on the successful application of the method to help elucidate the fluid evolution in a wide variety of mineralized settings, including porphyry Cu, magmatic Sn-W, evolved LCT pegmatites, carbonatites, orogenic- and intrusion-related gold, and carbonate replacement (i.e., MVT) deposits. The results of this work indicate that the following important aspects, all of which are important for understanding hydrothermal ore systems, are revealed by the use of this method: (1) Although Na is the most common cation, other solutes (Ca, K, Fe, Ba, Sr) occur depending on the setting and are important as sensitive indicators of processes such as fluid mixing and wall-rock contamination; (2) As noted before (Kontak 2004), Fe and Mn are most common in mineralized magmatic settings (e.g., porphyry and Sn-Cu); (3) Barium and Sr are most enriched in carbonatitic samples; (4) Solute chemistry is a good monitor of F:R interaction of either the host or the wall-rock environment; (5) Sulfur is common in samples from most mineralized settings, but its abundance can vary considerably; and (6) Fluorine is common in many of the samples studied and importantly this method offers an easy way to document its presence. Importantly if the presence of F is considered as a proxy for the contribution of magmatic fluids, then data for some orogenic gold deposits suggests affinities with a granitic source.

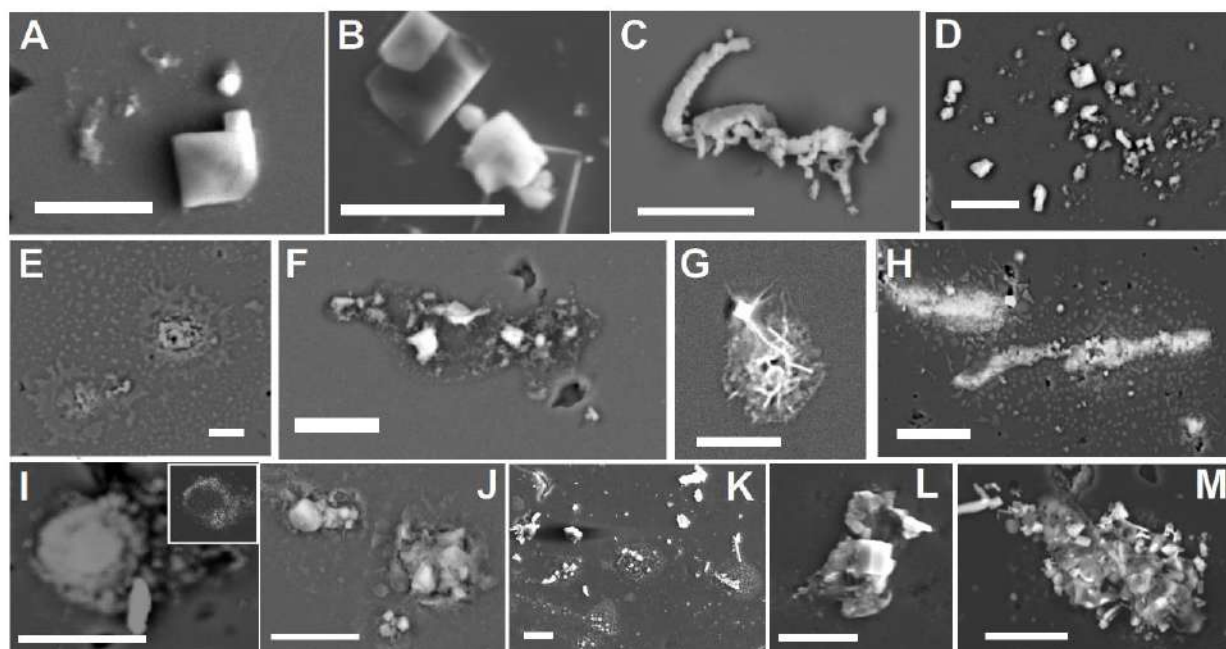


Fig. 1. Representative SEM-BSE images of decrepitate mounds from a variety of hydrothermal mineralized settings. The scale bar in all cases is 20 μm and the substrate is quartz except in A and B where it is sphalerite. (A, B) Mounds from the Nanisivik MVT deposit showing halite (A) and both halite horizon. (D) Mound field of halite mounds from base-metal rich quartz vein system. (E) Splatter mounds (Na-K-Ca-Mn-Fe-S) in quartz from the potassic zone of a porphyry Cu deposit. (F, G) Complex mounds (Na-Ca-F) from a mineralized peraluminous granite setting. (H) Mound trail due to leakage of secondary fluid inclusions from a healed fracture plane. (I) A zoned Na-K mound with the inset X-ray map showing a ring of K chloride mound about the Na-rich core. (J) Large Na-Ca mounds within near-surface cavities of high-salinity secondary inclusions in a mineralized granite. (K, L) Mounds from orogenic gold quartz veins. Importantly, the mound in L has a Na-Ca-F composition. (M) Large Na-Ca-Ba-Sr-Fe mound from a pegmatite hosting REE mineralization in a carbonatitic setting. The bright phases are stoichiometric SrCl_2 .

REFERENCES

- Bodnar, R.J. Interpretation of data from aqueous-electrolyte fluid inclusions. *In* Fluid Inclusions: Analysis and Interpretation. Mineralogical Association of Canada Short Course Series Vol. 32, 81-100.
- Crawford, M.L. (1981) Phase equilibria in aqueous fluid inclusions. *In* Short Course in Fluid Inclusions: Applications to Petrology, Mineralogical Association of Canada Short Course Notes, 75-100
- Gleeson, S.A. (2003) Bulk analysis of electrolytes in fluid inclusions. *In* Fluid Inclusions: Analysis and Interpretation. Mineralogical Association of Canada Short Course Series Vol. 32, 233-246.
- Haynes, F.M., Sterner, S.M., Bodnar, R.J. (1988) Synthetic fluid inclusions in natural quartz. IV. Chemical analyses of fluid inclusions by SEM/EDAS: evaluation of method. *Geochimica et Cosmochimica Acta* 52: 969-977.
- Heinrich, C.A., Günther, D., Aude'at, A., Ulrich T., Frischknecht R. (1999) Metal fractionation between magmatic brine and vapor, determined by microanalysis of fluid inclusions. *Geology* 27: 755-758.
- Eadington, P. (1974) Microprobe analysis of the non-volatile constituents of fluid inclusions. *Neues Jahrbuch Min. Mh.* 11: 518-525.
- Kontak, D.J. (2004): Analysis of decrepitate mounds as a complement to fluid inclusion thermometric data: Case studies from granitic environments in Nova Scotia and Peru. *Canadian Mineralogist*, vol. 42, p. 1315-1330.
- Roedder, E. (1984) Fluid Inclusions. Mineralogical Society of America, Reviews in Mineralogy, vo. 12, 646 p.

Using synthetic fluid inclusions in ultramafic minerals to monitor hydration – dehydration processes in the oceanic crust.

Lamadrid, H.M.*, Schwarzenback, E.*, Caddick, M.*, Rimstidt, D.*, Bodnar, R.J.*

**Department of Geosciences, Virginia Tech, Blacksburg, VA, USA,*

Synthetic fluid inclusions studies using the fracture – anneal technique, have been used for several decades to understand a wide variety of geologic processes, and have proven key to measure the P-V-T-X properties of fluids. We are using the synthetic fluid inclusion technique to monitor the hydration – dehydration processes of ultramafic minerals, in order to further understand the serpentinization processes occurring in the oceanic crust. Serpentinization is an important geological process that occurs where ultramafic rocks (mantle) are exposed to fluid circulation in the oceanic and continental crusts. This process not only induces huge magnetic, seismic and rheological changes in the oceanic crust and mantle wedge, but also produces highly unusual mineralogy and one of the most reduced fluid environments on the planet and other planetary bodies. The atypical geochemical characteristics of these fluids have been also proposed to be an ideal environment for the origin of life. Despite much recent attention, aspects of serpentinization such as the order of reactions, their timing and the direction in which they occur are still a matter of considerable debate in the literature.

We trap fluids of known composition at known P-T conditions in olivine crystals to follow in-situ serpentinization reactions in a closed system at low water/rock ratios. Pre-fractured olivine crystals were loaded into platinum capsules along with a H₂O-NaCl-MgCl₂ fluid of seawater concentration (3.5 wt.%) and Na/Mg ratio of 8:1, then welded shut (Bodnar & Sterner, 1987). The loaded capsules then were placed into high-pressure vessels, and P-T were increased to 5.6 kbar and 600 °C for 21 days. After trapping of fluid inclusions at the selected conditions in the samples, the inclusions were examined petrographically before the samples were placed into a furnace at ~280 °C and 1 atm.

Preliminary results show that serpentinization reactions start after a few days in some of the fluid inclusions. Mineralogy was monitored by Raman analysis, and we observed the formation of brucite and serpentine. After 28 days, some of the fluid inclusions had consumed nearly all of the fluid, leaving the cavity filled with brucite, serpentine and halite. Small fractures in the fluid inclusions reveal significant volume change during serpentinization. In at least one case, H₂ was detected in the fluid inclusion, showing that the reducing conditions inside the fluid inclusion are similar to what occurs in nature. However, no magnetite was observed in any of the fluid inclusions based on Raman analysis, suggesting that the reaction $2(\text{FeO})_{\text{rock}} + \text{H}_2\text{O} \rightarrow (\text{Fe}_2\text{O}_3)_{\text{magnetite}} + \text{H}_2$ did not occur, and that Fe³⁺ may instead be incorporated into serpentine or another phase. This observation concurs with thermodynamic calculations and observations of natural samples in which magnetite is formed preferentially by a secondary reaction of brucite and serpentine with higher fluid/rock ratios (Bach et al., 2006; Frost and Beard, 2007). Current experiments and thermodynamic modelling are being conducted in olivine, enstatite and diopside to constrain the rate of reaction of the trapped H₂O with hosts, to better understand these reactions and their overall implications of the serpentinization processes.

REFERENCES

- Bach et al. (2006) *Geophysical Research Letters* 33, L13306
Bodnar & Sterner (1987) *Hydrothermal experimental techniques* (ed. G.C. Ulmer and H.L. Barnes) 423-457.
Frost & Beard (2007) *Journal of Petrology* 48, 1351-1368

Vapor-saturated liquidus of the system $\text{H}_2\text{O}-\text{NaCl}-\text{FeCl}_2$

Lecumberri-Sanchez, P.*, Steele-MacInnis, M.*, Bodnar, R.J.**

**Institute for Geochemistry and Petrology, ETH Zurich, Clausstr. 25, 8092 Zurich, Switzerland*

***Department of Geosciences, Virginia Tech, 4044 Derring Hall, Blacksburg VA*

Magmatic-hydrothermal fluids are commonly FeCl_2 -rich (Yardley, 2005; Bodnar et al., 2014), but the effect of FeCl_2 on the $PVTx$ properties of fluid inclusions is essentially unknown (Liebscher, 2007). In this study, synthetic fluid inclusions experiments have been conducted to determine the vapor-saturated liquidus phase relations of the system $\text{H}_2\text{O}-\text{NaCl}-\text{FeCl}_2$, in order to allow compositional estimates for natural fluid inclusions based on ice- and halite-dissolution temperatures. Microthermometric and microanalytical measurements on synthetic fluid inclusions have been combined with the existing data to determine the phase boundaries and stability fields of ice, hydrohalite, halite and ferrous-chloride hydrates. The liquidus is qualitatively similar to those of other ternary systems of $\text{H}_2\text{O}-\text{NaCl}$ plus divalent-cation chlorides (MgCl_2 and CaCl_2) and has been characterized through empirical equations representing the liquid salinity on the ice- and halite-liquidus surfaces. The ice and halite liquidus intersect at a metastable cotectic curve, which can be used to determine fluid compositions in this system when metastable behavior is observed. Furthermore, based on the experimentally determined liquidus, bulk salinities of natural fluid inclusions can be determined from the last dissolution temperatures of ice and/or halite using the new empirical equations. This study provides the first comprehensive model for relating microthermometric and compositional data for iron-bearing fluid inclusions, which can be applied to fluid inclusion studies of magmatic-hydrothermal systems. In addition, the model allows improved major- and trace-element compositional estimates of iron-rich fluid inclusions by laser-ablation ICPMS.

REFERENCES

- Bodnar, R.J., Lecumberri-Sanchez, P., Moncada, D., Steele-MacInnis, M. (2014) Fluid inclusions in hydrothermal ore deposits. *Treatise on Geochemistry*. 13. 119-142.
- Liebscher, A. (2007) Experimental Studies in Model Fluid Systems. *Reviews in Mineralogy and Geochemistry*. 65. 15-47.
- Yardley, B.W.D. (2005) Metal Concentrations in Crustal Fluids and Their Relationship to Ore Formation *Economic Geology*. 100. 613-632.

Stable carbon isotope ratios of CH₄-rich gas inclusions in shale-hosted fracture-fill mineralization: a tool for tracing hydrocarbon generation and estimation of gas potential.

Lüders, V. and Plessen, B.

Helmholtz Centre Potsdam GFZ German Research Centre for Geosciences

Fluid inclusion gases in minerals from fracture-fill mineralization hosted in Paleozoic and Mesozoic shale have been analyzed for stable carbon isotopic ratios of CH₄ using a crushing device interfaced to an elemental analyzer (EA) and an isotopic ratio mass spectrometer (IRMS). Studied samples from Paleozoic strata originate from outcrops and wells in the Rhenohercynian Zone in Germany and the Campine Basin (Belgium). Fracture-fill mineralizations hosted by Mesozoic strata originate from drill cores in the Lower Saxony Basin. Some studied sites are under exploration for shale gas potential in Germany and Belgium.

The maturity of fracture-hosting shales varies from immature to overmature. The sample suite comprises mineral-filled horizontal as well as vertical fractures. Fracture fillings consist of calcite and/or quartz. The latter is mostly restricted to fracture-fill mineralization hosted in Paleozoic shales. The thickness of the sampled fracture fillings varies between some mm up to c. 20 cm.

Fluid inclusions in calcite from horizontal fractures hosted in shale with vitrinite reflectance $R_o < 0.8\%$ often show bluish-white fluorescence indicating the presence of oil besides gas in fluid inclusions. Calcite from fracture fillings hosted by higher mature shale contains either gaseous inclusions showing no UV fluorescence or no gas inclusions probably due to leakage and/or decrepitation of the latter. Quartz from vertical fracture fillings often contain gas-rich inclusions that were trapped under variable pressure conditions as indicated by phase transitions into the liquid or vapor phase. Gas-rich inclusions in quartz are often of primary origin (growth zones, clusters) and more or less associated with co-genetically formed aqueous 2-phase fluid inclusions showing variable salinity and homogenization temperatures. Gas compositions ranges from nearly pure CH₄ to variable CH₄-CO₂ or even CH₄-CO₂-N₂ composition.

Very negative $\delta^{13}\text{C}_{\text{CH}_4}$ values of fluid inclusions in calcite from horizontal fractures hosted in Mesozoic strata suggest that gaseous hydrocarbons generated during the oil/early gas window and that the formation of horizontal fractures seems to be related to hydraulic expulsion fracturing. The calculated maturity of the source rocks at the time of gas generation lies below the present-day measured maturity derived from vitrinite reflectance. Local unusual increasing vitrinite reflectance can be explained by hydrothermal alteration as indicated by less negative $\delta^{13}\text{C}_{\text{CH}_4}$ values and increasing CO₂ content in fluid inclusions. Vertical fracture filling minerals always yield gas generation from highly mature rocks by hydrothermal alteration of the latter after maximal burial.

In samples of quartz from fracture fillings hosted by Paleozoic shales from the Rhenohercynian Zone and the Campine Basin, no evidence is given for the presence of early generated gas. Since Paleozoic shales in the Harz Mountains and Rhenish Massif experienced deep burial and deformation, it appears likely that major gas loss from shales occurred due to deformation and uplift in response to the Variscan Orogeny.

Petrography of silicate melt inclusions in quartz phenocrysts from porphyry Mo deposit at Bangpu, Tibet, China

Luo, M.C.*, Moncada, D. ** and Bodnar, R.J. **

*School of Earth Sciences and Resources, China University of Geosciences, Beijing, China, lmc111@vt.edu

**Department of Geosciences, Virginia Tech, Blacksburg, VA, U.S.A., moncada@vt.edu, rjb@vt.edu

Porphyry-type ore deposits are commonly associated in space and time with intermediate to felsic magmas that are emplaced at depths of a few to perhaps 10 kilometers. Copper and other ore metals, including molybdenum, gold and silver, are extracted from the silicate melt when the volatiles exsolve from the parental magmas in response to decreasing pressure and crystallization (Cline and Bodnar, 1991). Melt inclusions represent samples of melt trapped during crystallization of magmas (Student and Bodnar, 2004) and melt inclusions provide the best-preserved samples of the earliest stage in the formation of porphyry type deposits. Based on petrographic analysis of 46 samples, we describe the petrography of silicate melt inclusions (SMI) in phenocrystic quartz from the porphyry Mo deposit at Bangpu (Tibet, China).

The porphyry Mo deposit at Bangpu, locating in the east section of Gangdese, Tibet, is hosted by a series of mid-Miocene (14.07-16.21 Ma) intrusions and contains 0.8 Mt of molybdenum with 0.079% average ore grade. The sequence of mineralizing porphyries as currently recognized is (1) monzogranite porphyry (MP) and (2) quartz monzonite porphyry (QMP). Most of the silicate melt inclusions occur within quartz phenocrysts from samples of MP and QMP, occasionally within quartz veins that have thin alteration envelopes containing biotite and K-feldspar.

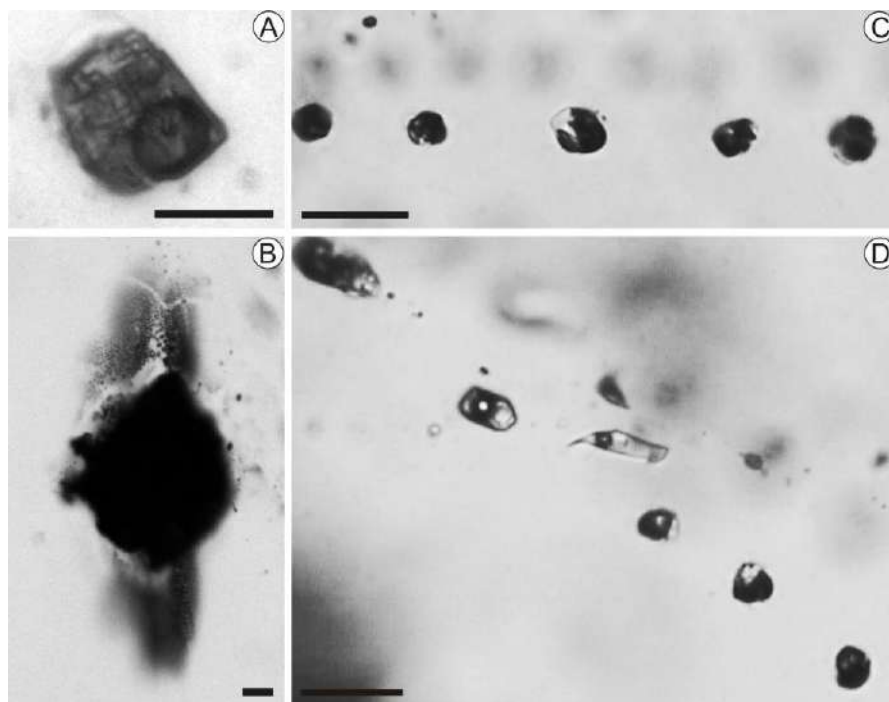


Fig. 1 Examples of SMI in quartz phenocrysts in MP and QMP from the Bangpu, Tibet, porphyry Mo deposit. (A) SMI consisting of crystals and vapor phase and (B) SMI trapped along a single fracture plane in phenocryst (ZK6804-195.2), (C) SMI with natural decrepitation features and (D) A secondary trail with coexisting brine fluid inclusions and SMI, occur in phenocryst (ZK6001-74.1). All scale bars represent 20 μm.

At room temperature, silicate melt inclusions examined in this study show variable proportions of glass, crystals and residual volatiles. The majority of silicate melt inclusions consist of one or more crystals and/or

glass and vapor. Some silicate melt inclusions contain liquid (Fig. 1A) in addition to crystals, glass and vapor. The variable phase relations observed in melt inclusions reflect the different rates of cooling of the melt inclusions (and host rocks) following entrapment. For a given size, glass-bearing inclusions were generally assumed to have cooled at a faster rate than crystallized inclusions (Roedder 1979). The size of melt inclusions ranges from >5 to $100\text{ }\mu\text{m}$, with most from >5 to about $25\text{ }\mu\text{m}$. Larger inclusions ($>40\text{ }\mu\text{m}$) generally show evidence of natural decrepitation, such as a halo of much smaller fluid inclusions surrounding a larger central melt inclusion (Fig. 1C), or radial fractures extending from the inclusion (Student and Bodnar, 2004). The shape of silicate melt inclusions includes rounded, rectangular, and hexagonal.

Quartz phenocrysts in MP and QMP show three distinct phases of quartz crystallization revealed by contrasting CL light intensity, recording a three-stage history of quartz phenocryst formation (Fig. 2B). Based on CL and photographic images, the timing of melt inclusion entrapment was related to the formation of Q1, Q2 and Q3 quartz. Most inclusions in quartz phenocrysts from Bangpu are isolated or distributed randomly within the quartz core (Q1, Fig. 2A), whereas some smaller inclusions are found along the growth zones (Q2 and Q3) or along trails (Fig. 1B, 2A), suggesting that these silicate melt inclusions were trapped at the same time (Bodnar and Student, 2006). Some silicate melt inclusions coexist with brine fluid inclusions along secondary trails (Fig. 1D), which is thought to be a result of immiscibility (Roedder, 1992).

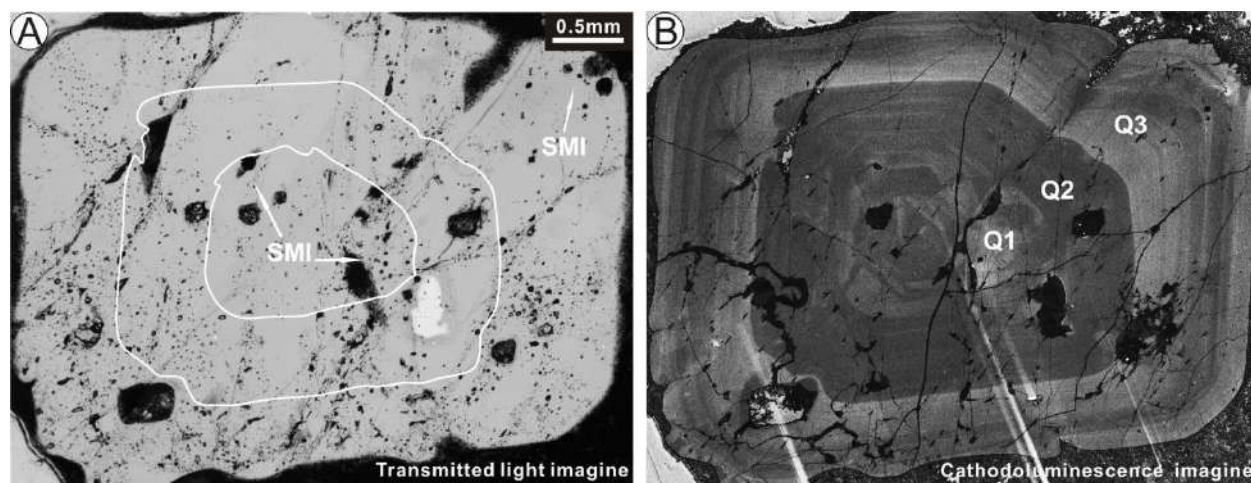


Fig. 2 CL mapping of SMI generations for sample ZK6001-281.4. The same phenocryst is shown in (A) transmitted light, (B) cathodoluminescence.

REFERENCES

- Bodnar R.J. and Student J.J. (2006) Melt inclusions in plutonic rocks: Petrography and microthermometry. In Webster J.D., ed. Melt inclusions in plutonic rocks. Mineralogical Association of Canada. Short Course 36. 1-26.
- Cline J.S. and Bodnar R.J. (1991) Can economic porphyry copper mineralization be generated by atypical calc-alkaline melt? *Journal of Geophysical Research*. Vol. 96. 8113-8126.
- Roedder E. (1979) Origin and significance of magmatic inclusions. *Bulletin de Mineralogie*. Vol. 102. 467-510.
- Roedder E. (1992) Fluid inclusion evidence for immiscibility in magmatic systems. *Geochimica et Cosmochimica Acta*. Vol. 56. 5-20.
- Student J.J. and Bodnar R.J. (2004) Silicate melt inclusions in porphyry copper deposits: identification and homogenization behavior. *The Canadian Mineralogist*. Vol. 42. 1583-1599.

Noble gas isotope data from the Goldfield high sulfidation epithermal deposit, Nevada: Evidence for helium input from a primitive mantle source during ore formation

Manning, A.H.* and Hofstra, A.H.*

**Denver Inclusion Analysis Laboratory, U.S.G.S., Denver, Colorado, amanning @usgs.gov*

Recent Pb, Cu, and Os isotopic studies of ore minerals in low-sulfidation (LS) epithermal Au-Ag deposits related to the Yellowstone plume (Nevada, Oregon, and Idaho, U.S.A.) suggest that metals were discharged directly from a mafic source. The role of mafic magmas in the formation of epithermal Au-Ag deposits in subduction-related magmatic arcs is poorly understood. To address this issue, noble gas isotope data were collected from fluid inclusions in ores from Goldfield, Nevada, which formed at 20.0 ± 0.5 Ma in an andesitic to rhyolitic volcanic field in the ancestral Cascades continental magmatic arc. It is the largest high-sulfidation (HS) epithermal gold mining district in the U.S., with over 130 t of gold production and 23 km² of argillic alteration (with alunite, pyrophyllite, or kaolinite). Previous stable isotope studies of quartz, alunite, and sulfide minerals suggest that the gold ores formed in a magmatic vapor plume, derived from a subjacent porphyry intrusion, which displaced and mixed with meteoric groundwater at shallow levels.

Helium, Ne, and Ar trapped in fluid inclusions in pyrite, enargite group minerals, sphalerite, and quartz were extracted by thermal decrepitation at 300°C and analyzed using a high resolution static sector mass spectrometer. The isotopic compositions of Ne and Ar are similar to air-saturated water (ASW), indicating an atmospheric source for these gases rather than nucleogenic or radiogenic subsurface sources (Fig. 1A,B). In contrast, He/Ne and He/Ar ratios are much greater than ASW, indicating that most of the He was produced in the subsurface. Measured He R/R_a values (0.4 to 20) suggest that He was derived from both crustal and mantle sources (Fig. 1C). The highest R/R_a values (15–20) require a juvenile mantle source, presumably located below the subducting slab. $^4\text{He}/^{40}\text{Ar}^*$ and $^4\text{He}/^{21}\text{Ne}^*$ systematics are characteristic of mantle magma degassing (Fig. 1D).

To place these data in context, we compiled published fluid inclusion He and Ar isotope data on epithermal and porphyry deposits from around the world (Figs. 1E,F). We found that Goldfield is the only HS epithermal deposit from which noble gas data have been collected, and that LS and intermediate-sulfidation (IS) epithermal deposits on average have greater R/R_a values than porphyry deposits. This could be because the latter cool more gradually, allowing more diffusive exchange with crustal He at elevated temperatures. The great majority of samples exceed the crustal R/R_a value of 0.01, many are >1 , and some extend into the magmatic arc and MORB fields, indicating that volatiles derived from mafic magmas were commonly present. The $^{40}\text{Ar}/^{36}\text{Ar}$ ratios are either atmospheric, as at Goldfield, or extend to greater values that reflect thermal degassing of older crust or mantle (Fig. 1F).

Goldfield R/R_a values are greater than those of LS and IS epithermal deposits, and the only ones reaching into the juvenile mantle field. Paleogeographic reconstructions suggest Goldfield was located above the Mendocino Fracture Zone in the subducted slab, which may have allowed magma and/or volatiles to migrate upward from deeper levels in the mantle through a slab tear. These mafic magmas and their degassed volatiles must have ascended sufficiently rapidly and directly so that mixing with crustal gases was minimized. Such inputs of hot, mantle-derived magma and/or volatiles may have triggered exsolution and discharge of fluid from porphyry intrusions. Additional work is needed to determine whether metals or ligands were derived from mantle sources.

Last, given that fluids in LS and IS deposits are often degassed due to boiling, we suspect that HS deposits are more likely to capture undiluted volatiles from depth because of their position in the vapor plume directly above the porphyry stock. More noble gas studies of HS deposits are clearly warranted.

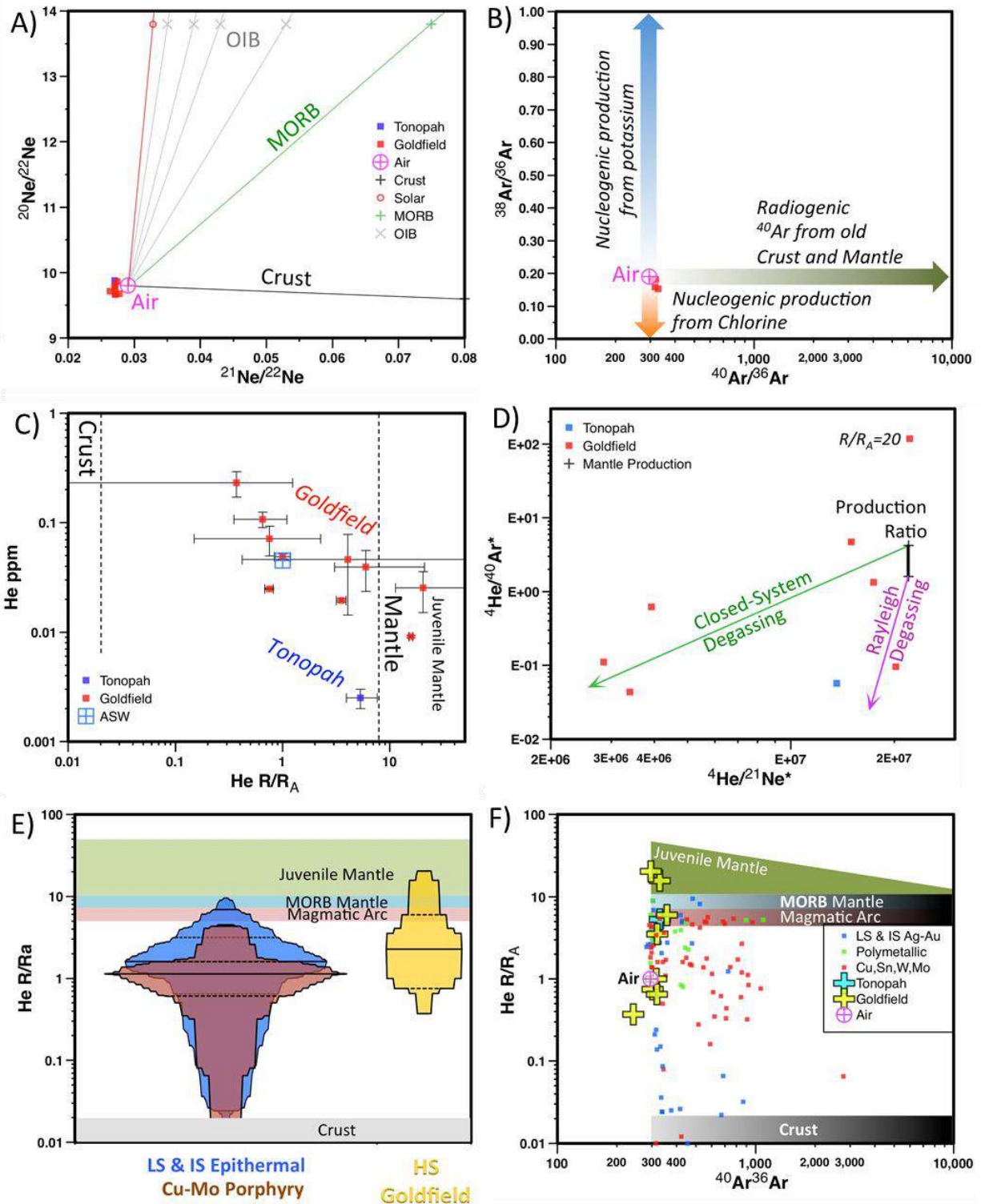


Figure 1. (A) Neon isotope results. (B) Argon isotope results. (C) Helium isotope results. (D) ^4He - $^{40}\text{Ar}^*$ - $^{21}\text{Ne}^*$ systematics for mantle magma degassing. (E) Proportional box plot comparing Goldfield to published He R/R_a values from porphyry (brown) and epithermal (blue) deposits. Width corresponds to number of samples. (F) R/R_a vs. $^{40}\text{Ar}/^{36}\text{Ar}$ plot comparing Goldfield to published data.

Pre-Eruptive Conditions of the Hideaway Park Topaz Rhyolite, Colorado: Insights into Metal Source and Evolution of Magma Parental to the Henderson Porphyry Mo Deposit

Mercer, C.N.* , Hofstra, A.H.* , Todorov, T.I.** , Roberge, J.*** , Sisson, T.W.**** , Burgisser, A.***** , Adams, D.T.***** , and Cosca, M*.

*Denver Inclusion Analysis Laboratory, USGS, Denver, CO 80225, USA

**Center for Food & Safety & Applied Nutrition, USFDA, College Park, MD 20740, USA

***ESIA-Ticomán, Instituto Politécnico Nacional, D.F. 07340, Mexico

****Volcano Hazards Program, USGS, Menlo Park, CA 94025, USA

*****Institut des Sciences de la Terre d'Orléans, Orléans, France

*****Department of Earth & Planetary Sciences, Macquarie University, Sydney, Australia

The pre-meeting field trip will include a visit to the Hideaway Park tuff, near the ski resort town of Winter Park, CO, with an opportunity to examine and collect rock specimens. The Hideaway Park tuff is the only preserved extrusive volcanic unit related to the Oligocene Red Mountain intrusive complex, which produced the world-class Henderson porphyry Mo deposit (Fig. 1). Located within the Colorado Mineral Belt, Henderson is the second largest Climax-type Mo deposit in the world, and is therefore an excellent location to investigate magmatic processes leading to Climax-type Mo mineralization. We combine an extensive dataset of major element, volatile, and trace element abundances in quartz-hosted melt inclusions and pumice matrix glass, and major element geochemistry from phenocrysts to reconstruct the pre-eruptive conditions and the source and evolution of metals within the Hideaway Park magma.

The tuff is poorly- to moderately-welded and contains tan pumice clasts and a variety of lithics within an ashy matrix. Hand specimens of the Hideaway Park tuff are light-gray to tan in color when fresh, and contain large (up to several mm) phenocrysts of sanidine, plagioclase, and smoky bipyramidal quartz, with accessory biotite, magnetite, ilmenite, titanite, zircon, and apatite. It is a peraluminous topaz rhyolite that is geochemically similar to the Henderson rhyolite stocks both in REE pattern and in containing characteristically F-rich biotite phenocrysts (up to 5 wt% F).

Our analyses of sanidine from the lower tuff yield an $^{40}\text{Ar}/^{39}\text{Ar}$ plateau date of 27.72 ± 0.28 (2 σ) Ma and we calculate a revised age of 27.49 ± 0.12 (2 σ) Ma for the upper tuff (revised from Knox, 2005), both of which are within the age range of Red Mountain intrusive rocks (29–25 Ma; Bookstrom et al. 1988; Geissman et al., 1992). The date on the lower tuff is essentially identical to the high-precision Re-Os date (27.656 ± 0.022 Ma; Markey et al., 2007) from Henderson molybdenite.

Quartz-hosted topaz rhyolite melt inclusions are volatile-charged (≤ 6 wt% H_2O , ≤ 600 ppm CO_2 , ≤ 150 ppm S, ~ 0.3 – 1.0 wt% F, ~ 2300 – 3500 ppm Cl) and metal-rich (~ 7 – 24 ppm Mo, ~ 4 – 14 ppm W, ~ 21 – 52 ppm Pb, ~ 28 – 2700 ppm Zn, < 0.1 – 29 ppm Cu, ~ 0.3 – 1.8 ppm Bi, ~ 40 – 760 ppb Ag, ~ 690 – 1400 ppm Mn). Melt inclusion and pumice matrix glass chemistry reveal that the Hideaway Park magma evolved by large degrees of fractional crystallization (≤ 60 – 70%) during melt inclusion entrapment in quartz at pressures of ≤ 300 MPa (≤ 8 km depth), with little to no quartz crystallization upon ascent and eruption. Filter pressing, crystal settling, magma recharge and mixing of less evolved rhyolite melt were important processes during magma evolution, and the low estimated viscosities ($\sim 10^5$ – 10^{10} Pa s) of these H_2O - and F-rich melts likely enhanced these processes.

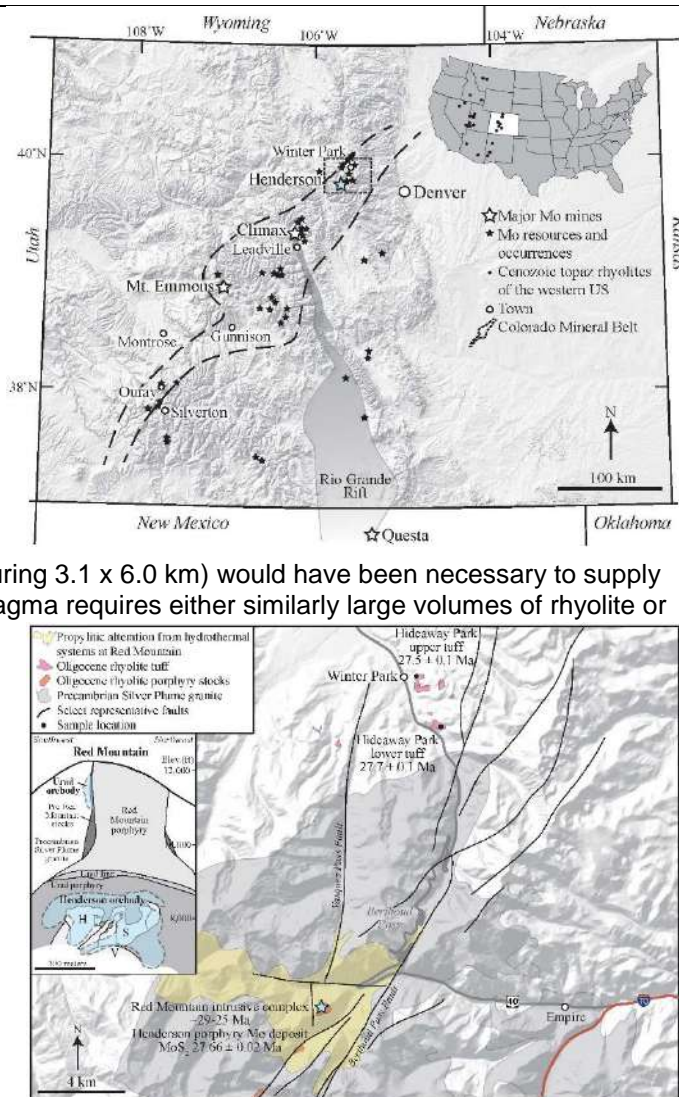
Decompression modeling of a S-O-H-C-bearing rhyolitic melt provides insight into the complex chemical evolution of exsolving volatiles. Preliminary modeling using the program *D-Compress* (Burgisser et al., in review) suggests that the fluid exsolving from the Hideaway Park magma was H_2O -dominated with large amounts of CH_4 , H_2 , CO_2 , and H_2S . Chlorine likely partitioned most strongly into the fluid at greater depth (~ 8 km), but continued to do so at shallower levels where it exsolved as HCl (e.g., Gardner et al., 2006). The capacity for metals to partition out of the magma and into the exsolving hydrosaline fluid requires the presence of hydroxyacid (for Mo and W) and chloride (for Pb, Zn, Cu, Sn, and Ag) ligands (e.g., Hedenquist and Lowenstern, 1994). Melt inclusions show an affinity for metals over the entrapment interval, displaying increasing metal concentrations (incompatible behaviour) with progressive melt evolution. However, a clear discrepancy in the concentration of some metals in the pumice matrix glass

compared to that in the melt inclusions provides evidence for strong partitioning of Mo, Bi, Ag, Zn, Mn, Cs, and Y into an exsolving magmatic fluid upon shallow magma ascent.

Given that the Henderson deposit is not only endowed with economic abundances of Mo, but also with anomalous concentrations of W, Pb, Zn, Cu, Bi, Ag, and Mn (Seedorff and Einaudi, 2004), we suggest these metals were sourced from similar fluids exsolved from un-erupted portions of the same magmatic system. Trace element ratios imply that Mo was sourced deep, either from the lower crust or metasomatized mantle. To account for the 437 Mt of MoS_2 ($\sim 1.0 \times 10^6$ t Mo) present in the Urad-Henderson ore deposit, a volume of $\sim 45 \text{ km}^3$ of Hideaway Park rhyolite magma (a cylindrical pluton measuring $3.1 \times 6.0 \text{ km}$) would have been necessary to supply the Mo. The extremely low S solubility of this magma requires either similarly large volumes of rhyolite or an alternative source of S to account for that present in the ore deposit, for example, S from co-magmatic, mantle-derived lamprophyres that occur in minor quantities with the voluminous topaz rhyolites in the area. Sparging (i.e., gas flushing) of $\sim 6.8 \times 10^5$ t of S from $\sim 0.05 \text{ km}^3$ of lamprophyre magma could supply the S budget. Ongoing decompression modelling will help distinguish the source of S.

REFERENCES

- Bookstrom A. A., Carten R. B., Shannon J. R. And Smith R. P. (1988) Origins of bimodal leucogranite-lamprophyre suites, Climax and Red Mountain porphyry molybdenum systems, Colorado: Petrologic and strontium isotopic evidence. In: J. W. Drexler and E. E. Larson (eds) *Colorado School of Mines Quarterly* 83, 1–24.
- Burgisser, A., Alletti, M., and Scaillet (in review) Simulating the behavior of volatiles belonging to the C-O-H-S-Fe system in silicate melts under magmatic conditions with the software D-Compress, *Computers & Geosciences*.
- Gardner J. E., Burgisser A., Hort M. and Rutherford M. (2006) Experimental and model constraints on degassing of magma during ascent and eruption. *Geological Society of America Special Papers* 402, 99.
- Geissman J. W., Snee L. W., Graaskamp G. W., Carten R. B. and Geraghty E. P. (1992) Deformation and age of the Red Mountain intrusive system (Urad-Henderson molybdenum deposits), Colorado: Evidence from paleomagnetic and $^{40}\text{Ar}/^{39}\text{Ar}$ data. *Geological Society of America Bulletin* 104, 1031–1047.
- Hedenquist J. and Lowenstern J. B. (1994) The role of magmas in the formation of hydrothermal ore deposits. *Nature* 370, 519–527.
- Knox K. L. (2005) Never Summer igneous complex- Evolution of a shallow magmatic system. M.S. thesis University of Colorado, 1–54.
- Markey R., Stein H. J., Hannah J. L., Zimmerman A., Selby D. and Creaser R. A. (2007) Standardizing Re–Os geochronology: A new molybdenite Reference Material (Henderson, USA) and the stoichiometry of Os salts. *Chemical Geology* 244, 74–87.
- Seedorff E. and Einaudi M. T. (2004) Henderson porphyry molybdenum system, Colorado: II. Decoupling of introduction and deposition of metals during geochemical evolution of hydrothermal fluids. *Economic Geology* 99, 39–72.



Fluid Inclusion and Mineral Texture based Exploration Targeting in the El Oro Gold District, Mexico and Michoacán states, Mexico.

Moncada, D.*, Freeze, J.**, and Bodnar R. J. *,

* Department of Geosciences, Virginia Tech, Blacksburg, VA 24061 USA, **Candente Gold Corporation, Suite 1650 400 Burrard Street Vancouver, BC Canada, V6C 3A6

Evidence of boiling is often associated with gold and silver mineralization in low sulfidation epithermal vein systems, so the presence of abundant boiling indicators should indicate a higher probability for finding precious metals compared to areas lacking this evidence. The El Oro-Tlalpujahua mining district lies approximately 120 km northwest of Mexico City, straddling the border between the states of Mexico and Michoacán, and hosts over 52 veins within an area of 257 km². Mined since the Spanish first discovered vein outcrops in the Tlalpujahua area in 1529, in the late 19th and early 20th century, El Oro was the most important gold-silver camp in Mexico. The important San Rafael and Veta Verde Veins have an estimated production of over 8 million gold equivalent ounces, but production from the balance of the district is poorly documented. The district's Cretaceous and Jurassic meta-sediments and meta-andesite host rocks are extensively overlain by post-mineral Tertiary and Quaternary andesitic flows and tuffs that greatly hamper exploration, so fluid inclusion and textural evidence for boiling has been marshalled as a tool to focus exploration.

The individual productive gold and silver-bearing quartz-bladed calcite veins vary in thickness from millimeters to over 70 m, and can be traced for over 3.5 km along strike. Most of the known veins in the El Oro district strike NW-SE with a steep westerly dip (65-80 degrees) for veins located in the eastern part of the property (San Rafael and Veta Verde veins) and easterly for veins located in the western part of the property in the Tlalpujahua area (Corona and Borda Veins).

Samples collected from underground workings, drill holes and surface outcrops in the El Oro gold district show a wide variety of silica and calcite textures and fluid inclusion types typical of boiling hydrothermal fluids. Fluid inclusions were examined from numerous samples of the major veins. Fluid inclusion assemblages (FIAs) consisting of coexisting liquid-rich and vapor-rich inclusions with a broad range in liquid-to-vapor ratios, as well as textural evidence of boiling, were observed at the northern and southern ends of the San Rafael vein, although samples from in the deepest part of the vein between Tiro Mexico Sur and Tiro Chuparrosa show only textural evidence of boiling (i.e., no fluid inclusion evidence was observed). Samples from Veta Borda, Veta Corona, Veta Verde, Veta Nueva, and Veta Monte show both fluid inclusion and textural evidence of boiling. Importantly, boiling indicators are present in samples from below the deepest levels explored in the El Oro District, thus increasing the exploration probability for additional gold and silver mineralization at depth.

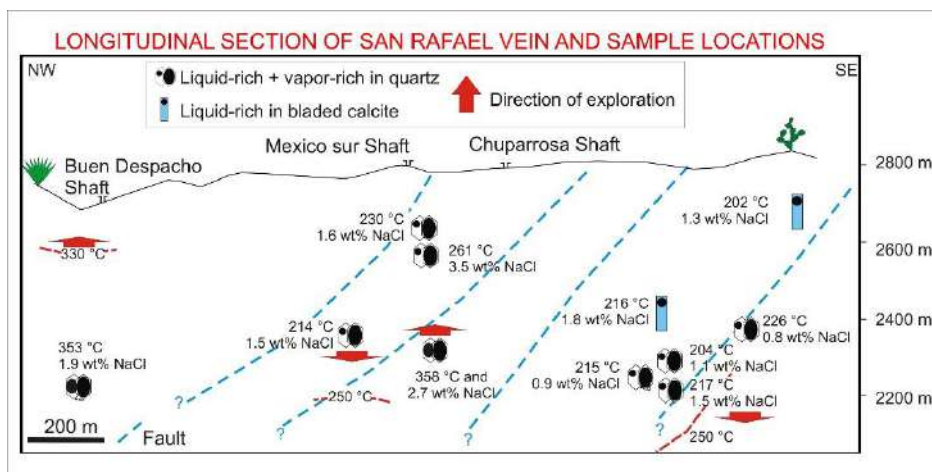


Figure 1. Results of reconnaissance microthermometric analyses of (1) coexisting liquid-rich and vapor-rich secondary fluid inclusions in quartz showing a broad range in liquid-to-vapor ratios, and (2) secondary liquid-rich fluid inclusions in bladed calcite.

Evidence for a magmatic source for Cu, Zn and Au in epithermal deposits in the Hauraki Goldfield, New Zealand

Sabina Strmic Palinkas*, Jeffrey L. Mauk**, Robert J. Bodnar***, Mathijs A. Booden****, Mark P. Simpson*****

* *School of Environment, The University of Auckland, P.B. 92019, Auckland 1142, New Zealand*

** *U.S. Geological Survey, P.O. Box 25046, MS 973, Denver, CO 80225, USA*

*** *Department of Geosciences, 4044 Derring Hall, Virginia Tech, Blacksburg, VA 24061, USA*

**** *Oude Singel 54, 2312RB, Leiden, The Netherlands*

***** *GNS Science - Wairakei Research Centre, 114 Karetoto Road - RD4, Taupo 3377, New Zealand*

The Hauraki Goldfield, North Island, New Zealand, contains approximately 50 adularia-sericite epithermal Au-Ag deposits. It coincides with the 200 km long and up to 40 km wide north-south-trending Coromandel Volcanic Zone (CVZ). The deposits occur as quartz veins that fill steep fractures. Total past production in the region exceeds 11 Moz Au and 48 Moz Ag. Approximately 97% of the Au has been recovered from CVZ andesite-hosted veins, while the remainder has come from veins in CVZ rhyolite, and veins in Late Jurassic greywacke basement (Christie et al., 2007).

The principal aim of the ongoing melt inclusion study is to understand the processes that link magmatic activity in the area to the epithermal mineralization, including chemical evolution of the melt, degassing of magmatic volatiles and exsolution of aqueous fluids. To achieve these goals we determined the chemical composition of silicate melt inclusions (LA-ICP-MS analyses) in unaltered plagioclase and pyroxene phenocrysts from barren and ore-hosting andesite, as well as rhyolite.

Subduction-related volcanism in the CVZ began in the early Miocene due to convergence along the Pacific-Australian plate boundary, erupting mainly andesitic and lesser dacitic magmas. In addition, a NNW-striking string of isolated volcanic centers, the Kiwitahi volcanic chain, erupted between 16 and 5.5 Ma along the western margin of the CVZ (Booden et al., 2012). The andesite occurs as massive flows, autoclastic breccias, lahars, tuffs and dikes. At about 11 Ma, propagation of the Colville-Lau oceanic island arc into the region resulted in a change from a compressional to extensional regime with corresponding bimodal rhyolitic (major) and basaltic (minor) volcanism. Rhyolitic volcanic rocks of the 11 to 1.5 Ma Whitianga Group overlie and interfinger with andesite and dacite of the Coromandel Group. In the late Pliocene (ca. 1.9–1.5 Ma), volcanic activity shifted from the CVZ to the Taupo Volcanic Zone (Booden et al., 2012).

The silicate melt inclusions are typically partly to completely crystallized and have variable proportions of glass, crystals, and vapor. Their size ranges from <5 μm up to 50 μm . Melt inclusions from the Coromandel Group andesite and the Whitianga Group rhyolite commonly coexist with fluid inclusions. The fluid inclusions show variable proportions of liquid, vapor, and isotropic and anisotropic solid phases, but their small size (<15 μm) precludes determination of their chemical composition by LA-ICP-MS. Nonetheless, coexisting melt and fluid inclusions indicates that magmas were H_2O -saturated (Student and Bodnar, 2004), so we conclude that the Coromandel Group andesite and the Whitianga Group rhyolite were H_2O -saturated, but the Kiwitahi andesite was not.

The LA-ICP-MS data for major (Na, Mg, Al, Si, K, Ca, Ti, Mn, and Fe) and trace elements (Li, Cu, Zn, As, Rb, Sr, Y, Zr, Nb, Ag, Sb, Cs, Ba, La, Nd, Sm, Eu, Dy, Yb, Au, Pb, Bi, Th, and U) were collected from complete (unhomogenized) silicate melt inclusions and reduced by AMS software (Mutchler et al, 2008). The concentrations of Al_2O_3 obtained from whole rock analyses of each sample were used as internal standards. Table 1 provides a summary of selected elements from the silicate melt inclusions analyzed by LA-ICP-MS.

Minor and trace element distributions in melt inclusions show trends similar to those in whole rock analyses (Booden et al., 2012). They are characterized by an arc-type signature with large ion lithophile element (LILE) enrichments, a positive Pb anomaly, negative anomalies for Nb, and Ti, enrichments of light REE, and depletion of heavy REE relative to bulk silicate Earth. The Coromandel Group and the Kiwitahi andesite melt inclusions show overlapping distributions with LILE enrichments of 50–100 times and Pb enrichment of 50 times. The Whitianga Group rhyolite melt inclusions are characterized by LILE and Pb enrichments up to 300 and 150 times, relative to bulk silicate Earth, respectively.

Elevated concentrations of Cu, Zn and Au in melt inclusions from the H₂O-unsaturated, barren Kiwitahi andesite, compared to the H₂O-saturated, mineralized Coromandel Group andesite and Whitianga Group rhyolite, suggest transfer of these metals from the melt into a magmatic hydrothermal fluid in the H₂O-saturated system. Absolute concentrations of As and Sb do not show significant differences among different rock types but As/Cs and Sb/Cs values are greater in the Kiwitahi andesite (As/Cs=2.1-3.3; Sb/Cs=0.4-0.5) compared to the Coromandel Group andesite (As/Cs=1.7-2.0; Sb/Cs=0.08-0.09) and Whitianga Group rhyolite (As/Cs=0.25-2.5; Sb/Cs=0.04-0.3) suggesting that exsolution of magmatic water contributed to the release of As and Sb as well (Student and Bodnar, 2004; Audétat et al., 2008; Zajacz et al., 2008). In contrast, Pb, Ag and Bi show differences in neither their absolute concentrations nor their metal/Cs ratios, suggesting that ore-bearing hydrothermal fluids leached these metals from the country rocks rather than deriving them from a magmatic source. Previously published Pb isotope data (Robinson, 1974) indicate that Pb in the orebodies was mostly leached from the underlying Mesozoic greywacke.

In summary, melt and fluid inclusion results suggest that Au, Cu, Zn, As, and Sb were transferred from melts of the Coromandel and Whitianga groups into magmatic hydrothermal fluids, and that these fluids may have played an important role in epithermal deposit formation.

Table 1. Summary LA-ICP-MS results with minimum, maximum and median element concentrations for silicate melt inclusions in volcanic rocks from the Hauraki goldfield, New Zealand

	SiO ₂	Li	Cu	Zn	As	Zr	Nb	Ag	Sb	Cs	Ba	Au	Pb	Bi
	wt. %													
ppm														
Rhyolite (Whitianga Group) (n=20)														
Min	68.19	<d.l.	<d.l.	19.4	<d.l.	113	5.94	<d.l.	<d.l.	6.04	603	<d.l.	11.9	0.03
Max	78.99	170	87.7	116	28.7	756	27.2	0.50	3.31	20.3	1379	0.07	46.6	0.67
Median*	75.54	86.9	38.3	40.5	16.6	255	11.0	0.38	1.26	10.3	879	n/a	27.2	0.29
Ore-hosting andesite (Coromandel Group) (n=13)														
Min	62.04	<d.l.	47.6	16.3	3.61	56.8	1.46	0.08	0.23	2.07	307	<d.l.	8.08	0.08
Max	64.74	59.5	147	29.3	8.55	202	8.02	0.32	0.38	4.59	453	<d.l.	11.5	0.19
Median	63.83	31.5	67.1	20.4	7.10	139	4.50	0.18	0.30	2.62	385	<d.l.	9.57	0.15
Barren andesite (Kiwitahi) (n=12)														
Min	52.65	<d.l.	290	51.2	7.30	183	4.20	0.17	1.32	1.86	446	0.13	8.59	0.10
Max	70.02	227	1082	130	10.1	243	8.63	0.31	1.32	3.49	646	0.20	11.0	0.32
Median	64.99	110	911	110	8.70	230	6.67	0.24	1.32	3.10	530	0.16	9.61	0.14

* Median values are calculated for elements with less than 50% censored data

<d.l. = concentration below detection limit

REFERENCES

- Audétat, A., Pettke, T., Heinrich, C.A., Bodnar, R.J. (2008) The composition of magmatic hydrothermal fluids in barren versus mineralized intrusions. *Economic Geology*, v. 103, p. 877-908.
- Booden, M.A., Smith, I.E.M., Mauk, J.L., Black, P.M. (2012) Geochemical and isotopic development of the Coromandel Volcanic Zone, northern New Zealand, since 18Ma. *Journal of Volcanology and Geothermal Research*, v. 219-220, p. 15–32.
- Christie, A.B., Simpson, M.P., Brathwaite, R.L., Mauk, J.L., Simmons, S.F. (2007) Epithermal Au-Ag and Related Deposits of the Hauraki Goldfield, Coromandel Volcanic Zone, New Zealand. *Economic Geology*, v. 102, p. 785–816.
- Mutchler, S.R., Fedele, L., Bodnar, R.J. (2008) Analysis Management System (AMS) for reduction of laser ablation ICP–MS data. *Mineralogical Association of Canada Short Course Series*, v. 40, p. 318-327.
- Robinson, B.W. (1974) The origin of mineralization at the Tui mine, Te Aroha, New Zealand, in the light of stable isotope studies. *Economic Geology*, v. 69, p. 910–925.
- Student, J.J. and Bodnar, R.J. (2004) Silicate melt inclusions in porphyry copper deposits: Identification and homogenization behavior. *Canadian Mineralogist*, v. 42, p. 1583-1599.
- Zajacz, Z., Halter, W.E., Pettke T., Guillon, M. (2008) Determination of fluid/melt partition coefficients by LA-ICPMS analysis of co-existing fluid and silicate melt inclusions: controls on element partitioning. *Geochimica et Cosmochimica Acta*, v. 72, p. 2169-2197.

Matching low-temperature microthermometric observations and LA-ICP-MS fluid composition data.

John Ridley

**Department of Geosciences, Colorado State University, Fort Collins, CO 80523, U.S.A*

Systematic patterns of hydrothermal fluid solute content are becoming apparent from the increasing number of fluid inclusion multi-element LA-ICP-MS data. An additional and independent recent important result is the recognition that many magmatic-hydrothermal fluids are undersaturated with respect to halite: They are low to moderate salinity fluids in which the last phase to dissolve on heating inclusions is typically ice, or clathrate if the fluid is gas bearing. The LA-ICP-MS fluid inclusion analyses (e.g. Audétat et al., 2008) show that in distinct contrast to inclusions of Na-Ca basinal waters, Na, K and Fe are in sub-equal concentrations in many of these lower-salinity magmatic-hydrothermal inclusion fluids. In view of these results, it is appropriate to reassess what we can and should infer about fluid solutes from inclusion petrography and from microthermometric observations and data on lower-salinity fluids.

Although there are almost no data, the known eutectic temperatures (e.g. Borisenko, 1977), phase relations at 0 °C (Atbir et al., 2000b), and the principle that ice-melting temperatures are functions of water activity, allow us to interpret that the low-temperature behaviour of the FeCl_2 – NaCl – H_2O system is very similar to that of the well studied CaCl_2 – NaCl – H_2O system. The eutectic composition in both systems is NaCl poor, and the sequence of dissolution on heating for almost all of the range of fluid compositions should be FeCl_2 -hydrate – hydrohalite – ice. FeCl_2 -hydrate dissolution will be at the eutectic, and we are thus unlikely to image and be able to identify crystals of this phase. Although eutectic temperatures in the Fe-bearing systems are higher than in Ca-bearing systems, in view of our observations that eutectic melting is often difficult to recognise (e.g. Samson and Walker, 2000), and may in any case be disequilibrium melting (e.g. Davis et al., 1990), recorded temperatures should be interpreted with caution. In fact, other than the equilibrium eutectic temperature, the solidus phase diagrams of all mixtures of NaCl and one or multiple of the common bivalent chloride salts are very similar if concentrations are considered on a molar basis. Unless we have specific evidence, we should describe all fluids in which hydrohalite and ice-melting temperatures are identified as *Na-bivalent cation-chloride* fluids, and quantify components on this basis.

Whether the inherent limitations on microthermometric observations are such that we should be even more circumspect and describe fluids with this behaviour as monovalent – bivalent chloride salt mixtures is unclear. The hydrohalite solidus field has a relatively restricted extent in the system NaCl – KCl – H_2O (Hall et al., 1988), and many analysed lower-salinity fluids have K:Na ratios greater than about 1:4, such that the predicted sequence of mineral dissolution is hydrohalite – sylvite – ice, with sylvite melting most likely between the eutectic temperature of -22.9 °C and about -15 °C. This sequence has however not been described.

There is no experimental data on the system KCl – FeCl_2 – H_2O for temperatures below 0 °C, nor on the three salt system NaCl – KCl – FeCl_2 . Phase diagrams at 0 °C imply that eutectic compositions are only slightly less FeCl_2 -rich than for the NaCl-bearing system (Atbir et al., 2000a). We do not however know the extent of the solidus hydrohalite field in the ternary salt system.

REFERENCES

- Atbir A, Aneflous L, Marrouche A, El Hadek M, Cohen-Adad R and Cohen-Adad M-Th, 2000a, Diagramme polythermique du système ternaire KCl-FeCl₂-H₂O entre 0 et 70°C. *Journal of Thermal Analysis and Calorimetry* 59, 891-900.
- Atbir A, Mancour-Billah S, Marrouche A, El Hadek M, Cohen-Adad R and Cohen-Adad M-Th, 2000b, Diagramme polythermique du système ternaire NaCl-FeCl₂-H₂O entre 0 et 70°C. *Journal of Thermal Analysis and Calorimetry* 61, 157-164.
- Audétat A, Pettke T, Heinrich C A and Bodnar R J, 2008, The composition of magmatic-hydrothermal fluids in barren and mineralized intrusions. *Economic Geology* 103, 877-907.
- Borisenko A S, 1977, Study of the salt composition of solutions of gas-liquid inclusion in minerals by the cryometric method. *Geologiya i Geofizika* 18, 16-27.
- Davis D W, Lowenstein T K and Spencer R J, 1990, Melting behavior of fluid inclusions in laboratory-grown halite crystals in the systems NaCl-H₂O, NaCl-KCl-H₂O, NaCl-MgCl₂-H₂O, and NaCl-CaCl₂-H₂O. *Geochimica et Cosmochimica Acta* 54, 591-601.
- Hall D L, Sterner S M and Bodnar R J, 1988, Freezing point depression of NaCl-KCl-H₂O solutions. *Economic Geology* 83, 197-202.
- Samson I and Walker R T, 2000, Cryogenic Raman spectroscopic studies in the system NaCl – CaCl₂ – H₂O and implications for low-temperature phase behaviour in aqueous fluid inclusions. *Canadian Mineralogist* 38, 35-43.

Petrogenesis and metal budget of three volcanoes in the Chichinautzin monogenetic field, Mexico: A Melt Inclusion Study

Roberge, J.*, Mercer, C.N.**, Kent, A.J.R.***, Guillbaud, M-N.****, Arrieta-Garcia G.****

*ESIA-Ticomán, Instituto Politécnico Nacional, Mexico City, Mexico

**USGS, Denver, CO USA

***College of Earth, Ocean and Atmospheric Sciences, Oregon State University, OR USA

****Instituto de Geofísica, UNAM, Mexico City, Mexico

Melt inclusions are becoming a powerful tool to track metal contents in magmatic reservoirs. In fact, metals like Li, Cu, Zn, Mo, Ag, Sn, W, and Pb, are becoming more common in trace element analyses. Investigating the metal contents in magma reservoirs of currently active volcanic systems provides insights into the partitioning behavior of metals between melts, minerals, and volatiles. This in turn, will help us understand the processes that form fossilized magmatic-hydrothermal ore deposits and barren systems. In this work, we present volatiles (H₂O, CO₂, S, Cl), major and trace element contents of olivine-hosted melt inclusions from three monogenetic volcanoes (Pelagatos, Xitle and Guespalapas) within the Sierra Chichinautzin volcanic field located in the central portion of the arc-related Trans Mexican Volcanic Belt (south-east of Mexico City). Documenting metal contents in monogenetic basaltic andesites is important because they may represent ordinary melts that could evolve into parental magmas that feed stratovolcanoes and produce porphyry ore deposits.

The melt inclusions presented in this work are basaltic to andesitic in composition (after post-entrapment crystallization corrections), with 1.84 - 6.02 wt% MgO, 51.95 – 60.91 wt% SiO₂ and 0.64 – 3.00 wt% K₂O. The H₂O content varies from 0.5 to 4.3 wt% whereas that of CO₂ varies from below detection up to 976 ppm. Sulfur contents vary from 35 to 1451 ppm, showing a decrease with increasing MgO (and K₂O) contents (Fig. 1) suggesting that S is being lost from the melt with progressive differentiation. But since S concentrations do not correlate with any other gas phase (H₂O, CO₂, Cl) we hypothesize that it partitioned into an immiscible fluid or mineral phase. On the other hand, Cl contents are broadly constant (900 to 1267 ppm), and show no correlation with MgO or K₂O.

All analyzed metals (Li, Cu, Zn, Mo, Ag, Sn, W, Pb) behave incompatibly showing a positive correlation with La (Fig. 1). Concentrations of Cu (18 to 82 ppm), Zn (30 to 107 ppm), Mo (X to X ppm), and Pb (2 to 8 ppm) correlate positively together indicating that fractional crystallization concentrates these elements. In this case crystal fractionation plays the primary role in controlling metal abundances, with Cu, Zn, Mo, W, and Pb showing similar variations to incompatible trace elements like Rb and Ba. During the course of basalt to basaltic-andesite generation in a monogenetic volcano, fractional crystallization selectively concentrates Cu and Sn to values above the average basaltic andesite, while the other metals such as Pb or Zn, nor Mo or W, which are still behaving incompatibly, remain at concentrations at or below average. Cu and Sn concentrations in the most evolved melt inclusions are above the average basalt - andesite abundance of Robb (2005), but are below ore-forming concentrations, such as those observed in melt inclusions from White Island, NZ (Rapien et al., 2003). Continuing work to document metal concentrations in the early stages of magma petrogenesis is a much needed step to help better understand the role of early magmatic processes in the development of more evolved ore-forming magmas.

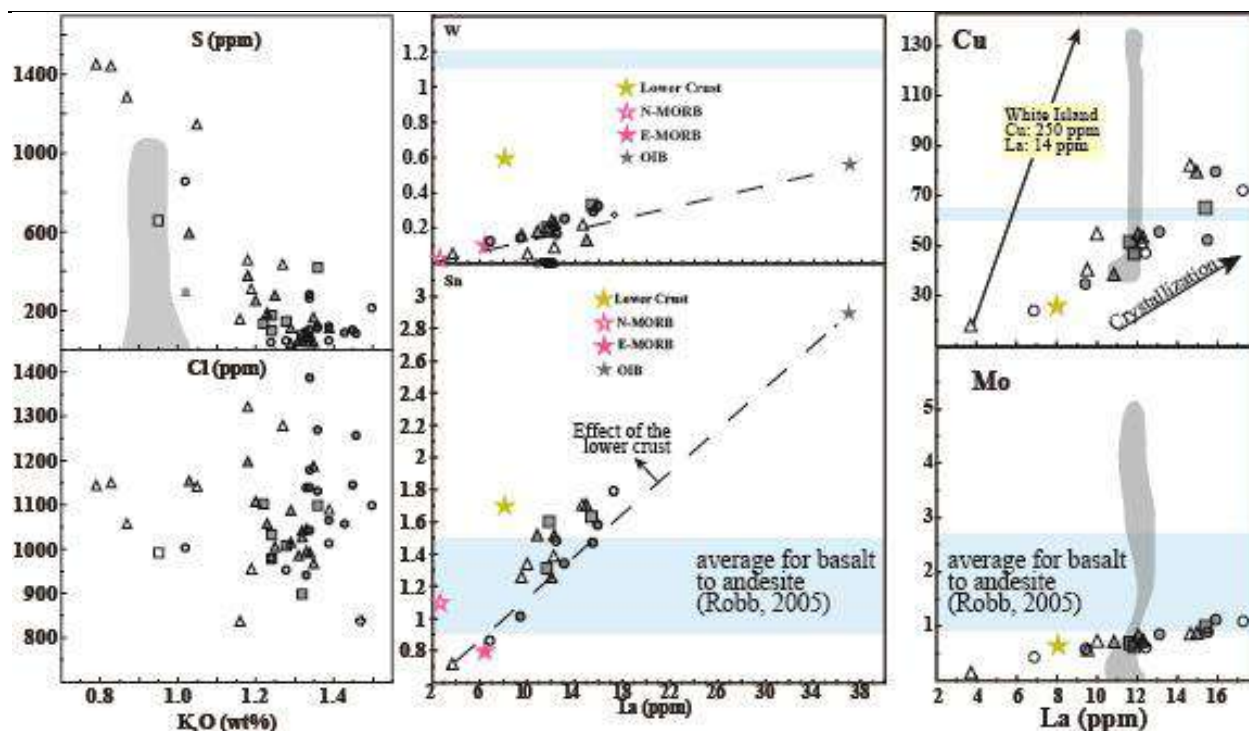


Figure 2: Graphs of selected volatiles and metals from Pelagatos, Guespalapas and Xitle monogenetic volcanoes, Sierra Chichinautzin, Mexico. The MORB and OIB data are from Sun and McDonough (1989), the upper crust data are from Rudnick and Gao (2003).

REFERENCES

- Rapien, M. H., R. J. Bodnar, S. F. Simmons, C. S. Szabo, C. P. Wood, and S. R. Sutton. "Melt inclusion study of the embryonic porphyry copper system at White Island, New Zealand." *Special Publication-Society of Economic Geologists* 10 (2003): 41-60.
- Robb, L. 2005. *Introduction to Ore-Forming Processes*. Blackwell Science Ltd. p 373.
- Rudnick, R. L. & Gao, S. (2003). The composition of the continental crust. In: Rudnick, R. L. (ed.) *Treatise on Geochemistry*, Vol. 3, The Crust. Oxford: Elsevier Pergamon, pp. 1-64.
- Sun, S. S. & McDonough, W. F. (1989). Chemical and isotopic systematics of oceanic basalts: implications for mantle composition and processes. In: Saunders, A. D. & Norry, M. J. (eds) *Magmatism in the Ocean Basins*. Geological Society, London, Special Publications 42, 313-345.

Ore-forming fluids associated with the early mineralization at Cerro de Pasco, Peru

Rottier B.*, Kouzmanov K.*, Fontboté L.*, Wälle M.,**

* Earth and Environmental Sciences, University of Geneva, 1205 Geneva, Switzerland
 Bertrand.Rottier@unige.ch

** Institute of Geochemistry and Petrology, ETH Zürich, 8092 Zürich, Switzerland

Cerro de Pasco, central Peru, is a large Cordilleran base metal deposit formed along the eastern margin of a diatreme-dome complex, as part of the Miocene metallogenic belt of central and northern Peru (Baumgartner et al, 2008). It was formed during successive stages of mineralization by fluids with contrasting fS_2 , fO_2 and pH. During the first stage, were emplaced a number of pyrrhotite pipes that contain minor arsenopyrite and Fe-rich sphalerite as well as traces of chalcopyrite, galena and stannite, they grade outwards into massive Fe-rich sphalerite and galena replacement bodies. They are structurally controlled by major N-S faults. During the second stage, a massive body consisting mainly of pyrite and quartz was emplaced. It is associated with a pervasive sericite-pyrite alteration affecting the diatreme-dome complex. Simultaneously, the root of the diatreme-dome complex (at a depth from 3350 to 3750 m.a.s.l.) is crosscut by structure-controlled pyrite-quartz veins with sericite alteration haloes. These veins are interpreted as feeders of the pyrite-quartz body. Following the emplacement of the pyrite-quartz body, high-sulfidation mineralization was formed, in the western part of the deposit as a set of E-W-trending Cu-Ag-(Au-Zn-Pb) enargite-pyrite veins hosted by the diatreme-dome complex, and, in the eastern part - as large well-zoned Zn-Pb-(Bi-Ag-Cu) carbonate replacement ore bodies (Figure 1).

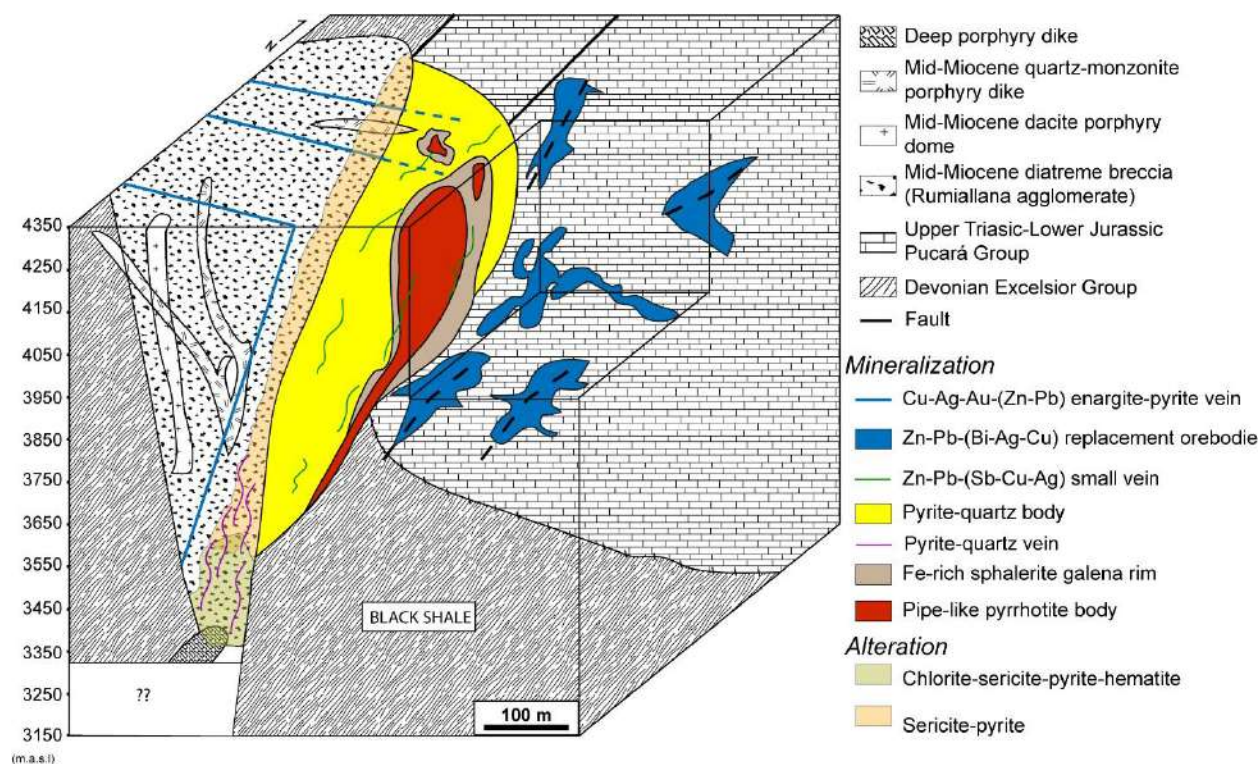


Figure 3: Block diagram showing the different mineralizing events (modified from Baumgartner et al., 2008).

In the present work, primary and pseudo-secondary fluid inclusion assemblages (FIAs) hosted in Fe-rich sphalerite and quartz from the pyrrhotite pipes and their rims and in quartz from the pyrite-quartz

body have been studied. In the deep pyrite-quartz veins, pseudo-secondary and secondary FIAs, clearly coeval with pyrite precipitation, have been used. All fluid inclusions are aqueous, liquid-rich, with 20-30 vol% vapor phase. No evidence of phase separation has been observed. FIAs show progressive salinity decrease with time from 18.5 to 2.7 wt% NaCl equiv. at relatively constant homogenization temperatures (Th) between 280 and 220°C; higher Th (up to 350°C) are also recorded in the deep pyrite-quartz veins.

Typical intermediate-density fluids exsolving directly from magma have salinities between 3 and 8 wt% NaCl equiv (Audétat et al., 2008). Fluid salinities above these values generally result from boiling and/or mixing with basinal brines. However, at Cerro de Pasco, neither boiling nor mixing with external brines could be evidenced. A way to explain such high salinity is to mix deep magmatic brines previously formed and stored at depth with less saline fluids.

Preliminary fluid inclusion analyses by LA-ICP-MS have been conducted on FIAs hosted by Fe-rich sphalerite from the pyrrhotite pipes and quartz from the deep pyrite-quartz veins. The results show that FIAs with higher salinity are highly enriched in metals, up to 1.3 wt% Mn, 0.9 wt% Pb, 0.5 wt% Sb in the pyrrhotite pipes, and up to 5.3 wt% Fe, 2.3 wt% Mn, 0.9 wt% Zn, 0.2 wt% Sb, 0.1 wt% Pb in the deep pyrite-quartz veins. Decrease of metal content correlates with decrease in salinity, less saline FIAs show metal contents which are at least two orders of magnitude lower. Our results are compatible with progressive dilution of stored metal-rich magmatic brines at depth. Significant differences in Pb, Sb and Mn contents between high-salinity fluids from the pyrrhotite pipes and the deep pyrite-quartz veins suggest that the two mineralization styles were formed by two separate mineralizing stages, related to chemically different fluids.

Origin of less saline fluid diluting the stored brines is quite puzzling. At Fresnillo, Simmons (1991), and Wilkinson et al. (2013) invoke implication of meteoric water. No low-salinity fluids (< 2 wt% NaCl equiv.), generally attributed to meteoric water, have been identified for the studied stages in the present work. Strong magmatic signature of the fluid is also supported by oxygen isotopes of hydrothermal quartz from the pyrite-quartz body $\delta^{18}\text{O}_{\text{quartz}} = 16.0 - 17.2\text{‰}$ VSMOW (Baumgartner et al., 2008) corresponding to $\delta^{18}\text{O}_{\text{water}} = 6.5 - 7.2\text{‰}$ VSMOW (at 250°C). These heavy $\delta^{18}\text{O}_{\text{water}}$ values are unlikely equilibrated meteoric waters. Modeled $\delta^{18}\text{O}$ values of exchanged with surrounding host rocks meteoric water, calculated using the equation of Ohmoto and Rye (1974), show that very low water/rock ratio (<0.1) and relatively important temperature (>250°C) are necessary to obtain such signatures. In addition, Cs content in the different FIAs is constant, which is incompatible with a mixing with meteoric water scenario. The new data are best explained by mixing between two different magmatic fluids, a brine previously formed by deep boiling and stored at depth, and a low-salinity one (≤ 3 wt% NaCl equiv.) probably exsolved directly from a new magma batch.

This mechanism, could explain the rise of base metal-rich high-salinity fluids derived from magmatic brines in the shallow epithermal environment of porphyry systems, and therefore the high Zn-Pb-(Ag) grades of such deposits, without invoking mixing with meteoric fluids at considerable depth.

REFERENCES

- Audétat A, Pettke T, Heinrich C, Bodnar R (2008) The composition of magmatic–hydrothermal fluids in barren versus mineralized intrusions. *Economic Geology*. V.103. p.877–908.
- Baumgartner R, Fontboté L, Vennemann T (2008) Mineral zoning and geochemistry of epithermal polymetallic Zn-Pb-Ag-Cu-Bi mineralization at Cerro de Pasco, Peru. *Economic Geology*. V.103. p.493-537.
- Simmons S (1991) Hydrologic Implications of Alteration and Fluid Inclusion Studies in the Fresnillo District, Mexico: Evidence for a Brine Reservoir and a Descending Water Table during the Formation of Hydrothermal Ag-Pb-Zn Orebodies. *Economic Geology*. V.86. p.1579-1601.
- Wilkinson J, Simmons S, Stoffell B (2013) How metalliferous brines line Mexican epithermal veins with silver. *Scientific reports*. V.3. 7p.
- Ohmoto H, Rye R (1974) Hydrogen and oxygen isotopic composition of fluid inclusions in the Kuroko deposits, Japan. *Economic Geology*. V.69. p.947-953.

Fluid evolution in an Andean geothermal system: coupling fluid inclusions thermometry, LA-ICP-MS and geochemical modeling

Sánchez-Alfaro, P.^{1,2}, Driesner, T.³, Heinrich, C.³, Reich, M.^{1,2}, Pérez-Flores, P.^{2,4}, Arancibia, G.^{2,4}, Cembrano, J.^{2,4}, Campos, E.^{2,5} and Lohmar, S.⁶

¹ Universidad de Chile, Santiago, Chile

² Centro de Excelencia en Geotermia de los Andes, Chile

³ ETH Zürich, Isotope Geochemistry and Mineral Resources, Zürich, Switzerland

⁴ Pontificia Universidad Católica de Chile, Santiago, Chile

⁵ Universidad Católica de Antofagasta, Chile

⁶ MRP Geotermia Chile

The nature of the interplay between active tectonics and fluid flow is a key feature to better understand the chemical evolution of fluids in geothermal and hydrothermal systems.

The objective of our current research is to assess the feedback between brittle deformation, chemical evolution of fluids and mineral paragenesis in the geothermal field of Tolhuaca in the Southern Andes volcanic zone. Tol-1 is a vertical 1.080 m deep core hole that yields relevant information regarding the evolution of the Tolhuaca geothermal system. The methodology includes fluid inclusion analysis using microthermometry and LA-ICP-MS in structurally-oriented fault-veins and veins hosted in the host rocks, and chemical analysis of the present-day vapor and liquid fluid phases from the geothermal reservoir. In order to establish the pressure (P)-temperature (T)-composition (X)-enthalpy (H) evolution of the fluids and determine the dominant mechanism(s) of heat transport, temperature-depth profiles of the geothermal wells and microthermometric/LA-ICP-MS data from fluid inclusions were combined with multiphase heat and mass transfer simulations using HYDROTHERM.

Our results indicate that the metalloid concentrations (e.g., B, As) in paleo-fluids and present-day fluids are significantly different, strongly suggesting changes in the deep magmatic vapor contribution. Moreover, the structural and mineralogical vertical segmentation and the evidence of brecciation and wide-spread boiling episodes reveal a periodical feedback between fault-fractures networks activation and mineralization sealing the conduits for fluid flow. Therefore, transient permeability changes due to the tectonic cycle (fault valve and/or suction pump mechanism) might be responsible for boiling episodes recorded in breccias and silica polymorph co-precipitation as has been reported in epithermal deposits. This hypothesis is being tested by numerical experiments of heat-fluid-rock interaction using GEMS code in geologically meaningful P-T-H conditions.

Developments in fluid inclusion compositional estimation from combined microthermometric and microanalytical data

Steele-MacInnis, M.*

*Institute for Geochemistry and Petrology, ETH Zurich, Clausstr. 25, 8092 Zurich, Switzerland

Fluid inclusions (FI) provide one of the best available means for determining the compositions of geologic fluids responsible for fluid-rock reactions and hydrothermal ore-forming processes. Compositions of fluid inclusions are commonly estimated based on the freezing point depression, according to the known vapor-saturated liquidus relations of model systems such as H₂O-NaCl (e.g., Bodnar, 1993). Moreover, microthermometry can provide some constraints on the presence and concentrations of additional salt (and/or gas) components, based on the observed eutectic temperature and/or second-to-last solid phase dissolution temperature. Recent advances in microanalytical techniques allow estimates of the ratios of elements in FI (LA-ICPMS; Heinrich et al., 2003) as well as estimates of the total molar concentration of chlorides (Raman spectroscopy; Mernagh and Wilde, 1989). When used together, these techniques can provide detailed and precise major- and trace-element compositional estimates for aqueous FI. However, at present the methods used for integrating microthermometric and microanalytical data for compositional estimates are empirical and semi-quantitative; meanwhile, experimental data on the freezing point depressions of complex, multicomponent fluids are scarce.

Recently, Leisen et al. (2012) suggested to determine FI compositions by combining microthermometric and microanalytical measurements through the thermodynamic formalisms pioneered by Pitzer (1973). In the present study, FI compositional determinations are extended to fluid inclusions with complex compositions using Pitzer's formalism, based on the extensive developments of Pitzer's model for salt- and gas-bearing fluids compiled by Marion and Kargel (2008). Pitzer's model has several advantages: (1) the model is applicable up to high solute concentrations (up to and exceeding salt saturation); (2) the model accurately predicts the solid-liquid-vapor equilibria of complex multicomponent systems based on only a few binary and ternary interaction parameters; (3) aqueous electrolytes of various cations and anions can be included simultaneously, as well as dissolved gases such as CO₂. In the present study the model is applied to aqueous FI containing Na-K-Ca-Mg-Fe-H chlorides. Vapor-saturated liquidus diagrams are predicted for these complex, multicomponent fluids. The effect of fluid pH on FI freezing point depressions is assessed, and the model is used to predict the role of additional anions (other than chloride), as well as various gases, on FI measurements. The model based on Pitzer's (1973) method is implemented in a new computer program to facilitate compositional estimates.

REFERENCES

- Bodnar, R.J. (1993) Revised equation and table for determining the freezing point depression of H₂O-NaCl solutions. *Geochimica et Cosmochimica Acta*. 57. 683-684.
- Heinrich, C.A., Pettke, T., Halter, W.E., et al. (2003) Quantitative multi-element analysis of minerals, fluid and melt inclusions by laser-ablation inductively-coupled-plasma mass-spectrometry. *Geochimica et Cosmochimica Acta*. 67. 3473-3496.
- Leisen, M., Dubessy, J., Boiron, M.-C., Lach, P. (2012) Improvement of the determination of element concentrations in quartz-hosted fluid inclusions by LA-ICP-MS and Pitzer thermodynamic modeling of ice melting temperature. *Geochimica et Cosmochimica Acta*. 90. 110-125.
- Marion, G.M., Kargel, J.S. (2008) *Cold Aqueous Planetary Geochemistry with FREZCHEM*. Springer-Verlag. 254 pp.
- Mernagh, T.P., Wilde, A.R., 1989. The use of laser Raman microprobe for the determination of salinity in fluid inclusions. *Geochimica et Cosmochimica Acta*. 53. 765–771.
- Pitzer, K.S. (1973) Thermodynamics of electrolytes. I. Theoretical basis and general equations. *Journal of Physical Chemistry*. 77. 268-277.

Liquid immiscibility – important processes during pegmatite formation

Thomas, R. *, Davidson, P. **

* GFZ German Research Centre for Geosciences, Potsdam, Germany

** ARC Centre of Excellence in Ore deposits, University of Tasmania, Hobart, Australia

The study of melt inclusions in minerals of granitic and pegmatitic rocks showed that there are usually two different types present, which differ principally in their bulk water content. Using the micro-Raman spectroscopic technique, since 1999 developed into a practical routine method, allows simple determination of water in glass and melt inclusions from 10 ppm to 40 % (g/g). However, there are also important differences in their concentrations of a number of elements (B, F, Cl, Li, Na, K, Rb, Cs, Be) and compounds (H_2O , OH^- , CO_2 , HCO_3^- , CO_3^{2-} , SO_4^{2-} , PO_4^{3-}) that can affect the solubility of silicates.

A comprehensive presentation of the water concentration in melt inclusions of granites and pegmatites are given in Thomas and Davidson (2012). According to the compiled data in it, the water concentration in granite melt inclusions is generally < 10% with three maxima at 4.0 ± 1.3 , 5.9 ± 1.2 and $8.1 \pm 1.1\%$ water. This data corresponds very well with data presented by Naumov et al. (2010). For granite pegmatites, a larger range of water contents was found: from 2 to more than 50% water with two distinct maxima at 10.5 ± 8.1 and $26.2 \pm 14.3\%$. In a number of papers (e.g., Thomas et al. 2012a, 2012b and references therein) we have shown that the great spread and generally high water content of the pegmatite-forming melts, conserved as melt inclusions in minerals, are the result of melt-melt immiscibility processes connected with the formation of conjugate melt fractions with contrasting physical and chemical characteristics, which also have a major influence on the element partitioning between such fractions.

Significantly, previous (Thomas et al. 2005) and more recent studies (Thomas et al. 2009) on melt inclusions in minerals of granitic rocks have shown that in quartz of these rocks very water-rich melt inclusions are also present. Originally, due to the very high number of these evolved melt inclusions we interpreted the Zinnwald topaz-albite rock as embryonic pegmatite with a too many crystallization nuclei to permit pegmatite crystallization. However further studies on very different granitic rocks (Precambrian Kymi granite, Finland, Variscan granites of the Erzgebirge in general, the granite from Königshain, Germany, and the Pliocene Eldzhurtinsk I-type biotite granite, Caucasus, Russia) have unambiguously shown that water-rich melt inclusions are rare, but nevertheless present in early generations of quartz in many different granites. Now, (Thomas and Davidson 2013) we have interpreted such early water-rich melt inclusions as remnants of the primary volatile-rich melt fractions formed by the crystallization of the anhydrous minerals quartz and feldspar. Due to the chemical difference in composition from point to point, their low density and high volatile concentration, resulting in low viscosity, and the tendency for decoupling from the bulk system by dewetting, such melt fractions will move rapidly away from the source region by intra-granular flow. We suggest that it is the merging of these different melt fractions that create pegmatite-forming magmas. According to their prevailing state of physical and chemical evolution such fractions can show very different compositions, which may produce equally diverse textures on crystallization. As long as the water concentration is high enough melt-melt-fluid immiscibility processes will operate.

As discussed, such melt fractions can move rapidly through the crystal mush and may achieve channelized flows to form pegmatitic structures of different types (e.g. schlieres, miarolitic pegmatites, veins or dykes) or may fail to be effectively drained and permeate the crystallized granite. Excellent examples of the last case are the fascinating pegmatitic granites in the Borborema pegmatite field/Brazil.

We have demonstrated (Thomas et al. 2012a, 2012b) using different pegmatites, that the process of liquid immiscibility is a widespread and very important process, for example for the extreme enrichment of rare elements to very high concentrations, exemplary shown by the behavior of Be in the Ehrenfriedersdorf granite-pegmatite system (Thomas et al. 2011). Volatile-rich melt inclusions contain as maximum 4.6 % (vol/vol) beryllonite [NaBePO_4] as daughter crystals, corresponding to nearby 10000 ppm Be. Such high enrichment would not be possible by the normal fractionated crystallization of a simple or evolved magma.

REFERENCES

- Naumov, V.B., Kovalenko, V.I., Dorofeeva, V.A., Girnis, A.V., Yarmolyuk, V.V. (2010) Average composition of igneous melts from main geodynamic settings according to investigation of melt inclusions in minerals and quenched glasses of rocks. *Geochem. Int.* 48. 1185-1207
- Thomas, R., Davidson, P. (2012) Water in granite and pegmatite-forming melts. *Ore Geology Reviews*. 46. 32-46
- Thomas, R., Davidson, P. (2013) The missing link between granites and granitic pegmatites. *Journal of Geosciences*. 58. 183-200
- Thomas, R., Davidson, P., Badanina, E. (2012a) Water- and boron-rich melt inclusions in quartz from the Malkhan pegmatite, Transbaikalia, Russia. *Minerals*. 2. 435-458
- Thomas, R., Davidson, P., Beurlen, H. (2012b) The competing models for the origin and the internal evolution of granitic pegmatites in the light of melt and fluid inclusion research. *Mineralogy and Petrology*. 106. 55-73
- Thomas, R., Davidson, P., Rhede, D., Leh, M. (2009) The miarolitic pegmatites from Königshain: a contribution to understanding the genesis of pegmatites. *Contribution to Mineralogy and Petrology*. 157. 505-523
- Thomas, R., Förster, H.-J., Rickers, K., Webster, J.D. (2005) Formation of extremely F-rich hydrous melt fractions and hydrothermal fluids during differentiation of highly evolved tin-granite magmas: a melt/fluid-inclusion study. *Contribution to Mineralogy and Petrology*. 148. 582-601
- Thomas, R., Webster, J.D., Davidson, P. (2011) Be-daughter minerals in fluid and melt inclusions: implications for the enrichment of Be in granite-pegmatite systems. *Contribution to Mineralogy and Petrology*. 161. 483-495

Using Evaporate Mound Chemistry of Fluid Inclusions to Assess the Metal Fertility and Fluid: Rock Interaction in a Large Peraluminous Batholith: A Case Study of the Mineralized (Sn-W-U-Cu-Zn-Ag) South Mountain Batholith, Nova Scotia, Canada

Tweedale, F. *, Hanley, J. *, Kontak, D.J. **, and Rogers, N. ***

**Department of Geology, Saint Mary's University, Halifax, Nova Scotia, Canada B3H 3C3
fergus.tweedale@smu.ca*

***Department of Earth Sciences, Laurentian University, 935 Ramsey Lake Rd, Sudbury Ontario, Canada P3E 2C6*

****Geological Survey of Canada, 601 Booth Street, Ottawa, Ontario, Canada K1A 0E8*

The 380 Ma South Mountain Batholith (SMB) of Nova Scotia is a large (~7300 km²), mesozonal granitoid intrusion that consists of 13 coalesced plutons of granodiorite to leucomonzogranitic composition which host a variety of mineralized zones (e.g., Sn-Zn-Cu-Ag, Mo, Mn-Fe-P, U, Cu-Ag). Given the hydrothermal nature of this mineralization, it is expected that a fingerprint of the mineralizing fluids might be manifested both petrographically and by the chemistry of secondary, quartz-hosted fluid inclusions (FIs) in the granites on a scale equal to or larger than the mineralized centres. In order to assess the potential of using the petrographic and chemical fingerprints as vector for exploration, a novel study integrating both these methods was investigated. The protocol involved in the study included the following: (1) completing a detailed petrographic study of archived samples (>500) that focused on the extent and degree of indices that reflect fluid: rock interaction. The indices included: (i) type and abundance of perthite, (ii) chloritic alteration of biotite, (iii) plagioclase alteration, (iv) amount of secondary muscovite, and (v) abundance of secondary FIs in quartz; and (2) determining the fluid chemistry of quartz-hosted FIs in >100 samples collected from a 100 km² grid superimposed on the SMB. The petrographic data are being used to design an alteration algorithm that can be used to map the extent of fluid: rock interaction throughout the batholith. The chemistry of the FIs was determined using SEM-EDS analysis of evaporate mounds which has previously been shown to be an effective means for determining the cation and anion contents fluids and that fluids in mineralized centres are often enriched in Fe, Mn and S (e.g., Kontak 2004). For this study, a protocol was specially designed (Tweedale et al. 2013) which first included making synthetic mounds to determine optimum counting times followed by making several runs on natural samples to determine the most effective temperature of decrepitation. Thus, in this study quartz chips were heated to 450°C and 16 mounds per sample were analysed (60 seconds) in raster mode, the latter to circumvent chemical variation related to elemental fractionation during mound formation. To date, the results for >700 mounds determined for 68 samples indicate that the fluids are dominated by Na-K-Ca-Cl-F with traces of Fe, Mn and S, and that two distinct types are present, one Na-K and the other Na-Ca-F, the latter being the more abundant in samples examined to date.

Although this study continues with the development of the alteration algorithm and completion of FI mound analysis still pending, some intriguing results are worthy of comment and we discuss two of these below which are recorded by the Na-Ca-F fluid: (1) the presence of elevated Ca in many samples, including those from chemically evolved and, hence, Ca-depleted rocks; and (2) the pervasive occurrence of F in mounds with up to 40 wt. % F (when normalized to 100%; Fig. 1) even in samples distal to known mineralization. The former feature is considered to reflect the petrographic observation of extensive albitization of plagioclase in all samples, although it is more pervasive in the most evolved rocks (e.g., leucomonzogranites). This alteration process involves a coupled dissolution-precipitation reaction (Putnis 2002) which leaves a distinct pitted texture in the product (i.e., albite; Fig. 2) and liberates Ca to the fluid. This process is attributed to the reaction of an orthomagmatic fluid with already crystallized granite, although it does not preclude some Ca contribution from a wall-rock derived metamorphic fluid, as indicated from stable isotopes (Carruzzo et al. 2004; Kontak and Kyser 2011). The second observation is the unexpected enrichment of F in one of the FI populations (Na-Ca-F), which is likely the first recognition of this phenomenon in granitic bodies on such a scale anywhere. That this fluid occurs in all rocks of the SMB,

including most primitive rocks (i.e., granodiorites), and across the entire intrusion suggests the generation of this F-rich fluid is part of the natural evolution of the system and consistent with the presence of topaz in both the most evolved magmatic rocks and as part mineralized greisens. Finally, that F enrichment occurs in the same fluid with Ca indicates a possible cause and effect relationship which we suggest relates to the reactive capacity of the original exsolved Na-F fluid.

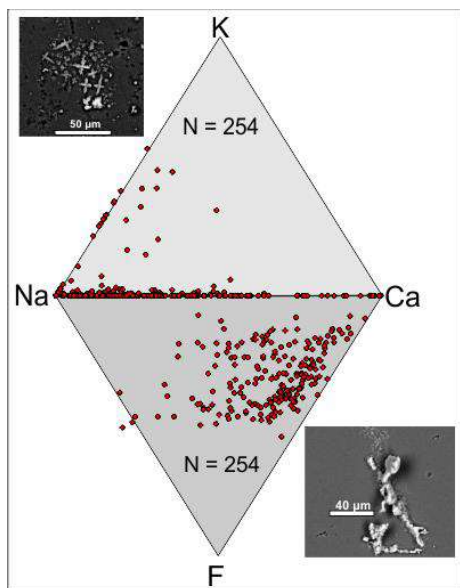
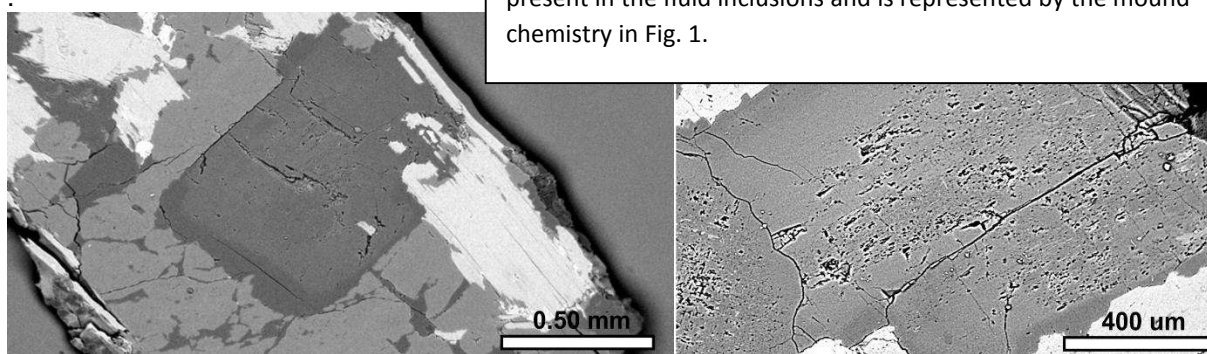


Fig. 1 (Left) Summary of SEM-EDS analysis of evaporate mounds from the South Mountain Batholith which shows two distinct fluid populations - Na(-K) and Na-Ca-F. Also shown as insets are representative mounds for these two fluid compositions and, as can be seen, there is a distinct difference in their shapes which relates to their different bulk compositions.

Fig. 2. (Below) Back-scattered SEM images of a monzogranite sample from the South Mountain Batholith. (Left) Plagioclase (An₃₀) grain surrounded by perthitic K-feldspar with mantle of albite and biotite (bright phase). (Right) Close-up of the core of the plagioclase grain showing a pitted area of An₀ composition that is surrounded by the original plagioclase of An₃₀ composition. This sample illustrates well the coupled dissolution-precipitation mechanism which released Ca to the fluid phase which is now present in the fluid inclusions and is represented by the mound chemistry in Fig. 1.



REFERENCES

- Carruzzo S., Kontak D.J., Clarke D.B., Kyser, T.K. (2004) Stable isotope study of mineralization in the New Ross area, South Mountain Batholith, Nova Scotia: evidence for multiple source reservoirs. *Canadian Mineralogist* 42:1425-1442.
- Kontak, D.J., Kyser, T.L. (2011) A fluid inclusion and isotopic study of an intrusion-related gold deposit (IRGD) setting in the 380 Ma South Mountain Batholith, Nova Scotia, Canada: evidence for multiple fluid reservoirs. *Mineralium Deposita* 46: 337-363.
- Putnis A. (2002) Mineral replacement reaction: from macroscopic observations to microscopic mechanisms. *Mineralogical Magazine* 66: 689-708.
- Tweedale, F., Hanley, J., Kontak, D.J., and Rogers, N. (2013) Petrographic observations and evaporate-mound analysis of quartz-hosted fluid inclusions: Applications to assess metal fertility in granites. Geological Association of Canada-Mineralogical Association of Canada Annual Meeting, Program with Abstracts, Winnipeg, MB, Canada.

Abstracts

Poster abstracts

Fluid Inclusions and Stable Isotopes (O, H, S, C) Document Fluid Mixing in the Ore-forming Systems of the Daraloo and Sarmeshk Porphyry Cu Deposits, Central Part of the Dehaj-Sardoeieh Belt, South Iran

Alimohammadi, M.* , Kontak, D.J.** , Alirezaei, S.* , and Kyser, K.T.**

* Faculty of Earth Sciences, Shahid Beheshti University, Tehran, Iran, Malimohammadi@laurentian.ca

** Department of Earth Sciences, Laurentian University, 935 Ramsey Lake Rd, Sudbury Ontario, Canada P3E 2C6,

Institution information for second author (if required) should be Arial italics 10 point font

***Department of Geological Sciences and Engineering, Queen's University, Kingston, Ontario, Canada K7L 3N6

The Daraloo and Sarmeshk porphyry Cu deposits occur in a NW-SE trending fault zone in the southern section of the Cenozoic Urumieh-Dokhtar Magmatic Belt of southern Iran. In this zone, a belt of alteration defines a NW-SE trending zone 10 km long and 0.5-1 km wide with the Daraloo and Sarmeshk deposits occurring at the NW and SE ends, respectively. The area is characterized by a series of porphyritic tonalite-granodiorite plutons of inferred Miocene age that intrude Eocene andesites and pyroclastic rocks; all these rocks are intruded by post-ore granodiorite plutons and dykes. Alteration assemblages present are comparable to those reported from many porphyry Cu \pm Mo systems globally and are well developed in both the Daraloo and Sarmeshk deposits, with phyllic alteration being the predominant alteration style observed at current exposures and in drill core. Based on the cross-cutting relations, vein mineralogy, textures and the associated alterations, several principal stages of vein formation can be distinguished. Fluid inclusion microthermometry and stable isotopic analysis (O, H, S, C) on representative samples from both mineralized and barren veins and various alteration assemblages are used to constrain the nature of the fluids and the PTX conditions of the mineralizing event.

Based on observations at room temperature, five fluid inclusion assemblages (FIAs) are observed in vein quartz from the different alteration zones and also as secondary inclusions in quartz grains hosted by porphyry stocks. In order of decreasing abundance, the 5 FIAs are (Fig. 1): (I) Liquid-rich L-V type; (II) Vapor-rich L-V type; (III) L-V-Halite type; (IV) L-V-Sylvite(?) -Hematite type; and (V) L-V-Multi-solid type. Type I inclusion are most abundant in vein quartz from the argillic zone, whereas high-salinity types (III, IV, V) are most abundant in quartz-magnetite veinlets from the potassic zone where they occur on healed fracture planes together with inclusion types I and II. Microthermometric data have been obtained from: (1) quartz-magnetite alteration in the potassic zone having disseminated copper, (2) quartz-chalcopyrite-pyrite veins from the phyllic-argillic zone, and (3) quartz grains in a porphyry stock. Thermometric runs for inclusion types (Fig. 2A) indicate the following: (1) ice was the last phase to melt in all L-V inclusions (-25° to 0°C), but rarely melting of hydrohalite (-38 to -21°C) was observed; (2) lack of clathrate formation or freezing of the vapor phase precludes the presence of significant condensed gases (e.g. CO₂); (3) fluid salinities range from 0 to 50 wt. % eq. NaCl with two distinct groupings that correspond to types I-II and type III inclusions (Fig. 2A); and (4) Th occurred over the range 200° to 425°C for types I-III. The compositions of the fluids are inferred based on: (1) melting of ice and hydrohalite; (2) dissolution of solid phases; and (3) SEM-EDS analysis of evaporate mounds. Integration of these data indicate the fluids are Na -rich with the addition of K, Fe, Ca and Mn with decoupling of K from Ca and Mn and lesser Fe, whereas Na is generally coupled with K and Fe and to a lesser extent Mn. The presence of considerable S, to 24 wt. % for mounds on a normalized basis, is noted in the potassic and phyllic alteration zones.

The FIAs record the evolution through the paragenesis, that is potassic to phyllic-argillic alteration, of an early higher T (Th = 230-400°C), saline (33-50 wt. % eq. NaCl) magmatic fluid possibly trapped at high P (Fig. 2B), to a lower-T, lower-salinity (0-23 wt. % eq. NaCl) fluid trapped at lower P that also records the ingress and mixing with meteoric fluids. The highest-T and most saline fluids are mainly recorded in early magnetite + quartz veins in the core of the alteration system and are considered to be the most primitive fluid in the deposit. Cooling of this fluid coincides with potassic-phyllic alteration and the main-stage copper mineralization. Dilution of the residual, cooler magmatic fluid after main-stage copper introduction is coincident with feldspar destructive (phyllic-argillic) alteration.

Isotopic data for vein minerals indicate $\delta^{18}\text{O}_{\text{H}_2\text{O}}$ values, calculated for 300° to 400°C, range from -4.5 to +6.8‰ for quartz (n=16), +2 to +4‰ for barite (n=2), and +3.2 to +5.2‰ for calcite (n=2). These data suggest mixing of magmatic-derived fluids with meteoric fluids, which is also supported by δD values (fluid inclusions in quartz) of -62 to -100‰. In addition, $\delta^{34}\text{S}$ for pyrite and chalcopyrite (+2.2 to +8.7‰, n=13) and barite (+13 to 14.6‰, n=2) suggest sulfur is either crustal in origin or represents mixing of mantle and crustal reservoirs, as does $\delta^{13}\text{C}$ for calcite (0 to +0.7‰, n=2).

This integrated fluid inclusion-stable isotope study shows that the fluid evolution of the Daraloo and Sarmeshk porphyry Cu deposits reflects interaction of a magmatic, metal-rich fluid that dominated the early, high-T, potassic-altered stages of the mineralized systems with incursion of later meteoric fluids coincident with the phyllic and argillic stages of alteration. The use of evaporate mound analysis also allows a more complete characterization of these fluids, in particular the documentation of the presence of K, Ca, Fe, and Mn, in addition to S in the early stage mineralizing fluids.



Figure 1. The five FIAs (from L to R types 1 to 5) in the Daraloo and Sarmeshk porphyry Cu deposits. Inclusions are all 15-30 μm in maximum length. Note the presence of red hematite in type IV FIA.

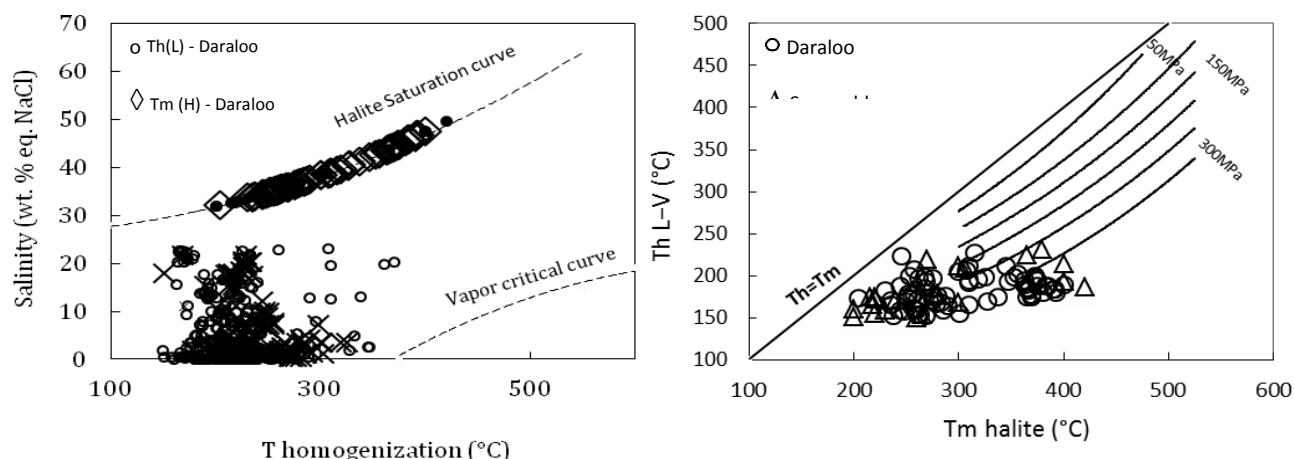


Figure 2. Thermometric data for fluid inclusions from the Daraloo and Sarmeshk porphyry Cu deposits. (A) Plot of salinity vs. Th (°C) for types I-III inclusions in Daraloo and Sarmeshk deposits; (B) Plot of Th L-V (°C) vs. Tm halite (°C) for type III inclusions with isobars (after Becker et al. 2008).

REFERENCES

Becker, S.P., Fall, A., Bodnar, R.J. (2008) Synthetic Fluid Inclusions. XVII.1 PVTX Properties of high salinity H_2O -NaCl solutions (>30 wt % NaCl): Application to fluid inclusions that homogenize by halite disappearance from porphyry copper and other hydrothermal ore deposits. *Economic Geology* 103: 539-554.

Testing Established Models of Hydrothermal Fluid Distribution Around Porphyry Deposits: The Application of Fluid Inclusion Research to Porphyry Exploration

Bain, W.B.*, Cline, J.S.*, Marsh, T.M.**

**University of Nevada, Las Vegas, 4505 S Maryland Pkwy, Las Vegas, NV 89119, USA*

***4750 N Bonanza Ave, Tucson AZ, 85749, USA*

Previous publications have summarized the physical and chemical characteristics and spatial distribution of ancient, ore-forming fluids trapped in fluid inclusions from productive porphyry deposits. These studies have provided an understanding of the fluids that form these deposits, and have established models of how fluid inclusions are distributed throughout porphyry systems (Reynolds and Beane, 1985; Hedenquist et al., 1998; Muntean and Einaudi, 2000; Ulrich et al, 2001; Rusk et al, 2008; Landtwing et al, 2010;). These fluid inclusion distribution models are important to our current understanding of porphyry deposits and should have predictive power that geologists can use to explore for new mineral resources.

The Kabba porphyry prospect in northwestern Arizona has been the focus of exploration and small-scale mining for over 90 years. This prospect contains two spatially related areas of pervasive porphyry style alteration and mineralization. One area on the eastern flanks of the Hualapai Mountains has surface exposures with pervasive quartz veining, sparse Cu-Mo mineralization, and porphyry style alteration. This area is hosted by Precambrian metamorphic and Laramide intrusive rocks, and has been the focus of most of the historic mining and exploration in the area. The other area is located under Quaternary gravels in the valley east of the Hualapai Mountains and was encountered during recent drilling by Bell Copper Corp. This area also contains pervasive quartz veining, porphyry style alteration, and Cu-Mo-Zn-Pb mineralization. Despite numerous exploration programs and drilling efforts in the area, no large-scale economic porphyry or base metal mineralization has been identified in this region. One hypothesis is that the mineralization and alteration exposed on the surface might be part of a porphyry system that has been dissected and exposed by Basin and Range faulting. A possible result is that the two zones of alteration and mineralization might represent the intermediate and deep zones of a single porphyry system that were separated by a north-south trending normal fault.

This study is testing the predictive power of established fluid inclusion distribution models by applying them to the Kabba porphyry prospect. If the two field areas do represent a faulted porphyry system, the chemical and physical characteristics and spatial distribution of fluid inclusions from these two areas should match the characteristics and pattern of spatial distribution of fluid inclusions found at similar depths in other porphyry systems. Furthermore, if the two field areas formed from a single hydrothermal system, they should contain fluid inclusions that show related pressure, temperature, and chemistry patterns and that have similar trace element abundances. The results of this study should determine whether or not the two field areas at Kabba are related and, depending on this relationship, may demonstrate the predictive power of established fluid inclusion distribution models and the practical application of fluid inclusion research in porphyry exploration.

Samples examined to date from the field area located under Quaternary gravels in the valley east of the Hualapai Mountains contain numerous A- and B-type quartz veins with secondary potassium feldspar and overprinting phyllosilicate alteration halos. Sulfide minerals in these samples occur along sulfide-rich center lines in quartz veins, as sulfide selvages along quartz vein margins, and disseminated adjacent to veins in the host rock. Based on mineral and textural relationships, precipitation of galena, chalcopyrite, and sphalerite was followed by partial pyrite replacement. Later, after formation of hypogene mineralization, pyrite, biotite, and chlorite were partially replaced by rutile and hematite, and a zone of supergene enrichment formed.

Fluid inclusion petrography has identified three dominant fluid inclusions assemblages (Goldstein and Reynolds, 1994) in the described samples from the valley east of the Hualapai Mountains:

Type 1a) Three-phase, aqueous liquid-rich, liquid + vapor + opaque daughter assemblage that contains ~10-30% vapor.

Type 1b) Four-phase, aqueous liquid-rich, liquid + vapor + opaque daughter + halite assemblage that contains ~10-30% vapor.

Type 2) Two-phase, aqueous vapor-rich, liquid + vapor +/- opaque daughter assemblage that contains ~75-85% vapor.

Type 3) Four-phase, CO₂-H₂O assemblage that contains ~10-15% CO₂ liquid + 20-35% CO₂ vapor + 50-70% H₂O + opaque daughter +/- halite.

In the shallow parts of this system (1078.8-1279.9 ft below surface), the vein and sulfide minerals coexist with Type 1a or 1b liquid-rich (10-30% vapor) and Type 2 vapor-rich (75-85% vapor) inclusions. However, with increased depth the mineralization is associated with coexisting Type 2 and Type 3 inclusions. Many porphyry systems contain coexisting assemblages of vapor-rich and liquid-rich, halite-bearing inclusions at intermediate depths (Reynolds and Beane, 1985; Hedenquist et al., 1998; Muntean and Einaudi, 2000; Ulrich et al, 2001; Rusk et al, 2008; Landtwing et al, 2010), thus the presence of similar assemblages of inclusions at Kabba may indicate the presence of the intermediate zone of a porphyry-like hydrothermal system. However, the presence of Type 3 inclusions that contain both CO₂ liquid and vapor is unusual for porphyry copper - molybdenum systems and is consistent with a formation pressure much greater than typical of known porphyry deposits (Rusk et al., 2008).

References:

Goldstein, R.H., and Reynolds, J.T., 1994, Systematics of Fluid Inclusions in Diagenetic Minerals: Society of Sedimentary Geology, SEPM Short Course 31, 199 p.

Hedenquist, J.W., Arribas, A., Reynolds, J.T., 1998, Evolution of an intrusion- centered hydrothermal system: Far Southeast-Lepanto porphyry and epithermal Cu-Au deposits, Philippines: *Economic Geology*, v. 93, p. 373–404.

Landtwing, M.R., Furrer, C., Redmond, P.B., Pettke, T., Guillong, M., Heinrich, C.A., 2010, The Bingham Canyon Porphyry Cu-Mo-Au Deposit. III. Zoned Copper-Gold Ore Deposition by Magmatic Vapor Expansion: *Economic Geology*, v. 105, p. 91-118.

Muntean, J.L., and Einaudi, M.T., 2001, Porphyry Gold Deposits of the Refugio District, Maricunga Belt, Northern Chile: *Economic Geology*, v. 95, p. 1445-1472.

Reynolds, J.T., and Beane, R.E., 1985, Evolution of Hydrothermal Fluid Characteristics at the Santa Rita, New Mexico, Porphyry Copper Deposit: *Economic Geology*, v. 80, p.1328-1347.

Rusk, B.G., Reed, M.H., and Dilles, J.H., 2008, Fluid Inclusion Evidence for Magmatic-Hydrothermal Fluid Evolution in the Porphyry Copper-Molybdenum Deposit at Butte, Montana: *Economic Geology*, v. 103, p. 307-334.

Ulrich, T., Gunther, D., Heinrich, C.A., 2001, The Evolution of a Porphyry Cu-Au Deposit, Based on LA-ICP-MS Analysis of Fluid Inclusions: Bajo de la Alumbrera, Argentina: *Economic Geology*, v. 96, p. 1743-1774.

Cathodoluminescence and Fluid Inclusion Characteristics of Porphyry Vein Quartz

Bennett, M.*, Monecke, T. *, Reynolds, T.J.**, Ricks, J. *, and Muntean, J.***

** Department of Geology and Geological Engineering, Colorado School of Mines, Golden, Colorado, USA, Email: mbennett@mymail.mines.edu*

*** FLUID INC., Denver, Colorado, USA*

**** Nevada Bureau of Mines and Geology, Mackay School of Earth Science and Engineering, University of Nevada, Reno*

Porphyry deposits represent one of the world's most important sources of copper, gold, and molybdenum. Integrated fluid inclusion petrography and cathodoluminescence microscopy showed that stockwork veins in porphyry deposits are universally composed of multiple quartz generations.

Early quartz shows a bright blue luminescence and commonly forms large anhedral grains, which may show oscillatory growth zoning. The early quartz precipitated at high-temperature (>400°C) from fluids that caused potassic alteration. Intermediate density fluid inclusions are the dominant fluid inclusion type in deep deposits such as Butte in Montana or Chuquibambilla in Chile while hypersaline liquid and vapor inclusions occur in abundance in deposits formed at intermediate depths, including Bingham Canyon in Utah, Far Southeast in the Philippines, and Santa Rita in New Mexico. Vapor inclusions predominate in shallow deposits such as those of the Maricunga belt in Chile.

The early quartz is interpreted to have formed at high temperatures from hydrothermal fluids derived from an actively degassing magma chamber at depth. At high pressures under lithostatic load, the hydrothermal fluids separating from the magma occurred as single-phase vapor-like fluids. The single-phase vapor-like fluids are entrapped in quartz veins formed in deep deposits, and appear as intermediate density fluid inclusions. During continued fluid ascent and related decompression, the single-phase vapor-like fluids of magmatic origin intersected the solvus of the H₂O-NaCl system. Condensation resulted in the formation of a hypersaline liquid and a coexisting low-salinity vapor. The hypersaline liquid and vapor entrapped in the early quartz of deposits formed at intermediate depth such as Far Southeast could have been derived from such single-phase vapor-like fluids undergoing phase separation below the current exposure of the deposit. Alternatively, the slightly lower pressure conditions could have allowed separation of hydrothermal fluids from a magma within the two-phase liquid plus vapor field of the H₂O-NaCl system, with no precursor single-phase fluid being produced. The shallow deposits of the Maricunga belt formed at even lower pressure conditions. In the case of these deposits, the early high-temperature magmatic-hydrothermal fluids were probably separated from the magma at lower pressure conditions and directly degassed from the magma within the liquid plus vapor field or even the vapor plus salt field of the H₂O-NaCl system.

In all deposits studied, early quartz in mineralized veins is overprinted by quartz showing a red-brown luminescence that precipitated from a distinctly lower temperature fluid (<400°C). The textural relationships between the early blue quartz and the later red-brown quartz are complex. A series of alteration processes is recognized, ranging from the modification and quenching of the cathodoluminescence signal of preexisting quartz to changes in the trace element abundances and structural reorganization resulting in the formation of subgrains or wholesale recrystallization of earlier quartz. At least in some cases, fluid inclusions can be inherited from the preexisting early quartz to its intensely altered equivalents without notable changes to their petrographic appearance. Careful investigations showed that the fluid inclusion inventory of the late red-brown quartz can be variable. At Bingham Canyon, the hydrothermal fluid forming this late quartz generation was a hypersaline liquid at 330-380°C. At Far Southeast, early red-brown quartz was formed from a hypersaline liquid, but is overprinted by a later generation of red-brown quartz characterized by low-salinity liquid inclusions that yield temperatures <350°C. A similar relationship may exist at Santa Rita in New Mexico. In the other deposits investigated, the red-brown quartz is dominated by low-salinity liquid inclusions associated with chlorite-sericite or sericite-pyrite alteration of the wall rocks.

The occurrence of low-temperature NaCl-saturated liquid inclusions in the late red-brown quartz can be explained by a fluid path of cooling, perhaps accompanied by decompression caused by a transition from lithostatic to hydrostatic conditions. The low-salinity hydrothermal liquid entrapped in red-brown quartz is interpreted to result from an entirely different fluid experiencing a different evolutionary path. This liquid probably formed from the early single-phase vapor-like hydrothermal fluid through isochemical contraction accompanying cooling at elevated pressures. Such a process could be related to the inward cooling of the source magma chamber, causing active degassing to occur at progressively increasing pressure conditions. Due to the increase in transport distance associated with the retreating magma front and conductive cooling of the intrusion, the fluids could cool towards lower temperatures during their ascent. As phase separation did not occur, this liquid of magmatic origin contains acidic volatile species, promoting the formation of sericite-pyrite or chlorite-sericite alteration at temperatures <400°C and hydrostatic pressure conditions. Textural relationships indicate that the late quartz encountered in the investigated porphyry deposits formed slightly before or during the formation of the ore minerals.

Fluid inclusion and stable isotope study of Magino; a magmatic related Archean gold deposit.

Haroldson, E.H.*, Brown, P.E.*

* *Department of Geoscience, University of Wisconsin-Madison, 1215 W. Dayton, Madison, WI, 53706 USA*

The Magino gold deposit is located approximately 45 km's Northeast of Wawa, Ontario, Canada in the Goudreau-Lochalsh area of the Michipicoten Greenstone Belt (MGB). The Archean aged gold deposit is a recently enlarged gold resource in a mining camp historically known to host deposits of ≤ 1 Moz. in total gold endowment. Gold was first discovered on the Magino project in 1917. Historic production on the property has been from two generations. The first generation was in the 1930's and approximately 10,000 oz. of gold were produced. The second more recent underground venture operated from 1987 to 1993 and an additional 105,000 oz. of gold was produced. As of December 2013; the Magino resource estimate is of 6.95 Moz of gold in various categories (Doerksen et al., 2014). On December 17, 2013 Argonaut Gold released the results of a Pre-Feasibility study (Doerksen et al., 2014) which showed positive economics related to recovering gold from the Magino deposit through a bulk-mining open pit operation, adding Magino to the growing list of open-pittable bulk tonnage deposits in the Superior province. The objective of this study is to better understand the mineralizing system(s) responsible for forming this gold deposit and to put that information in the context of the regional geology to better understand the economic potential of the deposit along with further exploration in the surrounding greenstone belt.

The Magino deposit is primarily hosted within an Archean trondhjemite (Sage, 1993) intrusion known as the Webb Lake Stock (WLS) with some mineralized structures extending into surrounding metavolcanic rocks of the MGB. The deposit is located at a bend within the Goudreau-Lochalsh Deformation Zone (GLDZ; (Heather and Arias, 1992)). The WLS cross-cuts the break between cycle 2 and cycle 3 volcanics in the MGB sequence which is marked by a formation of chemical metasediments. Other intrusive units in the area include felsic intrusions similar to the WLS, intermediate to mafic intrusives, quartz-feldspar porphyry intrusives, lamprophyre dikes, a nepheline-syenite intrusion (known as the Herman Lake Nepheline Syenite complex) and late diabase dikes (Sage, 1994).

Visible Gold is primarily observed hosted in or closely related to some form of silicification; either silica flooding or most commonly in the form of veins. Electron microprobe analyses show that gold is found in variable fineness values ranging from 812 to 957 with perhaps as many as 6 distinct modes. Under the microscope, gold is observed in two distinctive settings based on mineralogical and textural associations. Earlier gold is likely associated with a porphyry system and is commonly observed with chalcopyrite, sphalerite, pyrrhotite and trace galena, molybdenite and arsenopyrite hosted in 1-10mm sized pyrite grains. Pyrite grains which encase gold commonly display cores of earlier growth with BSE indicated arsenic concentric zonation. From a later event, gold is observed closely associated with hydrothermal calcite and Au, Ag, Te minerals hessite (Ag_2Te), petzite (AuAg_3Te_2) and rarely altaite (PbTe) along with some form of bismuth telluride (possibly tellurobismuthite (Bi_2Te_3)). In this second setting gold is found along fractures in pyrite (Borthwick, 1987) and as trails of small gold grains in healed quartz vein fractures, at quartz grain triple points and along quartz grain boundaries. It is unclear if the second gold mineralizing event contributed gold or was instead a re-mobilizing event.

Three main fluid types were identified using microthermometry and Raman spectroscopy as forming carbonic ($\text{CO}_2\text{-CH}_4, \pm\text{N}_2$), aqueous ($\text{H}_2\text{O-NaCl}$), and aqueo-carbonic ($\text{H}_2\text{O-CO}_2\text{-CH}_4\text{-NaCl}$) inclusions. Carbonic inclusion T_m range from -69 to -56.6 °C and T_h range from -69 to $+28.5$ °C. Aqueous fluid inclusions are often suspected of necking but when measurable were determined to have $T_m(\text{ice})$ ranging from -22 to 0 °C (equiv. salinities of 23.7 to 0 wt. %) and T_h ranging from $+70$ to $>+525$ °C. Rarely observed eutectic melting temperatures range from -55 to -21 °C (suggesting variable amounts of divalent cations in the fluids). Aqueo-carbonic $T_m(\text{car})$ range from -63.9 to -56.6 °C, $T_h(\text{car})$ range from -43 to $+26$ °C and $T_m(\text{cla})$ range from -10 to $+23.6$ °C. Nahcolite solids were observed in carbonic and aqueo-carbonic fluid inclusions.

At least four generations of fluids (Fluid I-IV) have been identified in at least two auriferous (Fluid II, IV?) and multiple barren fluid (Fluids I, III, more?) events at Magino. Fluid I is a high density carbonic

fluid ($\text{CO}_2\text{-CH}_4$, $\pm\text{N}_2$) related to late magmatic emplacement of the WLS quartz and initially barren quartz veins (Q1). A second generation of fluid (Fluid II), believed to be the first auriferous fluid event, is a variable salinity aqueous fluid which was trapped in inclusions along healed fractures in quartz veins and healed fractures in WLS quartz phenocrysts. This second fluid generation is likely associated with porphyry intrusives which cross-cut the WLS, but intruded prior to or perhaps during the initial stages of regional deformation. A third generation (Fluid III) of fluid was best preserved in tension gash veins oriented perpendicular to shear bands formed during the regional deformation. The primary fluid (Fluid III) formed in these barren tension gash veins is an aqueo-carbonic fluid ($\text{H}_2\text{O-CO}_2\text{-CH}_4\text{-NaCl}$). Moderately to highly saline aqueous fluid (Fluid IV) is observed in late secondary fractures which cross-cut all quartz types including fine-grained quartz that formed in veins during regional deformation (Q2).

Textural evidence suggests calcite was emplaced along with the later gold event. Calcite $\delta^{13}\text{C}$ values fall in a narrow range between -3.27 ‰ to -1.48 ‰ (PDB). Mineral (ankerite, calcite) $\delta^{18}\text{O}$ values range from 8.85 ‰ to 11.14 ‰ (VSMOW) and mineral (ankerite, calcite) $\delta^{13}\text{C}$ values range from -6.74 ‰ to -1.48 ‰ (PDB). $\delta^{18}\text{O}$ values for nearby carbonate iron formation were measured for calcite and ankerite separately with values of 10.74 ‰ and 10.22 ‰ (VSMOW) respectively and calcite and ankerite mineral $\delta^{13}\text{C}$ values in the iron formation were 0.13 ‰ and 0.85 ‰ (PDB) respectively. The mineral $\delta^{18}\text{O}$ values show a relatively low $\delta^{18}\text{O}$ value for deposits in the MGB area when compared to deposits in the Abitibi which has been shown to suggest similarities in the hydrothermal system(s) throughout the MGB (Studemeister and Kilias, 1987; Samson et al., 1997). Fluid $\delta^{18}\text{O}$ values range from 5.22 ‰ to 7.51 ‰ (VSMOW) calculated using equations from (Zheng, 1999) and an estimated temperature for this second mineralizing event (350 °C). Both the mineral $\delta^{13}\text{C}$ values and the calculated fluid $\delta^{18}\text{O}$ values suggest a magmatic fluid source.

Coupling the textural and mineralogical evidence, the interpretation calls for two separate gold mineralizing events with the first and possibly the second being related to variably saline aqueous magmatic derived fluids that, respectively, post-date the two vein formation events (Q1 - magmatic, Q2 - regional deformation). It is worth noting that in similar settings, a saline aqueous fluid has been interpreted as an unmixed end member of the aqueo-carbonic fluid and that fluid separation was a mechanism for gold deposition. Quartz veins are the dominate host at Magino, however it appears that the gold mineralization post-dates their formation, and that the quartz veins simply provide a rheological, and perhaps a chemical trap for gold mineralization?

The recent expansion of the Magino resource raises the exploration potential of the MGB significantly. Fluid inclusion and stable isotope studies have hinted strongly at a regional genetic link between various widespread MGB study areas. A new interpretation of the magmatic contribution to the mineralization at Magino should aid in the development of new exploration models in the MGB.

REFERENCES

- Borthwick R. (1987) The distribution and association of gold within quartz Veins, Magino mine prospect, Wawa, Ontario. A thesis submitted to the Department of Geological Sciences Brock University. 115 p.
- Doerksen, G. Pilotto, D. Boehnke, R. Bender, M. Khosrow, A. Kirkham, G. Hutchinson, I. and Buter, L. (2014) Preliminary feasibility study technical report for the Magino project, Wawa, Ontario, Canada. 513 p.
- Heather, K. and Arias, Z. (1992) Geological and structural setting of gold mineralization in the Goudreau-Lochalsh area, Wawa gold camp. Ontario Geological Society. Open File Report 5832. 159 p.
- Sage, R. (1993) Geology of Aguonie, Bird, Finan and Jacobson townships, district of Algoma. Ontario Geological Society. Open File Report 5588. 286 p.
- Sage, R. (1994) Geology of the Michipicoten greenstone belt. Ontario Geological Society. Open File Report 5888. 592 p.
- Samson, I. (1997) Hydrothermal evolution of auriferous shear zones, Wawa, Ontario. *Economic Geology*. vol 92. no 3. p 325-342.
- Studemeister P. and Kilias, S. (1987) Alteration pattern and fluid inclusions of gold-bearing quartz veins in Archean trondhjemite near Wawa, Ontario, Canada. *Economic Geology*. vol 82. no 2. p 429-439.
- Zheng, Y. (1999) Oxygen isotope fractionation in carbonate and sulfate minerals. *Geochemical Journal*. vol 33. no 2. p 109-126.

Geochemistry of Fluid Inclusions in the Vazante Zinc Deposit, Minas Gerais, Brazil.

Hassan, A. M* and Appold, M. S*

**Department of Geological Sciences, University of Missouri-Columbia, Columbia, MO, 65211, USA*

ABSTRACT

The Vazante deposit in Minas Gerais, southeast-central Brazil is the world's largest known occurrence of hypogene non-sulfide zinc (HNSZ) mineralization, originally consisting of about 28.5 million tonnes of ore at an average grade of 18% zinc. The zinc mineralization consists mainly of willemite with lesser, broadly coeval sphalerite and is hosted by sheared Proterozoic slaty dolomites. The Vazante deposit lies at the southern end of the 120 km long Vazante-Unai trend, the largest district of Zn-Pb mineralization in Brazil, which consists of both hypogene non-sulfide and sulfide deposits. All of the Vazante-Unai mineralization lies within the Brasília fold belt in the western part of the Bambuí foreland basin and is thought to be a product of fluids mobilized by the 630-610 Ma Brasiliano orogeny.

Little is known about the nature of the fluids that form HNSZ deposits beyond fluid inclusion bulk salinities and homogenization temperatures. The present study of the Vazante deposit is the first to measure the elemental composition of potential mineralizing fluids in a HNSZ deposit, and was carried out using LA-ICP-MS and microthermometry. The analyses were all performed on fluid inclusions hosted by sphalerite, as no primary fluid inclusions were identified in willemite.

Most of the primary fluid inclusions in sphalerite were found to contain aqueous liquid and vapor in highly variable proportions. Some primary fluid inclusions (~20%) consist entirely of aqueous liquid. Most secondary fluid inclusions were found to consist of a single aqueous liquid phase with about 10% consisting of aqueous liquid + vapor. A few fluid inclusions were observed to contain rhombohedral crystals, which were interpreted to be accidental carbonate mineral inclusions rather than daughter minerals based on their inconsistent occurrence within fluid inclusion assemblages, variable sizes in proportion to their host fluid inclusion sizes, and the abundance of carbonate mineral inclusions in the sphalerite matrix.

Microthermometry was performed only on the liquid-vapor primary fluid inclusions and yielded highly variable homogenization temperatures ranging between 46.7 and 351.7 °C). This high degree of variability is interpreted to be a product of the deformation and low grade metamorphism that affected the Vazante-Unai trend during the Brasiliano orogeny. Salinities were also found to be highly variable, ranging from 0.9 to 18.7 equivalent weight percent NaCl, and are interpreted to reflect mixing of a saline fluid with a dilute fluid. No correlation between salinity and homogenization temperature was observed.

LA-ICP-MS analyses were performed after the microthermometry analyses to determine the elemental compositions of the fluid inclusions. Absolute elemental concentrations varied widely in keeping with the wide range of fluid inclusion salinities, but the atomic ratios of elements with respect to Na were relatively constant as a function of salinity, consistent with the pattern expected from the dilution of a saline fluid. Average atomic ratios were K/Na = 0.36, Mg/Na = 0.078, Ca/Na = 0.12, and Sr/Na = 0.001. Ba was consistently detected in the fluid inclusions at concentrations of 10's to 100's of ppm. Pb was quantifiable in about 14% of the fluid inclusions in concentrations of 100's to 1000's of ppm.

Vazante fluid inclusion compositions obtained from the present study were compared to Morro Agudo fluid inclusion compositions obtained from previous studies. Vazante and Morro Agudo fluid inclusions were found to have similar K/Na and Ba/Na ratios but Vazante fluid inclusions were found to have significantly lower Mg/Na, Ca/Na, and Sr/Na ratios and to be overall more dilute. Also, none of the Morro Agudo fluid inclusions contained any detectable Pb. Thus, the Vazante and Morro Agudo deposits and their corresponding different styles of mineralization appear to have been formed by different fluids. The compositions of Vazante fluid inclusions were also compared to the compositions of fluid inclusions in Mississippi Valley-type (MVT) deposits of the Ozark Plateau in the central United States and in the Irish deposits. Vazante fluid inclusions were found to have higher Ba/Na, K/Na, and Mg/Na but lower Ca/Na and Sr/Na atomic ratios than Ozark MVT fluid inclusions. Vazante fluid inclusions were also found to be

distinct from Irish fluid inclusions, having higher Ca/Na, K/Na, and Mg/Na ratios but lower Ba/Na and Sr/Na ratios than Irish fluid inclusions.

The fluid inclusion microthermometry and LA-ICP-MS data suggest that the Vazante mineralization formed as a result of dilution of a brine. Willemite and sphalerite solubility are identically sensitive to salinity, but willemite solubility decreases more strongly than sphalerite solubility with respect to pH increase. If the diluting fluid had a higher pH than the brine, then the higher fraction of dilute fluid present in Vazante fluid inclusions compared to Morro Agudo fluid inclusions may mean that the pH of the ore fluid mixture at Vazante was higher than at Morro Agudo, which would favor willemite precipitation and explain its predominance at Vazante. This hypothesis was tested using reaction path modeling, in which potential end member ore fluids were extracted from the fluid inclusion data and allowed to mix. The results confirmed that willemite precipitation should predominate over sphalerite when a cool, dilute, basic, oxidizing fluid mixes with a hotter, saline, acidic, reducing fluid, and produce an overall ore mineral assemblage that resembles what is observed in the field.

Petrography of fluid inclusions in modern gypsum precipitated from volcanoclastic hosted acid saline Salar Ignorado, northern Chile

Karmanocky, F.J. and Benison, K.C.*

*West Virginia University, Department of Geology

Few mentions of fluid inclusions in gypsum have been made in the literature. Observations by Sorby (1858) have quickly dismissed fluid inclusions in gypsum due to the ease and readiness of gypsum to alter and transition to anhydrite. Workers such as Sabouraud-Rosset (1976) and Attia (1994) have carefully demonstrated evidence of primary fluid inclusions in gypsum from Oligocene and Miocene coastal deposits. Little is known of fluid inclusions in modern gypsum forming in continental evaporite basins, specifically not in gypsum forming in intervolcanic basins. In the Cordillera de los Andes of South America, salars, or salt-pans, contain pools that precipitate evaporite mineral assemblages, including gypsum. Shallow acidic (pH 2.65 to 3.88) pools at Salar Ignorado precipitate abundant gypsum and provide a unique opportunity to investigate the petrographic characteristics of fluid inclusion assemblages (FIAs) of modern *in situ* bottom growth gypsum in volcanic terrain.

Salar Ignorado gypsum precipitates in shallow (< 1m deep) pools of acid, saline (TDS 4.05 to 97.4 ppt) waters rich in SO₄-Al-Cl-Na-K with lesser amounts of Si-Mg-B (listed by relative abundance; Risacher et al., 2002). Two primary growth morphologies of gypsum include: (1) mounds of 'needle-shaped', or acicular, gypsum mounds (similar in appearance to a sea urchin) and (2) larger 'stock-work' masses of prismatic/hemi-bipyramidal selenite crystals of various orientations.

'Needle-shaped', or acicular, gypsum crystals have been observed to be a maximum of 7 cm in length and 1.5 cm wide, but most are quite small, averaging ~4 cm long and ~1 cm wide. These gypsum crystals tend to grow with the crystals radiating from a similar central point. Mounds of semi-transparent needle shaped gypsum crystals were collected from the bottom of the pools, below the air-water interface. Primary FIAs in 'needle'-shaped gypsum indicate the growth faces of the gypsum crystals and form at an oblique angle to the twinned (101) crystal face. 'Needle-shaped' crystals also host secondary and pseudo-secondary FIAs.

'Stock-work' masses of prismatic/hemi-bipyramidal selenite crystals are much larger than the 'needle-shaped' gypsum to be ~21 cm long and 3 cm wide. These crystals were likely precipitated as bottom growth gypsum crystals; however, they have been reworked by the wind. Abrasion of the crystals is evident at the macro- and microscopic scales. Primary FIAs line the crystal growth face and occur normal to the (103). 'Stock-work' crystals can also host secondary and pseudo-secondary FIAs.

Primary fluid inclusions in both needle-shaped and stock-work gypsum are aligned in rows parallel to the direction of growth. These inclusions point in the direction of growth with the fluid inclusion broadest at its base and tapering upward. Two types of primary FIAs can be identified petrographically:

1. Type I primary FIA inclusions range in size from ~2 to 15 μm long and are negative crystal to sub-horn shaped in two-dimensional space. Each Type I primary FIAs typically form consists of 10 to 25 fluid inclusions; however, in rare cases the number of fluid inclusions is indiscernible. Type I primary FIA L-V (or gas) ratios are highly variable. Some of these inclusions also trap microorganisms and organic compounds. In 'needle'-shaped gypsum crystals Type I FIAs form at oblique angles to the (101) twinning plane and can even appear to curve toward the (101) twinning plane.
2. The Type II primary FIAs are triangular-shaped in two-dimensional space and typically consist of groups of 2 or 3 and can be quite large (~50 to 200 μm). There can be some difficulty in discerning

Type II FIAs from fluid inclusions of unknown origin or IDKs. The large, Type II primary FIAs tend to have an obtuse-scalene-triangular morphology that point in the direction of crystal growth and the base of the fluid inclusion is parallel to the growth plane. While IDKs display similar features, they cannot be evaluated due to the unknown nature of their genesis. Type II primary FIAs have considerable variation in the L-V ratio and can trap microorganisms such as *Dunaliella* algae, diatoms, and organic compounds.

3. Type III primary FIAs are horn-shaped in two dimensional space and typically consist of groups of 4 to 35 and are intermediate in size, ranging in size from ~20 to 60 μm , and are consistently all liquid. These fluid inclusions also trap sediment, microorganisms such as diatoms and carotenoids, and organic material. Type III primary fluid inclusions have only been documented in needle-shaped gypsum.

Secondary FIAs occur as linear or curved trails that can cross cut many generations of primary FIAs and terminate at the crystal face. Secondary fluid inclusions range in size but are typically 2 to 10 μm long and have a variety of shapes; most are slightly negative crystal to cubic, yet some can be triangular. Secondary fluid inclusions have inconsistent and varying L-V ratios. A second type of secondary fluid inclusions includes large amorphous fluid inclusions that lack any consistent shape or arrangement. These inclusions are located along the cleavage planes of the gypsum crystal and appear flat. They do have the potential to trap both liquid and microorganisms.

Pseudo-secondary FIAs share similar morphologies as secondary FIAs, however pseudo-secondary FIAs terminate at a previous growth face within the crystal. The pseudo-secondary inclusions tend to be negative crystal to cubic in shape and range from ~2 to 8 μm long.

Petrography of primary, secondary, and pseudo-secondary fluid inclusions in modern naturally occurring gypsum crystals can aid in studying gypsum in the rock record on Earth or other planetary bodies. Carefully petrographic evaluation gypsum is a critical first step in performing subsequent microthermometric and geochemical investigations. With sound petrography, fluid inclusions in gypsum may yield important environmental data.

REFERENCES

- Attia, O. E., Lowenstein, T. K., & Wali, A. M. A. (1995) Middle Miocene gypsum, Gulf of Suez; marine or nonmarine?. *Journal of Sedimentary Research*. 65. 614-626.
- Risacher, F., Alonso, H., and Salazar, C. (2002) Hydrochemistry of two adjacent acid saline lakes in the Andes of northern Chile. *Chemical Geology*. 187. 39-57.
- Sarbouraud, C. (1994) Solid and fluid inclusions of evaporites: Gypsum. In M. Majithia (Ed.), *Evaporative sequences in petroleum exploration: 1. geological methods* [Les series a evaporites en exploration petroliere. 1. 136-145.
- Sorby, H.C. (1858) On the microscopic structure of crystals, indicating the origin of minerals and rocks. *Quarterly Journal of Geology, Society of London*. 14. 453–500.

Low-salinity fluids associated with the Geumeum Mo mineralization in the late Cretaceous granitic rocks of the Gyeongsang Basin, South Korea

Kim, H.* , Seo, M.* , Yang, K.*

*Dept. of Geology, Pusan National University, Busan, 609-735, South Korea

Molybdenum mineralization hosted in the late Cretaceous granitic rocks at the Geumeum deposit in the northern part of the Gyeongsang Basin, South Korea is associated with two types of fluids that boiled and mixed. These two types of fluids can be represented by two types of primary fluid inclusions (e.g., liquid-rich Type I and CO₂-bearing Type IV) trapped in the fissure-filling quartz veins. Based on vein ore mineralogy and paragenesis, the quartz veins crosscutting the host granitic rocks can be classified into (1) the earliest Mo type containing major molybdenite with a minor amount of chalcopyrite and pyrite, (2) the intermediate Cu-Mo type containing major chalcopyrite with a minor amount of molybdenite, pyrite, and sphalerite, and (3) the late barren type containing no ore minerals. The earliest Mo type quartz started to precipitate against the wall of the host granitic rocks, followed by precipitation of the Cu-Mo type and barren type quartz towards the interior part of the quartz vein (Fig. 1).

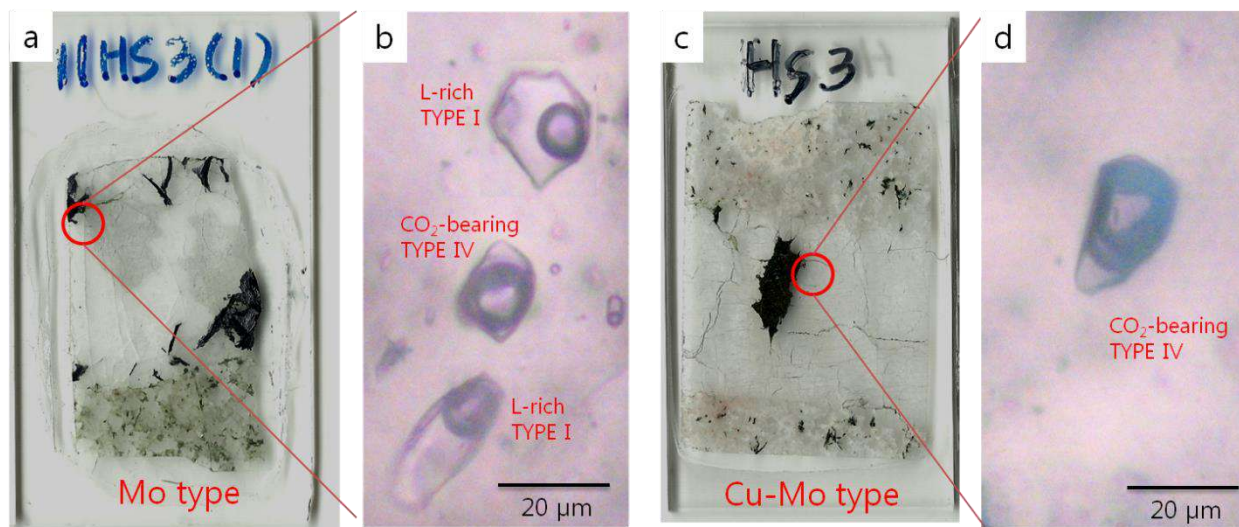


Fig. 1. Aqueous fluid inclusions trapped in quartz vein from the Geumeum Mo deposit (a) A polished section showing molybdenite at the contact with the host granite. (b) Type IV inclusion coexisting two Type I inclusions trapped in Mo-type quartz vein. (c) A polished section showing chalcopyrite and pyrite in the interior part of quartz vein. (d) Type IV inclusion trapped in Cu-Mo type quartz vein.

The earliest fluid can be represented by Type I inclusion which have salinities of 0.4-1.7 wt% NaCl equiv. and homogenize from 310 to 381 °C (Th total) (in liquid phases). The earliest fluid was trapped in Mo type quartz veins during the initial stage of the Geumeum Mo mineralization. The second fluids can be represented by boiling assemblages Type I (salinities of 4.6-5.3 wt% NaCl, Th=298-317 °C) homogenized by vapor-bubble disappearance and the coexisting Type IV inclusions (salinities of 2.5 wt% NaCl, Th=364 °C) homogenized by vapour-expansion. The second fluid was trapped during the main stage of Mo mineralization in Mo type quartz veins. The third fluid can be represented by Type I (salinities of 5.0-7.2

wt% NaCl, Th=300-344 °C) homogenized by vapor-bubble disappearance and Type IV (salinities of 2-3 wt% NaCl, Th=332-340 °C) homogenized by vapor-bubble disappearance. The third fluid was trapped in Cu-Mo type quartz veins during the Cu mineralization stage. The latest fluid can be represented by Type I (salinities of 0.9-1.4 wt% NaCl, Th=162-300 °C) homogenized by vapor-bubble disappearance. The latest fluid was trapped in barren type quartz veins. In addition, to help constrain the source of the mineralizing fluids, oxygen and hydrogen isotopic compositions of quartz crosscutting the host granitic rocks were measured. The oxygen and hydrogen isotopic compositions of the fluid have $\delta^{18}\text{O}_{\text{SMOW}} = -4.9$ to -2.3‰ and $\delta\text{D}_{\text{SMOW}} = -84$ to -65‰ at 350 °C, suggesting a significant contribution of a meteoric or basinal fluids to the magmatic water.

The fluids that transported and precipitated molybdenum and altered the host granitic rocks at the Geumeum deposit are unique because they exhibit significantly low-salinity fluids throughout the whole stages of the hydrothermal activity for Mo-mineralization. Furthermore, similar homogenization temperatures in different types of fluid inclusions and the phase behaviour during microthermometry may indicate that these fluids were trapped at near critical conditions in the H₂O-NaCl-CO₂ system. Stable isotopic compositions and the presence of co-existing Type I and IV inclusions, the variable range of vapor volume ratios, low density vapor and relatively low homogenization temperatures clearly indicate that Geumeum Mo-mineralization and alteration are products of fluid mixing and fluid boiling at near critical conditions.

Characteristics of tin-tungsten mineralizing fluids at Panasqueira, Portugal

Lecumberri-Sanchez, P.* , Heinrich, C. A.* , Wälle, M.* , Vieira, R.** , Pinto, F.**

**Institute for Geochemistry and Petrology, ETH Zurich, Clausstr. 25, 8092 Zurich, Switzerland*

***Sojitz-Beralt Tin and Wolfram, Barroca Grande, Portugal*

Tungsten has many industrial applications due to its heat resistance, density and hardness (tungsten carbides). Tungsten deposits typically form due to the interaction of a magmatic-derived fluid with the rocks in which the deposit is emplaced or with other fluids. However there are no modern quantitative analytical studies of the fluids responsible for the formation of the highest-grade deposit type (tungsten vein deposits; Bodnar et al., 2014). Panasqueira (Portugal) is a tungsten vein deposit, one of the leading tungsten producers in Europe and one of the best geologically characterized tungsten vein deposits (Kelly and Rye, 1979).

In this study, compositions of the mineralizing fluids at Panasqueira have been determined through combination of detailed petrography, microthermometric measurements and LA-ICPMS analyses. We characterize the fluids related to the various mineralizing stages in the system: the oxide stage (tin and tungsten mineralization)- and the sulfide stage (chalcopyrite and sphalerite mineralization). Thus, our results provide information on the properties of fluids related with specific paragenetic stages.

This study provides the first quantitative analytical data on fluid composition for tungsten vein deposits and thus helps to constrain the mechanisms of formation of the Panasqueira tin-tungsten deposit.

REFERENCES

- Bodnar, R.J., Lecumberri-Sanchez, P., Moncada, D., Steele-MacInnis, M. (2014) Fluid inclusions in hydrothermal ore deposits. *Treatise on Geochemistry*. 13. 119-142.
- Kelley, W. C., Rye, R. O. (1979) Geologic, Fluid Inclusion, and Stable Isotope Studies of the Tin-Tungsten Deposits of Panasqueira, Portugal. *Economic Geology*. 74. 1721-1822.

Paragenesis of quartz, FIA's, and associated alteration and sulfide minerals in the Pebble Porphyry Cu-Au-Mo Deposit, SW Alaska resolved by Cathodoluminescence

Marsh, E.E.

Denver Inclusion Analysis Laboratory, U.S.G.S., Box 25046 MS 973, Denver, CO 80225
emarsh@usgs.gov

Fluid inclusions are often relied upon in ore deposit research to determine the temperature, pressure, composition, and density of hydrothermal fluids. To elucidate connections between fluid inclusion PTX_d and ore forming processes, it is critical to define the paragenesis of transparent minerals, such as quartz, and the fluid inclusion assemblages (FIAs) within them. This endeavor is difficult in porphyry systems with complex paragenesis and fluid histories. This preliminary investigation describes the paragenesis of quartz and fluid inclusions in a small suite of representative samples from the Pebble Porphyry Cu-Au-Mo Deposit, SW Alaska which holds 80.6 billion pounds of copper, 107.6 million ounces of gold, and 5.6 billion pounds of molybdenum (<http://www.pebblepartnership.com/geology.html#section-deposit>).

Previous work by Tracey (2001) and Gregory (2012) suggests that mineralization developed from two phases, initially with sodic-potassic and potassic alteration at temperatures of 343 to 519°C and 313 to 419°C, respectively, with Gregory (2012) stating that samples most endowed in chalcopyrite have related fluid temperature of 400 to 438°C and elevated salinities. Their determined second phase of mineralization is described to be associated with advanced argillic alteration at temperatures of 290–390°C. It is possible that without more concrete paragenetic control of the quartz generations in these previous studies the relation between fluid inclusions, quartz generations, and ore minerals is not well constrained.

Scanning electron microscope-cathodoluminescence (SEM-CL) images of quartz from Pebble east, a deeper portion of the deposit, reveal a complex paragenesis not visible in transmitted or reflected light microscopy. SEM-CL textures are very similar to those reported in samples from the Butte porphyry copper deposit, Montana (Rusk and Reed, 2002). Quartz textures observed include: 1) bright-CL on medium grain size primary quartz, 2) dull-CL quartz that appears to etch primary quartz, occurs in narrow bands along the bright-CL quartz grain boundaries, and exhibits growth zonation of various CL intensities, none as bright as the primary quartz, 3) dull-CL quartz sharply cutting bright-CL quartz in very thin veinlets, and 4) bright-CL quartz in hairline veinlets lining the boundary between the vein and altered granodiorite. Chalcopyrite +/- pyrite and molybdenite as well as sericite and chlorite are associated with dull-CL quartz (2) along the crystal edges and fractures in the bright-CL quartz (1). The fabric created by planes of secondary fluid inclusions can be followed into the altered granodiorite where disseminated chalcopyrite mineralization occurs.

In primary quartz (1), fluid inclusions are either hypersaline and liquid-rich or dilute and vapor-rich (Figure 1). They appear to be an immiscible pair derived from a moderately saline parent fluid. Primary quartz growth occurred at elevated temperatures (425–550°C). Preliminary Raman microscopy shows minor amounts of CO₂ in the vapor-rich inclusions in the primary quartz. The secondary quartz (2) with the dull CL response contains liquid-rich inclusions that formed at a noticeably lower temperature (300–350°C) (Figure 1).

It is reasoned from the paragenesis that copper mineralization and associated sericite alteration formed as fluids cooled to temperatures ≤350°C, as found in analogous studies of the Far Southeast deposit in the Philippines and the Grasberg porphyry Cu-Au deposit, Indonesia (Bennett et al., in review; Penniston-Dorland, 2001).

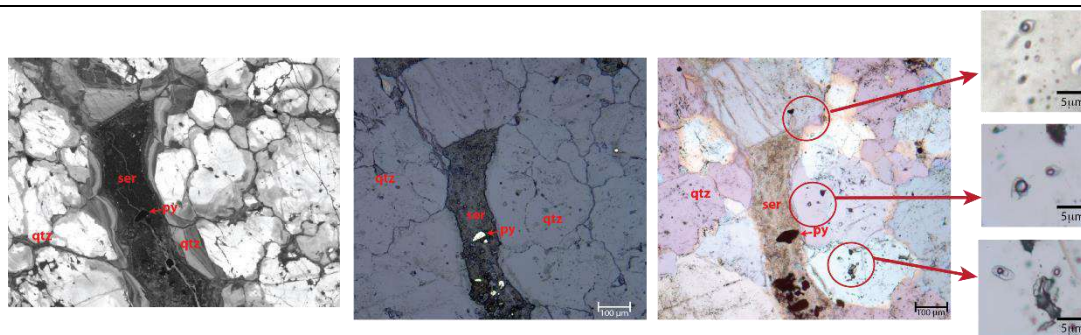


Figure 1. SEM-CL, reflected light, and transmitted light photomicrographs of quartz vein cutting sample 5330-3263, an altered and mineralized granodiorite. The SEM-CL reveals a dissolution texture with secondary quartz and sericite associated with chalcopyrite and pyrite. Fluid inclusion within the quartz phenocrysts represent alteration and quartz growth phases prior to mineralization. Fluid inclusions following the alteration and dissolution trend are associated with mineralization.

REFERENCES

- Bennet, M.M., Monecke, T., Reynolds, J., Kelly, N.M., Lowers, H., Gotze, J., and Arribas, A., SUBMITTED (Economic Geology), Hydrothermal alteration of quartz and inheritance of fluid inclusion assemblages: A case study on vein quartz from the Far Southeast porphyry Cu-Au Deposit, Philippines.
- Gregory, M., 2012, Fluid evolution in the Pebble Porphyry Cu-Au-Mo Deposit, Alaska: SEG 2012 September 23-26, poster presentation 045, Lima, Peru.
- Penniston-Dorland, S.C., 2001, Illumination of vein quartz textures in a porphyry copper ore deposit using scanned cathodoluminescence: Grasberg Igneous Complex, Irian Jaya, Indonesia: American Mineralogist, v. 86, p. 652–666.
- Rusk, B.G., and Reed, M.H., 2002, Scanning electron microscope-cathodoluminescence of quartz reveals complex growth histories in veins from the Butte porphyry copper deposit, Montana: Geology, v. 30, p. 727–730.
- Tracy, B.J., 2001, Geology and ore fluid geochemistry of the Pebble Cu-Au porphyry deposit, southwest Alaska. Unpub. M.Sc thesis, University of Georgia, Athens, 148 p.

Generation of monazite and other REE-bearing phases during secondary fluid events: Pea Ridge iron oxide-apatite-REE deposit, Southeast Missouri, USA

Meighan, C.J.* , Hofstra, A.H.* , Marsh, E.E.* , Lowers, H.A.* , Emsbo, P.* , Hitzman, M.W.**

*U.S. Geological Survey, Denver, CO. 80225

**Department of Geology and Geological Engineering, Colorado School of Mines, Golden, CO. 80401

The Pea Ridge iron oxide-apatite (IOA) deposit, classified as a “Kiruna-type” magnetite deposit (Frietsch & Perdahl 1995), is located in southeast Missouri within the ~1470 Ma St. Francois Mountains granite-rhyolite terrane known for its numerous iron occurrences (Kisvarsanyi, 1974). The steeply dipping magnetite ore body and its REE breccia pipes has been described by Nuelle and others (1992). The IOA deposit is hosted in a series of subalkaline rhyolites and consists of magnetite (>75 wt%) with lesser intergrown coarse apatite, actinolite, phlogopite, and quartz. The central magnetite body is broadly mantled by a hematite-quartz zone and is enveloped by an amphibole-quartz zone. The amphibole zone grades into a silica zone on the footwall. The magnetite body is cut by several REE breccia pipes that contain ~ 600,000 t @ 12% REO. The breccia pipes are composed of specular hematite, apatite, and quartz with lesser barite and REE minerals.

Both the magnetite body and the REE breccia pipes contain monazite with lesser xenotime and REE-bearing carbonates. In the magnetite body, monazite and xenotime are generally found along fractures and cleavage planes within apatite. Rare coarse monazite occurs with hydrous phases such as actinolite and phlogopite. Minor Y-bearing carbonates and/or oxides occur in vugs or along fractures that cut quartz and magnetite. In the REE breccia pipes, monazite and xenotime occur along fractures and as inclusions in other phases such as specular hematite. REE-bearing carbonates are abundant in vugs.

Monazite and xenotime in apatite have been interpreted to be exsolution features that formed during cooling (Sidder et al. 1993). A more recent study suggests that late acidic fluids mobilized REE's from the lattice of apatite into monazite along cleavage planes and fractures (Harlov et al., 2005). To constrain the mechanism and conditions of phosphate mineral growth, we combine textural and chemical relationships between monazite, xenotime, apatite, and quartz with fluid inclusion data and Ti-in-Qtz thermometry.

Ti concentrations in quartz decrease through the paragenetic sequence. In the magnetite body, quartz intergrown with apatite contains ~15 ppm Ti whereas later recrystallized quartz contains ~5 ppm Ti. In the outer silica zone, primary quartz with euhedral growth zones is cut by recrystallized quartz. Primary quartz lacks fluid inclusions and contains significant titanium (~40 ppm). Recrystallized quartz contains ~16 ppm Ti as well as abundant planes of secondary fluid inclusions and submicron mineral inclusions of Y-bearing carbonates/oxides and lesser monazite. Recrystallized and drusy quartz in the REE breccia pipes has the lowest Ti concentrations (≤ 1.5 ppm - the Detection limit (DL) of LAICPMS).

The X-site in apatite contains ~1.30 OH, ~0.67 F (apfu), and little or no Cl. Ce, La, and Nd concentrations in apatite decrease through the paragenetic sequence. In the magnetite body, primary apatite lacks inclusions of monazite and/or xenotime and has high Ce, La, and Nd concentrations (~1700 ppm, ~750 ppm, and ~1600 ppm). Recrystallized apatite in the magnetite body lacks fluid inclusions, but contains ubiquitous monazite along cleavage planes. Where xenotime is present, it encases monazite and tends to follow secondary fractures that are perpendicular to cleavage. Relative to primary domains, recrystallized apatite is depleted in Ce, La, and Nd (≤ 1080 ppm - the DL of Electron Microprobe analysis (EMP), ~300 ppm, and ~600 ppm). In the REE breccia pipes, apatite is thoroughly recrystallized. Monazite and xenotime are present in relic core domains; apatite rims are devoid of mineral inclusions and are depleted in Ce, La, and Nd to levels less than the DL of EMP (1080 ppm, 260 ppm, 248 ppm).

Nd and Gd concentrations in monazite decrease through the paragenetic sequence whereas Yb and Lu concentrations in xenotime increase in REE breccia pipes. In the magnetite body, monazite associated with xenotime often has enriched Nd and Gd cores (~10.70 wt% and ~0.80 wt%) and depleted fractures and rims (~8 wt% and ~0.40 wt%). Xenotime exhibits patchy zoning with some zones containing slightly elevated concentrations of Yb and Lu (~4 wt% and ~0.57 wt%) and others with lower concentrations (~3.35 wt% and ~0.48 wt%). In REE breccia pipes, Nd and Gd concentrations in monazite cluster at 9.15 wt% and 0.68 wt%. Xenotime has high Yb and Lu concentrations (~5.8 wt% and ~1.0 wt%).

Sidder et al. (1993) and Song (2002) described 3 major inclusion populations: dilute (0-6 wt.% NaCl eqvl.), brine (12-28 wt.% NaCl eqvl.), and hypersaline (34-60 wt.% NaCl eqvl.). Current work suggests these inclusion populations are mostly secondary in origin. Dilute inclusions are prevalent in quartz in REE breccia pipes. These inclusions are often necked and yield a wide range of Th (100-400 °C). They are morphologically typical of fluid inclusions found in the epithermal environment and may represent condensed magmatic vapor. Brine inclusions are common in quartz ± barite from the magnetite ore body and surrounding domains. Their homogenization P and T suggest that they may have been trapped when ascending fluids split into brine and vapor at T < 350 °C and P < 15 MPa. The maximum pressure corresponds to a depth of 1.5 km, assuming hydrostatic conditions, which is well within the 3 km maximum depth estimate of Kisvarsanyi (1974). Hypersaline inclusions (60 wt. % NaCl eqvl.) homogenize by halite dissolution and yield errant T and P values of up to 530°C and 790 MPa or more due to heterogeneous trapping of L+H. Such inclusions are characteristic of a porphyry environment and indicate that ascending fluids intersected the V+L+H surface (i.e. halite saturation). The eutectic ice melting T of the brine and hypersaline inclusions (-65 to -20 °C), together with the existence of halite, sylvite, and hematite daughter minerals, suggest that Na, K, Ca, Mg, and Fe were important cations in the fluids.

To further constrain the composition and source of salt in fluid inclusions, extracts from ore and gangue minerals were analyzed by ion chromatography. The results confirm that Na, Ca, K, and Mg are the principal cations with lesser NH₄ and Li; Fe was not analyzed. Cl is the principal anion, with significant SO₄ and lesser F, acetate, and Br (CO₃ was detected but not quantified). Na/Cl and Cl/Br ratios suggest that saline fluids were derived primarily from a magmatic source that mixed with external fluids derived from either basinal (evaporated seawater) or metamorphic (or simply CO₃ & SO₄ rich) sources.

Ti-in-Qtz thermometry (Huang & Audétat 2012) was applied to quartz from the magnetite body, silica zone, and REE-rich breccia pipes. T's were calculated assuming a pressure of 15 MPa. Accessory rutile and zircon are common in the silica zone, but are absent in the magnetite body. Therefore a Ti activity of 1 is valid for the silica zone, but not the magnetite body. Consequently, T estimates for the magnetite body assuming unit activity are minimum values. In the magnetite body, primary quartz yields T 400-450 °C and recrystallized quartz T 300-400 °C. In the silica zone, primary quartz yields a T 475-525 °C and recrystallized quartz a T 300-480 °C. A Ti activity of 0.5 is required to raise the T estimates for the magnetite body to those of the silica zone. The REE breccia pipes yield maximum T < 325 °C. These temperatures are at, or above, those recorded by homogenization T's of secondary fluid inclusions, which suggests they were trapped as the system cooled or that they require a pressure correction.

Texturally it appears that monazite formed along fractures from hydrothermal fluids that leached components from primary apatite in the magnetite body. The texture is not compatible with formation from a cooling melt. Monazites may have formed from the fluids represented by the secondary brine and/or hypersaline fluid inclusion populations present in quartz. These fluids were probably derived from a magmatic source. Xenotime, specular hematite, and (REE)-bearing carbonates in the REE breccia pipes appear to be related to later, more dilute, low T fluids, and do not appear to have obtained components directly from apatite.

REFERENCES

- Frietsch R & Perdahl JA (1995) Rare earth elements in apatite and magnetite in Kiruna-type iron ores and some other iron ore types. *Ore Geology Reviews*. 9. 489-510.
- Harlov D, Wirth R, & Forster HJ (2005) An experimental study of dissolution-reprecipitation in fluorapatite: fluid infiltration and the formation of monazite. *Contrib Mineral Petrol*. 150. 268-286.
- Huang R & Audétat A (2012) The titanium-in-quartz (TitaniQ) thermobarometer: a critical examination and re-calibration. *Geochim et Cosmochim Acta*. 84. 75-89.
- Kisvarsanyi EB (1974) Operation Basement: buried Precambrian rocks of Missouri – their petrography and structure: *American Association of Petroleum Geologists Bulletin*. 58. 674-684.
- Nuelle and others, 1992, *Geology and origin of the Pea Ridge iron ore mine, Missouri*. USGS Bulletin 1989. A1-A11.
- Sidder GB, Day WC, Nuelle LM, Seeger CM, and Kisvarsanyi EB (1993) Mineralogic and fluid-inclusion studies of the Pea Ridge iron-rare-earth-element deposit, southeast Missouri. *U.S. Geological Survey Bulletin* 2039.
- Song X (2002) Fluid inclusion studies of the Pea Ridge iron-oxide rare earth elements deposit, Missouri. University of Windsor Theses and Dissertation. Paper 2130.

Estimates of the amount of time required to form an epithermal precious metal deposit based on ore grade & tonnage, fluid flow rate, and metal content of ore fluids.

Moncada, D.* , Rimstidt, J.D.* , and Bodnar, R.J.*

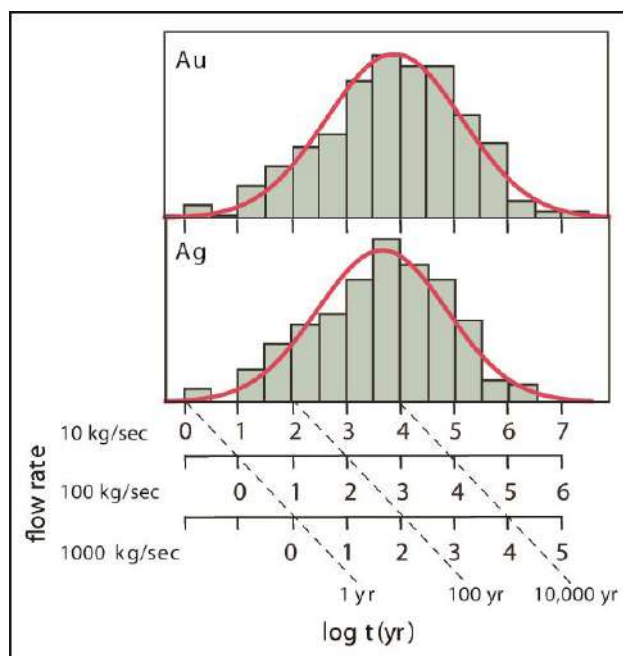
* Department of Geosciences, Virginia Tech, Blacksburg, VA 24061 USA

Over the past three decades there have been numerous studies of the physical and chemical environment in both active terrestrial geothermal systems and their fossil equivalents, the epithermal precious metals deposits. There is now a large database on fluid inclusions and mineralogy in these systems that shows that boiling is closely associated with mineralization in the epithermal environment. In these boiling systems, the highest gold grades often occur at the bottom of the boiling horizon, and there is a sharp decrease in gold grades and increase in base metal grades beneath the boiling level. Once boiling begins at depth, the fluid usually will continue to boil to the surface . Thus, the presence of fluid inclusions indicative of boiling in surface outcrops suggests that the base of the boiling zone, and the highest gold grades, are likely to be encountered at depth.

One of the least understood aspects of ore genesis concerns the duration of the mineralizing event. We have used ore tonnage (production + reserves) and grade information along with observed fluid flow rates in active geothermal systems to estimate the amount of time required to form an epithermal Au-Ag deposit. Total gold tonnage for 279 epithermal veins and deposits ranges from 0.0002 T (6t oz; Wharekirau- ponga, NZ) to 2,170 T (69 x 10⁶ t oz; Yanacocha, Peru), with an average of 4.1 T. Total silver tonnage for 252 epithermal deposits ranges from 0.0004 T (12t oz; Wharekirau- ponga, NZ) to 62,207 T (2.0 billion t oz; Cerro Rico de Potosi, Bolivia), with an average of 29.4 T (1.94 million t oz). The average gold grade, based on 241 deposits, is 4.5 g/T, and the average silver grade is 87.2 g/T. Reported flow rates for 693 active continental geothermal systems and hot springs average 5.9 kg/sec. Assuming a gold content in the ore-forming fluid of 1.8 µg/kg (1.8 ppb), the amount of time required to deposit the average amount of Au estimated for epithermal deposits is 7,940 yr, with 68% (one standard deviation) of the deposits requiring between 132 and 479,000 yr to form. Assuming a silver content in the ore-forming fluid of 33.9 µg/kg (33.9 ppb), the amount of time required to deposit the average amount of Ag estimated for epithermal deposits is 9,330 yr, with 68% of the deposits between 120 and 724,000 yr.

Results of this assessment indicate that the duration of active mineralization in epithermal systems need not be longer than ~10⁴ yr, assuming continuous deposition. Field and laboratory data suggest, however, that mineralization is not continuous but, rather, is episodic and associated with discrete hydrothermal eruption events that lead to boiling and the quantitative precipitation of all metal in solution. As such, gold and/or silver deposition is likely occurring over only a small fraction of the total lifetime of the hydrothermal system. Results of this study also suggest that formation of giant deposits in a geologically reasonable amount of time requires hydrothermal systems that were active for longer periods of time and were characterized by higher fluid flow rates.

Figure 1. Estimated times needed to deposit the Au or Ag reported for the epithermal precious metal deposits in our data base based on the mass of fluid and the range of flow rates (10 to 1000 kg/sec) of geothermal systems.



Fluid inclusion & stable isotopic evidence for extreme degassing of melt & condensation of brine in the Henderson porphyry Mo deposit

Melanie N. Newton* and Albert H. Hofstra**

*Dept. of Geoscience, Univ. of Nevada - Las Vegas, NV 89154, USA, newtonm8@unlv.nevada.edu

**Denver Inclusion Analysis Laboratory, USGS, Denver, CO 80225, USA, ahofstra@usgs.gov

The pre-meeting field trip will include a visit to the Henderson molybdenum (Mo) mine in the Front Range about 80 km west of Denver, Colorado, USA. It is the largest primary producer of molybdenum in the world with production over the past 27 years of more than 160 million tons of ore and 770 million pounds of molybdenum (Climax Molybdenum, 2014). Climax-type Mo deposits, such as Henderson, are products of hydrothermal systems associated with silicic magmatic centers that formed after the transition from contraction to extension and calc-alkaline to bimodal volcanism in the western United States (Ludington and Plumlee, 2009). The Henderson ore body is related to 30-27 Ma high-silica rhyolite porphyry intrusions and lamprophyre dikes of the Red Mtn. Intrusive Complex (Shannon et al., 2004).

Henderson was the subject of a Ph.D. dissertation by E. Seedorff at Stanford (Seedorff, 1987; Seedorff and Einaudi, 2004) and a postdoctoral investigation at the U.S. Geological Survey by R. Carten (Carten et al., 1988b). These seminal studies generated fluid inclusion and stable isotopic data that can be further interpreted in light of current understanding. To aid interpretation of such data, quartz cathodoluminescence and optical microscopy were used to determine the type and origin of fluid inclusions present. Crenulate unidirectional solidification texture quartz (i.e. "brain rock") is extremely fractured to comminuted, etched, and cemented. These textures suggest that quartz was brittle during plastic deformation of enclosing porphyry. Euhedral quartz in vein dikes exhibits subtle growth zones and an abundance of etched and healed fractures. No primary fluid inclusions were recognized. Secondary fluid inclusions, 5-25 microns in size, are abundant in all of the quartz studied and the majority are hypersaline, although vapor- and liquid-rich inclusions are also present. Though secondary with respect to their host mineral, the inclusion types present are typical of the porphyry environment. Based on these observations, we infer that most of the inclusions studied by Seedorff (1987) are secondary in origin and that most of the fluid inclusion water extracted from quartz for H isotopic analysis by Carten et al. (1988b) was derived predominantly from secondary hypersaline inclusions. To further characterize the population of hypersaline inclusions, extracts were analyzed by ion chromatography (à la Landis and Hofstra, 2012).

Seedorff's (1987) microthermometric data were used to estimate the T, P, d, and salinity of the inclusions at homogenization (à la Steele-McInnis et al., 2012). Remarkably, most of the T_h and P_h data coincide with the vertical T-P path in the porphyry fluid flow model of Weis et al. (2012). Thus, we surmise that the T+P at homogenization \approx T+P of trapping. The few inclusions that deviate from the model T-P path have $T_{m(Halite)} > T_{h(V+L \rightarrow L)}$ and yield errant P_h , up to 250 MPa, which likely reflect heterogeneous trapping of L+H from halite saturated fluids. The T_h , P_h and salinity of the main population of hypersaline brine inclusions (33 ± 5 wt. % NaCl eq.) suggests that input fluids split into liquid and vapor at $T < 475^\circ\text{C}$ and $P < 42$ MPa and that immiscibility extended to much lower T (200°C) and P (1 MPa). A plot of the P_h data relative to sample elevations and the reconstructed elevation of the paleosurface (from Carten et al., 1988a) shows that fluids were trapped over an enormous pressure range that extended from near lithostatic through hydrostatic to vaporstatic conditions.

Carten and others (1988b) O isotope data on biotite (i.e. fluorophlogopite) and quartz yield a median $\delta^{18}\text{O}_{\text{H}_2\text{O}}$ of 8‰, which is typical of magmatic water, and a $\Delta^{18}\text{O}_{\text{qtz-Fphl}}$ of 2.6‰, which corresponds to a temperature of 520°C . Remarkably, the calculated $\delta\text{D}_{\text{H}_2\text{O}}$ values for biotite from vein dikes, UST's, and

potassic alteration zones at this temperature (-128 to -112‰, median -115‰) are similar to the measured δD_{H_2O} values for fluid inclusion water extracted from quartz (-140 to -92‰, median -116‰). Such δD_{H_2O} values are much lower than typical magmatic water (-80 to -40‰) and have been attributed to open system magma degassing and condensation of brine from magmatic vapor in Cu porphyries (Hedenquist and Richards, 1998). The ion ratio results show that more volatile ions, such as Li and Na, are enriched in fluids from less degassed melts and less condensed brine with higher δD_{H_2O} values, whereas less volatile elements, such as K and F, are enriched in fluids from more degassed melts and more condensed brines with lower δD_{H_2O} values. There is little or no evidence for the involvement of meteoric water.

We conclude that the extreme negative H isotopic shift at Henderson resulted from the combined effects of open system magma degassing with progressive condensation of brine from magmatic vapor, during a large pressure drop, as the vapor plume discharged to the paleosurface. The shallow manifestation of such hot, low density, vapor discharges are not preserved at Henderson, but may have been magmatic steam alunite veins (Rye et al., 1992), such as those preserved in a down dropped fault block in the Questa Climax-type porphyry Mo district in New Mexico (Ludington et al., 2005).

REFERENCES

- Carten, R.B., Geraghty, E.P., Walker, B.M., and Shannon, J.R. (1988a) Cyclic development of igneous features and their relationship to high-temperature hydrothermal features in the Henderson Porphyry Molybdenum deposit, Colorado. *Economic Geology*. 83. 266–296.
- Carten, R.B., Rye, R.O., and Landis, G.P. (1988b) Effects of igneous and hydrothermal processes on the composition of ore-forming fluids; stable isotope and fluid inclusion evidence, Henderson porphyry molybdenum deposit, Colorado. *GSA Abstracts with Programs*, 19, A94.
- Climax Molybdenum, 2014, website,
<http://www.climaxmolybdenum.com/worldwidelocations/usa_colorado_henderson.htm>
- Goldstein, R.H. and Reynolds, T.J. (1994) Systematics of fluid inclusions in diagenetic minerals. *SEPM Short Course*, 31, 199.
- Landis, G.P., and Hofstra, A.H. (2012) Genetic Constraints on the Idaho Cobalt Belt from gas, noble gas isotope, and ion ratio analyses of fluid inclusions. *Economic Geology*. 107. 1189–1205.
- Ludington, S. and Plumlee, G.S. (2009) Climax-type porphyry molybdenum deposits. *U.S. Geological Survey Open-File Report*. 2009–1215. 16.
- Hedenquist, J. W. and Richards, Jeremy P. (1998) The influence of geochemical techniques on the development of genetic models for porphyry copper deposits. *Rev. Economic Geology*. 10. 235–256.
- Rye, R.O., Bethke, P. M. and Wasserman, M.D. (1992) The stable isotope geochemistry of acid sulfate alteration. *Economic Geology*. 87. 225–262.
- Seedorff, C.E. (1987) Henderson porphyry molybdenum deposit: Cyclic alteration-mineralization and geochemical evolution of topaz- and magnetite-bearing assemblages. Ph.D. dissertation, Stanford University, Stanford, CA, 432.
- Seedorff, E., and Einaudi, M.T., 2004, Henderson porphyry molybdenum system, Colorado; I & II. *Economic Geology*, v. 99, p. 3–72.
- Shannon, J.R., Nelson, E.P., and Golden, Jr., R.J. (2004) Surface and underground geology of the world-class Henderson molybdenum porphyry mine, Colorado. *In* Nelson, E.P. and Erslev, E.A., eds., *Field trips in the southern Rocky Mountains, USA: GSA Field Guide* 5, p. 207–218.
- Weis, P. et al. (2012) Porphyry-copper ore shells form at stable pressure-temperature fronts within dynamic fluid plumes. *Science*. 338. 1613.

Critical *PTX* properties of FeCl₂-bearing fluids

Steele-MacInnis, M.*, Lecumberri-Sanchez, P.*, Bodnar, R.J.**

*Institute for Geochemistry and Petrology, ETH Zurich, Clausstr. 25, 8092 Zurich, Switzerland

*Department of Geosciences, Virginia Tech, 4044 Derring Hall, Blacksburg VA

Ferrous chloride (FeCl₂) is a common and abundant component in magmatic-hydrothermal fluids, occurring in concentrations up to several 10's of wt% in fluids in some hydrothermal systems (Yardley, 2005). Thus, the effect of FeCl₂ on the phase equilibria of aqueous fluids is a significant factor in interpreting fluid evolution in iron-rich, ore-forming environments such as granite-related tin-tungsten deposits (e.g., Audétat et al., 2005) and some porphyry copper systems (Bodnar et al., 2013). However, there are few available experimental data on the phase equilibria and thermodynamic properties of iron-bearing aqueous fluids (Liebscher, 2007).

We used synthetic fluid inclusions to investigate the pressure-temperature conditions along the critical curve in the system H₂O-FeCl₂, from 0 to 35 wt% FeCl₂, using methods similar to those described by Knight and Bodnar (1989). This information constrains the conditions at which immiscibility ("boiling") can occur in hydrothermal systems, because at any given temperature, the critical curve represents the highest pressure at which immiscibility occurs. Stated differently, at pressures above the critical curve, fluids are always in the single-phase field, whereas boiling may occur at lower pressures.

The critical curve for H₂O-FeCl₂ fluids occurs at lower pressure (at any given temperature) compared to fluids in the system H₂O-NaCl. For example, the average dP/dT slope of the H₂O-NaCl critical curve is about 3.5 bar/°C up to 550 °C, whereas the average slope of the H₂O-FeCl₂ critical curve is only 2 bar/°C over the same range. Thus, the critical pressure at 500 °C for H₂O-FeCl₂ fluids is about 500 bar, compared to about 560 bar for H₂O-NaCl. The low dP/dT slope of the H₂O-FeCl₂ critical curve is in contrast to other H₂O-salt binaries containing divalent cation chlorides such as CaCl₂ or MgCl₂, for which the critical curves occur at higher pressure compared to NaCl (Liebscher, 2007). Thus, immiscibility in FeCl₂-rich fluids can occur only at relatively low pressures, or at relatively shallow depths in the crust. These data provide a basis for interpreting the fluid evolution and pressure-temperature conditions of Fe-rich, boiling hydrothermal systems (e.g., Audétat et al., 2000).

REFERENCES

- Audétat, A., Günther, D., Heinrich, C.A. (2000) Causes for Large-Scale Metal Zonation around Mineralized Plutons: Fluid Inclusion LA-ICP-MS Evidence from the Mole Granite, Australia. *Economic Geology*. 95. 1563-1581.
- Bodnar, R.J., Lecumberri-Sanchez, P., Moncada, D., Steele-MacInnis, M. (2014) Fluid inclusions in hydrothermal ore deposits. *Treatise on Geochemistry*. 13. 119-142.
- Knight, C.L., Bodnar, R.J. (1989) Synthetic fluid inclusions: IX. Critical PVTX properties of NaCl-H₂O solutions. *Geochimica et Cosmochimica Acta*. 53. 3-8.
- Liebscher, A. (2007) Experimental Studies in Model Fluid Systems. *Reviews in Mineralogy and Geochemistry*. 65. 15-47.
- Yardley, B.W.D. (2005) Metal Concentrations in Crustal Fluids and Their Relationship to Ore Formation. *Economic Geology*. 100. 613-632.

CO₂-rich fluid inclusions in Silica- and LREE-enriched spinel peridotite xenoliths from the Quaternary intraplate alkali basalt, Jeju island, South Korea: A preliminary study

Woo, Y.H. , Yang, K.H

Dept. of Geological Sciences, Pusan national University, Busan 609-735, South Korea

Spinel harzburgite to lherzolite peridotite xenoliths trapped in Quaternary intraplate alkali basalts in Jeju Island, South Korea are silica- and LREE-enriched, containing late-stage secondary orthopyroxene as the main pervasive metasomatic mineral. Moreover, primary CO₂-rich inclusions with negative crystal shapes (5-30µm in diameter) are trapped in the late-stage secondary orthopyroxene or fine-grained neoblasts (Fig.1), although they are extremely rare. Most CO₂-rich inclusions in the coarse-grained porphyroclasts are considered as secondary in origin and are decrepitated. During microthermometry, solid CO₂ melting temperatures of the inclusions are -56.6°C (± 0.8°C), indicating the presence of essentially pure CO₂ phase.

Homogenization temperatures of CO₂ to the liquid phase range from - 34 to -22°C, corresponding to CO₂ density of 1.1–1.0 g/cm³. The high CO₂ density and a negative crystal shape support that the entrapment of the fluids occurred at lithospheric mantle conditions prior to sampling by upwelling alkali basalt.

On the other hand, the studied xenoliths are characterized by the high Mg# [=100×Mg/(Mg+Fe_{total}) atomic ratio] of olivine, orthopyroxene and clinopyroxene (89-93) and the variable Cr# [=100×Cr/(Cr+Al) atomic ratio] of spinel (9-53), representing residues left after variable fractional melt extraction. In contrast to their depleted major element compositions, the clinopyroxenes of the xenoliths are mostly enriched in incompatible trace elements, exhibiting enrichment in light rare earth elements (LREE), negative Ce-anomalies, and depletion in Ba and high field strength elements (HFSE; e.g., Nb-Ta, Zr-Hf, Ti). The chemical evidence, in addition to the formation of secondary orthopyroxene, clearly indicates that Jeju peridotite series have been subjected to different degrees of metasomatism by subduction-related silica- and LREE-enriched fluids. In addition, the secondary orthopyroxenes, which are characterized by high Cr₂O₃ (0.28-0.59 wt%) and Al₂O₃ (1.98-4.86 wt%) and moderate CaO (0.57-0.80 wt%) contents, resemble those of continental arc peridotites from the eastern Pacific.

Although we still have incomplete knowledge about whether the silica- and LREE-enrichment was controlled by the CO₂-rich fluids and about understanding the effect of such a CO₂ fluid, it is highly likely that the observed CO₂-rich fluids in the lithospheric mantle may have played a significant role in transporting significant amounts of dissolved silicate components and trace elements at the mantle wedge environment. Following the enrichment in the peridotites protolith at the mantle wedge, the upper mantle beneath proto-Jeju Island was transformed from a subarc environment to an intraplate environment as a consequence of geodynamics, possibly due to the formation of the back arc basin (e.g., East Sea) in the

western Pacific. The resulting Jeju peridotites, representing old subarc fragments, were subsequently transported rapidly to the surface, as captured in ascending Quaternary intraplate alkali basalt.

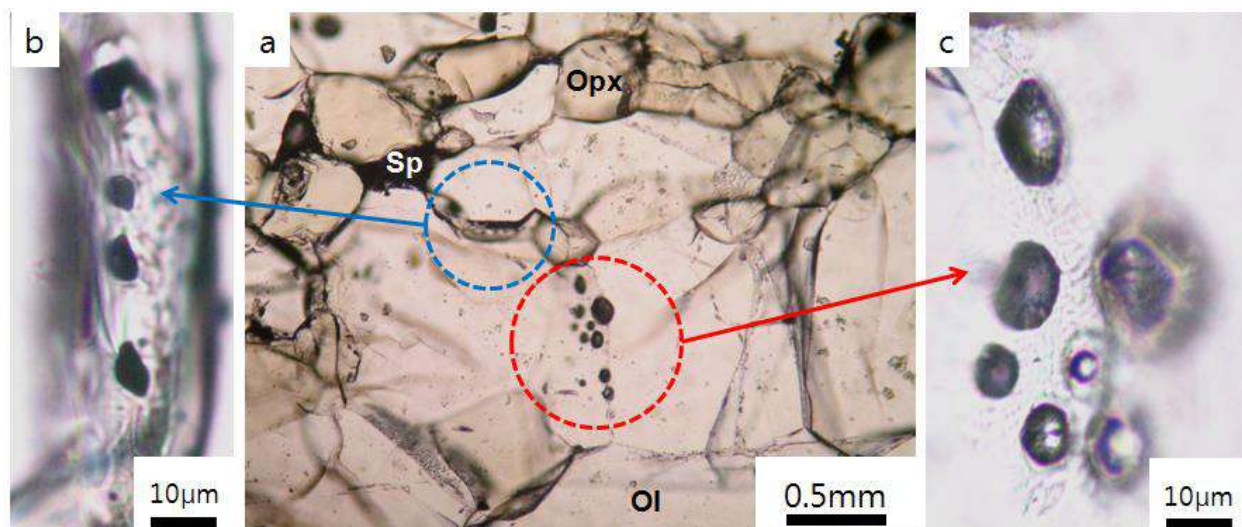


Fig. 2. Primary CO₂-rich inclusions trapped in the alkali basalt from Jeju Island, South Korea. (a) Spinel lherzolite xenoliths, containing primary CO₂-rich inclusions trapped (b) in late-stage secondary orthopyroxene and (c) along the olivine subgrain boundary.

Author Index

- Adams, D.T., 4, 39
Alimohammadi, M., 8, 57
Alirezaei, S., 8, 57
Appold, M.S., 8, 65
Arancibia, G., 4, 50
Arrieta-Garcia G., 5, 46
Audétat, A., 1, 13
Bain, W.B., 8, 59
Benison, K.C., 6, 8, 23, 67
Bennett, M., 8, 61
Bodnar, R.J., 2, 3, 4, 6, 9, 11, 27, 31, 33, 35, 41, 42, 76, 79
Booden, M.A., 6, 42
Brown, P.E., 8, 63
Burgisser, A., 4, 39
Caddick, M., 2, 31
Cai, Y-C., 5, 19
Campos, E., 4, 50
Casanova, V., 1, 13
Cembrano, J., 4, 50
Cline, J.S., 8, 59
Cosca, M., 4, 39
Davidson, P., 4, 52
Diamond, L.W., 2, 15
Driesner, T., 2, 4, 27, 50
Emsbo, P., 6, 9, 17, 74
Esposito, R., 3, 11
Fall, A., 3, 11
Fan, H-R., 5, 19
Fontboté, L., 1, 5, 13, 48
Freeze, J., 6, 41
Gazel, P., 3, 11
Guilbaud, M-N., 5, 46
Hanley, J., 4, 54
Haroldson, E.H., 8, 63
Hassan, A.M., 8, 65
Heinrich, C., 4, 50
Heinrich, C.A., 8, 71
Hitzman, M.W., 6, 9, 17, 74
Hofstra, A.H., 1, 4, 6, 9, 21, 37, 39, 74, 77
Hu, F-F., 5, 19
Karmanocky, F.J., 6, 8, 23, 67
Kendrick, M.A., 1, 25
Kent, A.J.R., 5, 46
Kim, H., 8, 69
Klyukin, Y.I., 2, 27
Kontak, D.J., 1, 4, 8, 29, 54, 57
Kouzmanov, K., 1, 5, 13, 48
Kyser, K.T., 8, 57
Lamadrid, H.M., 2, 31
Lambrecht, G., 2, 15
Landis, G.P., 4, 21
Lecumberri-Sanchez, P., 3, 8, 9, 33, 71, 79
Lohmar, S., 4, 50
Lowell, R.P., 2, 27
Lowers, H.A., 9, 74
Lüders, V., 6, 34
Luo, M.C., 4, 35
Manning, A.H., 6, 37
Marsh, E.E., 9, 72, 74
Marsh, T.M., 8, 59
Mauk, J.L., 6, 42
Meighan, C.J., 9, 74
Mercer, C.N., 4, 5, 39, 46
Moncada, D., 4, 6, 9, 35, 41, 76
Monecke, T., 8, 61
Moore, L., 3, 11
Muntean, J., 8, 61
Newton, M.N., 9, 77
Palinkas, S.S., 6, 42
Pérez-Flores, P., 4, 50
Pinto, F., 8, 71
Plessen, B., 6, 34
Reich, M., 4, 50
Reynolds, T.J., 8, 61
Ricks, J., 8, 61
Ridley, J., 2, 44
Rimstidt, D., 2, 31
Rimstidt, J.D., 9, 76
Roberge, J., 4, 5, 39, 46
Rogers, N., 4, 54
Rottier B., 5, 48
Rye, R.O., 4, 21
Sánchez-Alfaro, P., 4, 50
Schwarzenback, E., 2, 31
Seo, M., 8, 69
Simpson, M.P., 6, 42
Sisson, T.W., 4, 39
Steele-MacInnis, M., 3, 9, 33, 51, 79
Thomas, R., 4, 52
Todorov, T.I., 4, 39
Tweedale, F., 4, 54
Vieira, R., 8, 71
Wälle, M., 5, 8, 48, 71
Woo, Y.H., 9, 80
Yang, K., 8, 69
Yang, K.H., 9, 80
Yang, K-F., 5, 19